Expansion and contraction of anoxia during OAE-2 as inferred by sedimentary $\delta^{238}U$ values in the Portland #1 Core, Western Interior Seaway, Colorado

A Thesis Submitted to the College of Graduate and Postdoctoral Studies

In Partial Fulfillment of the Requirements

For the Degree of Master of Science

In the Department of Geological Sciences

University of Saskatchewan

By

Brayden Scott McDonald

Saskatoon, Saskatchewan

© Copyright Brayden S. McDonald, August 2018. All rights reserved

Permission to use:

In presenting this thesis/dissertation in partial fulfillment of the requirements for a Postgraduate degree from the University of Saskatchewan, I agree that the Libraries of this University may make it freely available for inspection. I further agree that permission for copying of this thesis in any manner, in whole or in part, for scholarly purposes may be granted by the professor or professors who supervised my thesis work or, in their absence, by the Head of the Department or the Dean of the College in which my thesis work was done. It is understood that any copying or publication or use of this thesis or parts thereof for financial gain shall not be allowed without my written permission. It is also understood that due recognition shall be given to me and to the University of Saskatchewan in any scholarly use which may be made of any material in my thesis.

Requests for permission to copy or to make other uses of materials in this thesis in whole or part should be addressed to:

Dean
College of Graduate and Postdoctoral Studies
University of Saskatchewan
116 Thorvaldson Building, 110 Science Place
Saskatoon, Saskatchewan S7N 5C9
Canada

Head of the Department of Geological Sciences
University of Saskatchewan
114 Science Place
Saskatoon, Saskatchewan S7N 5E2
Canada

Abstract

Oceanic Anoxic Event 2 (OAE-2) records a dramatic increase in organic carbon burial in marine sediments straddling the Cenomanian-Turonian boundary (93.9 Ma). This large increase in the flux of organic matter to the seafloor reduced the dissolved oxygen inventory of deep oceanic waters, particularly in the proto-North Atlantic Ocean. Development of a greater anoxic sink during this time led to increased burial rates of some redox sensitive elements. Based on modern analogues, redox sensitive elements, such as U, can be used to estimate the extent of anoxia in the geologic past. This research measures uranium isotopes ($\delta^{238}U$) in a pelagic carbonate and shale succession deposited in the Western Interior Seaway during OAE-2, which is interpreted to represent the authigenic record of seawater uranium. The measured $\delta^{238}U$ profile for the Portland core records a much larger negative excursion (-1.2‰) than previously reported for other OAE-2 sections (-0.15‰ in shale at Demerara Rise; Montoya-Pino et al., 2010 and -0.47‰ in limestone at Eastbourne; Clarkson et al., 2018). Accounting for fractionation associated with syndepositional reduction of uranium into anoxic sediments, the relative size of the $\delta^{238}U$ excursion in the Portland core can be decreased to -0.64‰, decreasing the differences between the two carbonate profiles. The recent focus on the incorporation of uranium into carbonate precipitates has found evidence for a small diagenetic alteration of primary seawater $\delta^{238}U$ values during carbonate deposition, could possible explain the difference between the two profiles (0.20 to 0.40‰). Therefore, the $\delta^{238}U$ profile from the Portland core might be a more accurate reflection of the uranium isotopic composition of coeval seawater during OAE-2.

Acknowledgments

I would like to thank both Dr. Camille Partin and Dr. Chris Holmden for their untold patience with me during this project. I know if it were not for their advice and high expectations, I would not be where I am today. I would like to specially thank Camille for taking a chance on me right from the get go and giving me the opportunity to pursue something I never thought possible. I would also like to thank Nasreen for her guidance in the lab, as well as the rest of the group for their willingness to listen and give advice. A special thanks to Brad Sageman for the samples. Lastly, I would like to thank my friends and family, if it were not for all of you this experience would not have been successful nor as rewarding.

Dedication

To my friends, family, and Kendall... Thanks for everything, always.

Table of Contents

List of Tables

List of Figures

List of Abbreviations

BOZ – Benthic oxic zone

C-T – Cenomanian – Turonian

CAS – Central American Seaway

IOC – Interpreted oxygen content

IODP – Integrated Ocean Drilling Program

LIP – Large igneous province

MBD – Maximum burrow diameter

MRB – Metal reducing bacteria

OAE – Oceanic Anoxic Event

ODP – Ocean Drilling Program

OMZ – Oxygen minimum zone

PNAO – Proto-North Atlantic Ocean

PCE – Plenus Cold Event

PCP – Primary carbonate precipitates

PO – Portland Core

SST – Sea surface temperature

TE – Trace Elements

TOC – Total organic content

USGS – United States Geological Survey

WIB – Western Interior Basin

WIS – Western Interior Seaway

CHAPTER 1

Introduction

Modern climate science shows that increasing temperatures could be devastating to some modern plant life, aquatic life, and terrestrial life (Meisner et al., 1987; De Boeck et al., 2007; Stirling and Derocher, 2012). As atmospheric temperatures increase, and in turn sea-surface temperatures, the ability for the oceans to retain oxygen decreases (e.g., oxygen saturation is 20% lower in seawater of 15°C than it is at 0°C ocean water temperature; Huber et al., 2002) allowing low oxygen or oxygen free (anoxic) zones within the water column to more readily form (Trabucho Alexandre et al., 2010). Due to the broader consequences that a warming climate has on the Earth, the geologic past can help understand the effects an expanding anoxic zone would have. Our planet has been well oxygenated for the last 500 Ma. Relative to today, atmospheric oxygen levels were 1 to 2 orders of magnitude less prior to the Phanerozoic (Berner and Canfield, 1989) (Figure 1.1). Discrete intervals exist throughout Earth history, however, where the oceans are estimated to be up to 50 times more anoxic than present day (Jenkyns, 2010; Zhang et al., 2018). Primarily occurring during the Cretaceous Period (145 – 66 Ma), these discrete intervals represent periods of significant organic carbon sequestration and preservation, extinction, and faunal turnover (Jenkyns, 2010). Most commonly referred to as Oceanic Anoxic Events (OAE), these events provide a unique snapshot into a time interval when the oceans were poorly oxygenated relative to today. OAEs provide the opportunity to better understand possible predictions for future realities facing modern Earth, but also allow us to gain a framework to interpret and understand the Earth further back in time, when an oxygenated atmosphere was first forming (2.4 – 2.1 Ga; Bekker et al., 2004). Spanning from the early to mid-Jurassic Period (183 Ma) to the late-Cretaceous Period (~ 85 Ma), eight separate OAEs have been identified, with three of them being considered globally significant (Early Toarcian Oceanic Anoxic Event, Early Aptian Oceanic Anoxic Event, and Cenomanian-Turonian Oceanic Anoxic Event; Figure 1.2). Of those three, OAE-2 or the Cenomanian - Turonian OAE, is widely studied largely due to its longevity, global distribution, and its easily identifiable geochemical signatures.

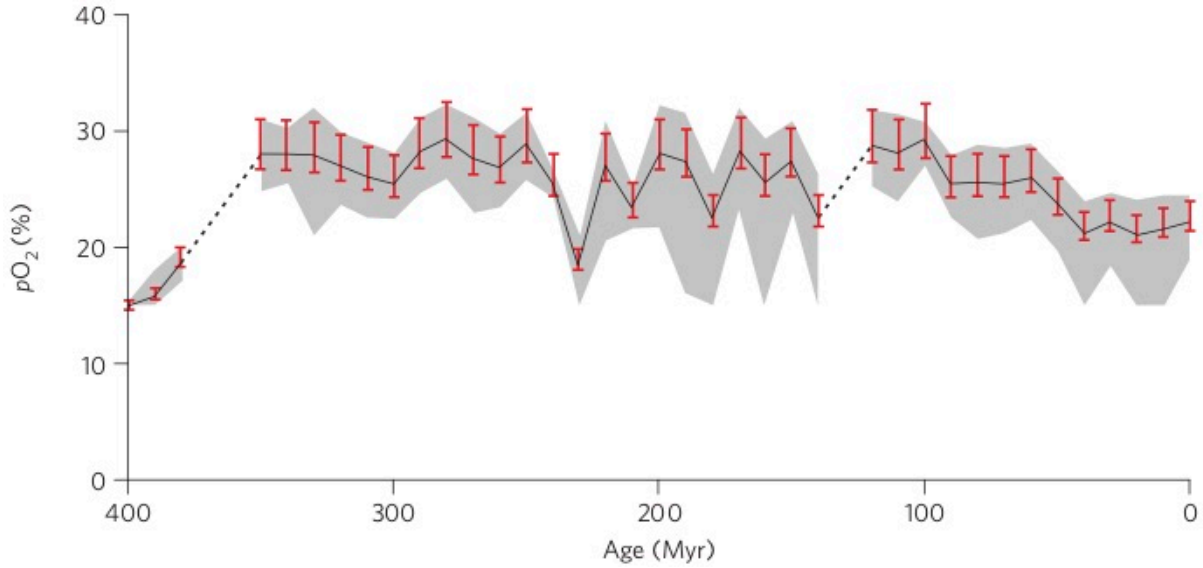

Figure 1.1 Evolution of Earth's atmospheric oxygen content through the Phanerozoic Era. Figure from Glasspool and Scott (2010).

Since its discovery by Schlanger and Jenkyns (1976), OAE-2 has become a major focal point in paleo-redox research. Schlanger and Jenkyns (1976) found evidence of widespread organic-rich sediments in several Aptian-Albanian and Cenomanian-Turonian sedimentary sequences from Deep Sea Drilling Program (DSDP) core in both the south central and western North Pacific Ocean. Further investigation led to the discovery of similar $\delta^{13}C$ excursions in Aptian-Albanian and Cenomanian-Turonian aged organic-rich sediments in various depositional environments from around the world (Figure 1.3; Hetzel et al., 2006; Tucholke and Vogt, 1979; Murdmaa, 1978; Tucholke et al., 2006; Thurow et al., 1988; Kuypers et al., 2004; Monaco et al., 2002; Curiale, 1994). When initially discovered, Schlanger and Jenkyns (1976) attributed the widespread preservation of organic-rich black shales and the associated anoxia to be a result of increased organic productivity due to increased nutrient supply to the oceans. Although the ideas presented in Schlanger and Jenkyns (1976) still have merit, new ideas have been proposed for the cause of the increased nutrient supply. Some postulated the reason behind the increased nutrient supply had been intensified weathering processes during the Cretaceous due to a more humid climate and higher freshwater runoff (Arthur et al., 1987). A combination of a humid climate and increased runoff would supply the excess nutrients to the oceans. The expansion of anoxia was also suggested to be the result of a salinity stratified water column due to a sea level rise. As a result, organic matter would be trapped within the lower most level and eventually preserved (Arthur et al., 1987). Alternatively, more recent work, such as Sinton and Duncan (1997); Snow

et al. (2005); Turgeon and Brumsack (2006); and Holmden et al. (2016), has suggested that there was an additional or complementary source for the nutrients. They suggest that the arrival of a short lived, massive, underwater eruption, known as a Large Igneous Province (LIP), acted as the principle source of nutrients for primary production to increase. Large amounts of basalt were erupted onto the ocean floor and along with it the release of bio-essential metals (i.e., Fe, Cu, and V) contained in thermally buoyant plumes. Sinton and Duncan (1997) postulated that the addition of ferrous Fe from the erupting LIP stimulated primary productivity. Regardless of the cause, all theories as to why or how widespread anoxia occurred during OAE-2 share a common theme of increased nutrient supply.

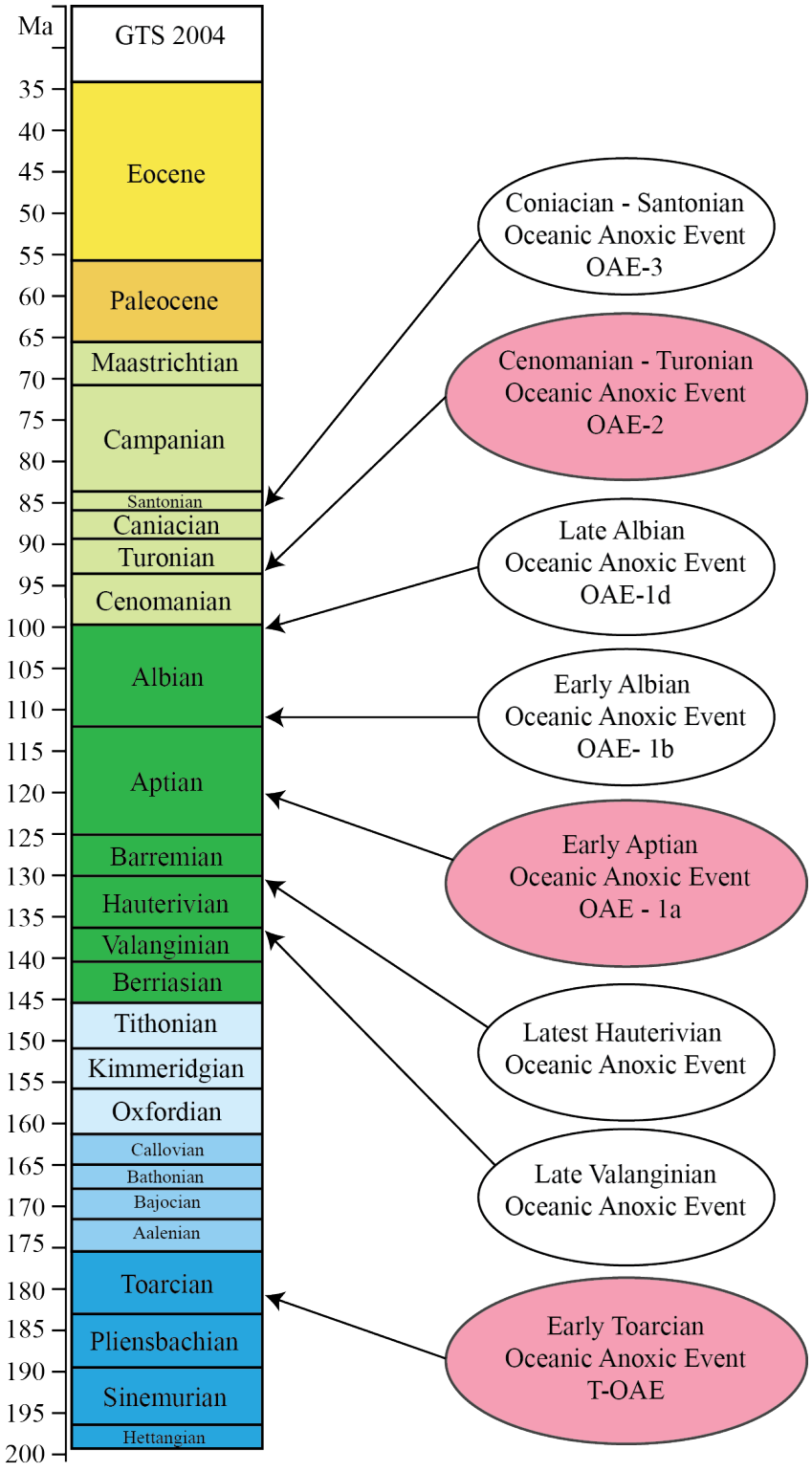

Figure 1.2 Geologic time scale depicting eight known oceanic anoxic events in the last 200 Ma. Pink ovals indicate globally significant anoxic events. Modified from Jenkyns (2010).

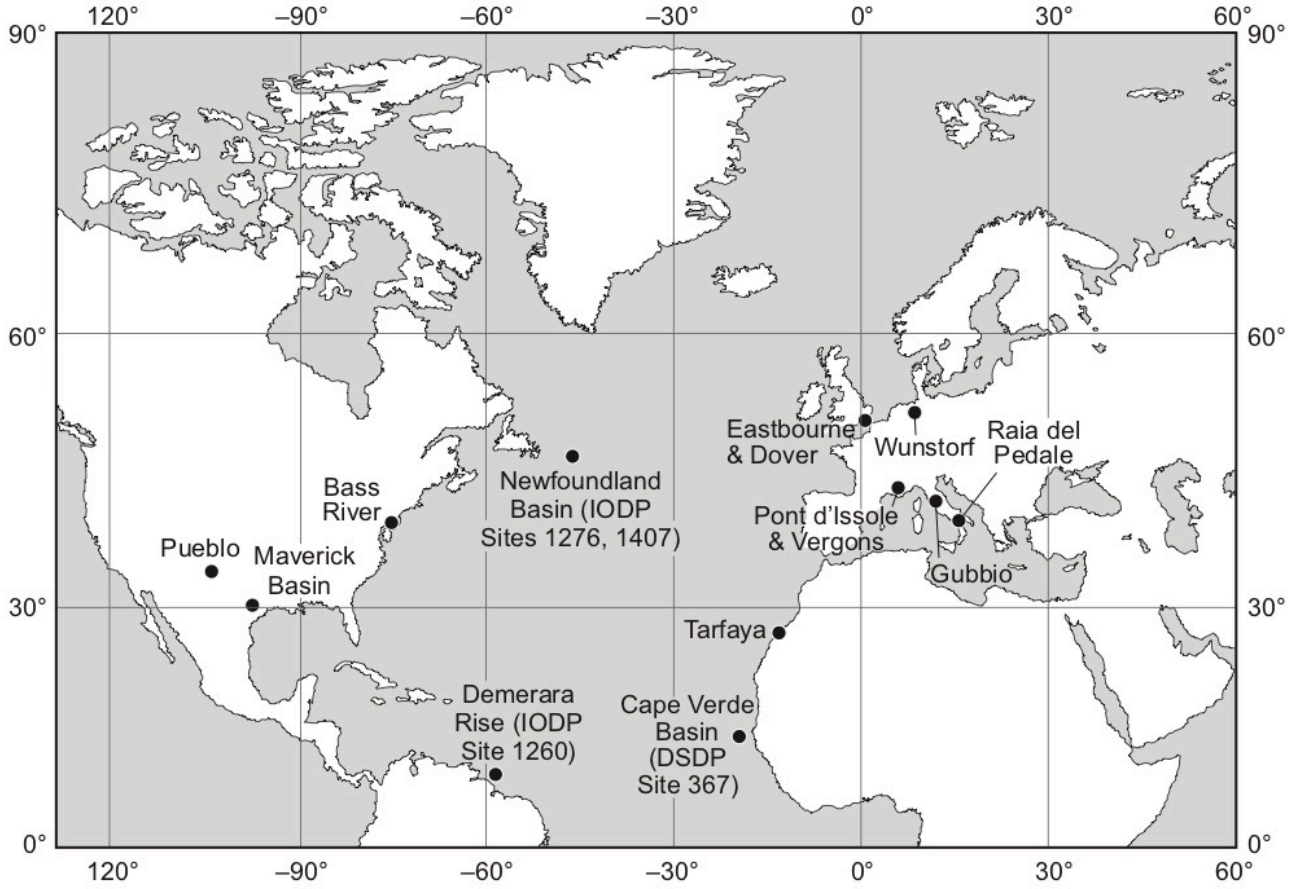

Figure 1.3 Key localities of the Cenomanian-Turonian boundary locations in which the OAE-2 event has been studied. From Jenkyns et al., (2017).

1.1 Evidence for enhanced anoxia during OAE-2

Ocean circulation patterns for the Proto-North Atlantic Ocean (PNAO) were conducive to the formation of organic-rich sediments along the eastern margins of the PNAO. Within the organic-rich sediments forming under these conditions, redox sensitive elements will be preferentially removed from seawater into the sediment. As a result of the increased drawdown and preservation of some redox sensitive elements, organic-rich shales offer an excellent record of TE enrichments. By measuring the relative abundances of redox elements in marine sediments it is possible to understand the state of atmospheric oxygen throughout Earth's history. Elevated concentrations of many redox sensitive elements suggest the presence of a well oxygenated atmosphere because the processes that remove them into the sediments are dominated by reductive mechanisms, therefore the higher the concentration of the element the less anoxic sediments there are globally. Elevated

levels of redox metals in organic-rich sediments such as uranium, which are introduced through oxidative processes (discussed below), demonstrates that marine anoxia for most of the Phanerozoic was minimal relative to the Precambrian (Figure 1.4; Partin et al., 2013). Concentration data is a useful first order approach to understanding the redox state of the oceans. Concentrations of U, Mo, and Fe through the Cenomanian-Turonian boundary in organic-rich sediment (Figure 1.5 and 1.6) demonstrate the ability for concentrations to record major perturbations to the marine redox state. However, they do not allow us to discriminate between the cause of the perturbation. Instead isotopes have the potential to narrow in on the specific source or sink that is controlling the change and can allow us to estimate the relative change the source or sinks underwent.

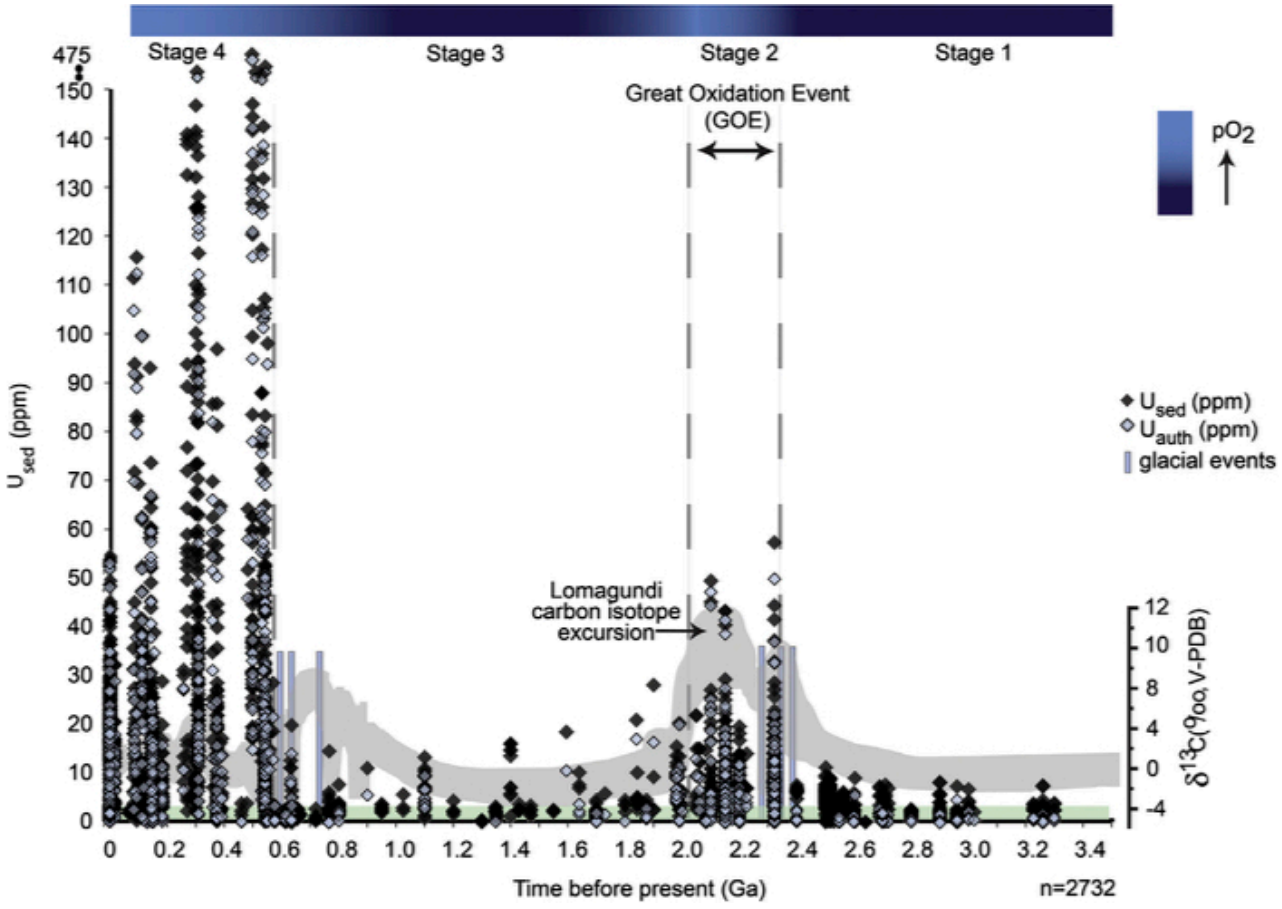

Figure 1.4 U concentration for organic-rich shales through time. [U] follows closely to pO_2 estimates, illustrating the point that during increased oxygen levels of the Phanerozoic were associated with higher seawater U concentrations. Green bar represents average continental crust U content of 2.7 ppm. From Partin et al. (2013).

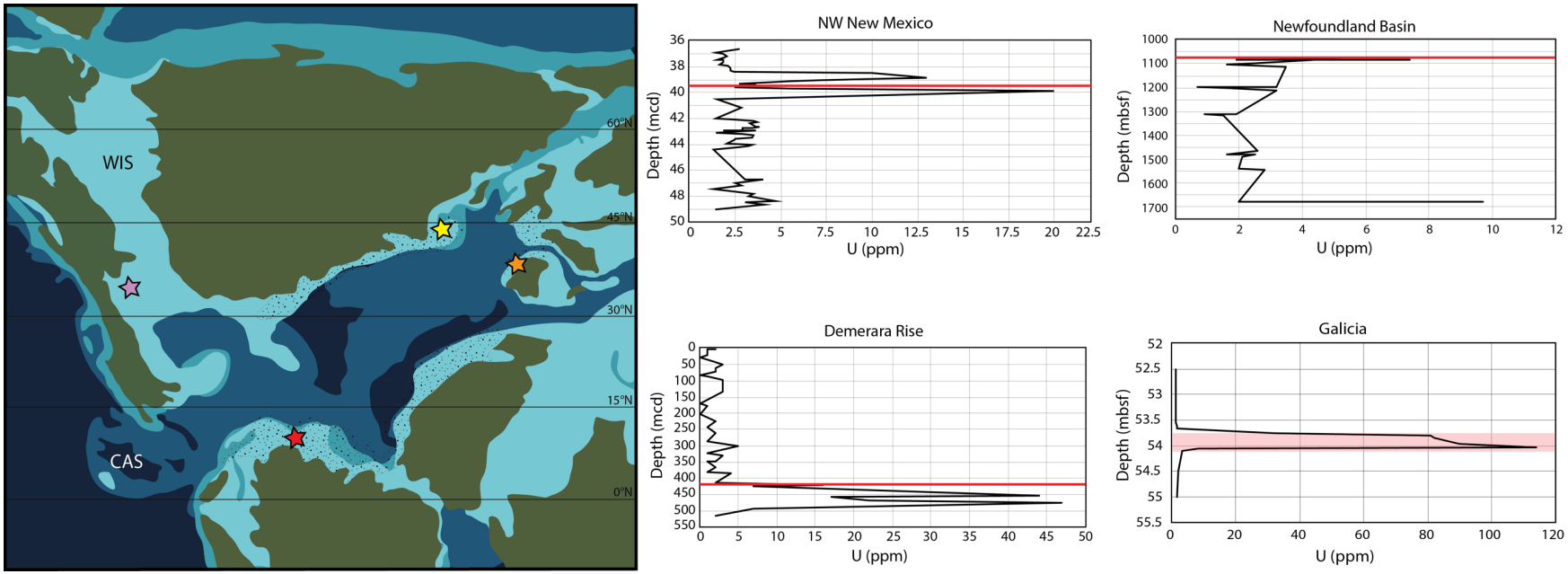

Figure 1.5 Plots of changing uranium concentration from black shales in four stratigraphic sections in the proto-North Atlantic Ocean that record OAE-2. With the onset of OAE-2, uranium concentration in the sediments increases, due to its preference to be sequestered into anoxic sediments as the OAE progresses, while the concentration of uranium within seawater decreases due to this drawdown. This trend can be seen from four localities in the proto-Atlantic Ocean (red star denotes Demerara Rise, orange is Galicia, yellow star is the Newfoundland Basin, and the purple star represents New Mexico) with data plotted from literature sources (Thurow et al., 1988; Curiale, 1994; Hetzel et al., 2006; Tucholke et al., 2006). Red line represents the approximate Cenomanian – Turonian Boundary. Each graph shows uranium concentrations with core depth, which gives an indication that uranium is indeed responding to the OAE. Map modified from Trabucho Alexandre et al. (2010).

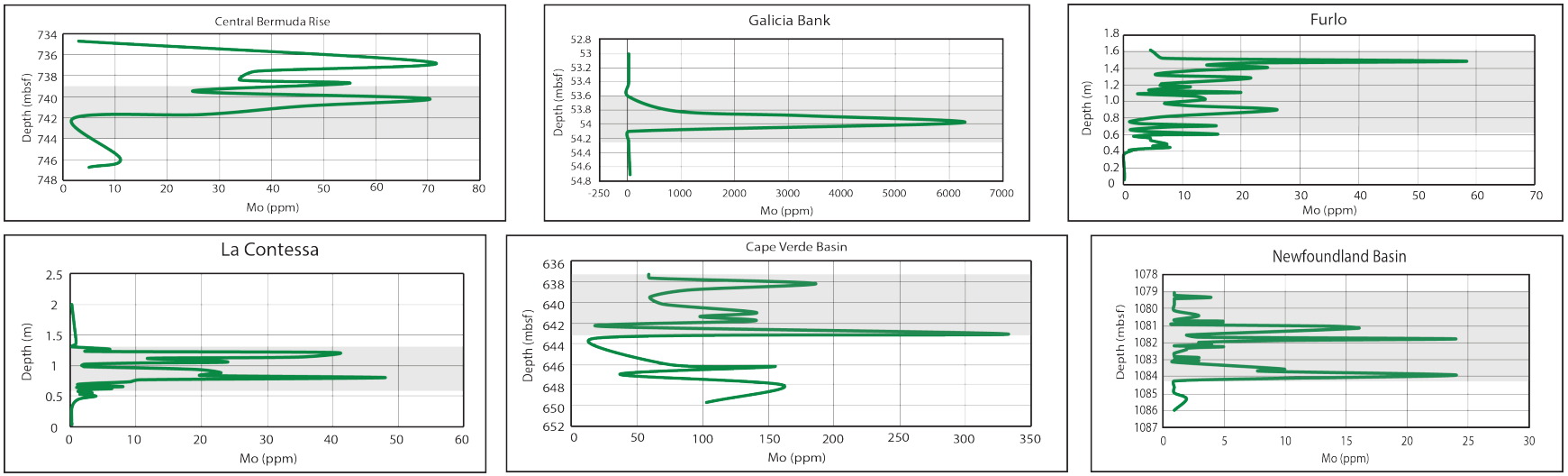

Figure 1.6 Plots depicting Mo enrichment in OAE-2 aged sediments from select locations around the PNAO (van Helmond et al., 2014). The removal of Mo from seawater, resulting in a large enrichment within the sediments, can be used as an indicator for the expansion of poorly oxygenated waters. Grey bars represent the OAE-2 interval.

1.2 Thesis Overview

Chapter 2 explains the background of the thesis, covering climate during OAE-2, the geometry and importance of both the Proto-North Atlantic Ocean and the Western Interior Seaway to the causation and preservation of OAE-2. Chapter 3 discusses the geological background of the study area. Chapter 4 discusses the processes and mechanisms by which the uranium isotope system fractionates within the modern oceans. Chapter 5 describes the analytical procedures used and Chapter 6 presents the results of those procedures. Chapter 7 discusses the results in context of OAE-2 and the implications of those results on the chemical state of the oceans and finally Chapter 8 concludes the thesis and presents possible considerations for future work.

CHAPTER 2

Framework, Background, and Research Hypotheses

2.1 The Proto-North Atlantic Ocean

OAE-2 occurred when the Atlantic Ocean was still relatively young. Since the initial breakup of Pangea (~180 Ma), the North American, European, and African continents continued to drift apart forming the Proto-North Atlantic Ocean (PNAO) (Figure 2.1). During this time the PNAO acted as a semi-restricted basin, resulting in the cold, deep, nutrient rich waters of the Pacific Ocean to be trapped within the PNAO (Trabucho Alexandre et al., 2010). Topper et al. (2011) attributes sea level changes throughout the pre- to post OAE period as a major reason as to why OAE-2 occurred. Based on the seawater curves of Miller et al. (2005) (Figure 2.2), Topper et al. (2011) concludes that prior to OAE-2 sea level was roughly 150 m lower than during OAE-2 (Figure 2.2) and was not conducive to allowing circulation of Pacific waters into the PNAO. Early research on the organic-rich shales suggested that the lack of incoming Pacific Ocean water would result in a lack of water renewal to the PNAO, reducing the oxygen content of the waters. Later it was suggested that the PNAO was cut off due to low sea-level and allowed for the anoxic conditions to more readily develop (Bralower and Thierstein, 1984). However, counter to these ideas, Trabucho Alexandre et al. (2010) suggested that circulation was less of a factor in the creation of anoxic bottom water conditions instead, they suggested the paleo-geometry of the PNAO basin was a more important factor in facilitating anoxic conditions, a claim later repeated by Topper et al. (2011). Just prior to OAE-2, the Caribbean Large Igneous Province (LIP) was erupting near the Central American Gateway (Figure 2.1). Recent studies (Snow et al., 2005; Holmden et al., 2016) have suggested that the intruding Caribbean LIP was the dominant cause of OAE-2. The authors suggest that the ensuing hydrothermal activity introduced vast amounts of bio-essential metals in the form of anoxic plumes that worked their way into the PNAO. The close connection between atmospheric and ocean circulation would have also seen an intensified wind driven ocean surface circulation resulting in more intensified storm systems (Föllmi, 2012). An overall increase of ocean surface circulation would have help fuel Ekman transport-driven upwelling processes that supplied the nutrients for the increase in primary producers. Due to the enhanced primary productivity, an increase of organic matter deposition occurred (Figure 2.3). As organic matter settles, the available oxygen is used up during microbial degradation of the organic

material and through a host of other abiotic and biotic processes, then combined with sedimentation rates and water column circulation and stratification soon leads the eventual disappearance of available oxygen. This drove the oceans to transition from being oxic to less oxic (up to 4x more anoxic; Montoya-Pino et al., 2010)). Circulation models for the PNAO before, during, and after OAE-2 all support the intensified upwelling and the ensuing increase in primary productivity. When all combined, poor circulation and low nutrients limit the production of organic matter. Prior to OAE-2 ocean turnover was relatively low due to sluggish upwelling rates and poor water exchange with the global oceans (Topper et al., 2011). During the marine transgression at the onset of OAE-2, the intermediate inflow became more prominent and exchange with the global oceans increased, eventually intensifying the upwelling mechanism (Topper et al., 2011). Deposition of organic-rich sediments along the eastern margins of the PNAO and lack of organic-rich sediments along the northern edges support the increased input from the Pacific Ocean (Topper et al., 2011). Eventually, seafloor conditions, because of the intensified cycling, transitioned back to a more oxygenated state. With the decrease of primary production and the intense bottom water re-oxygenation, organic matter preservation became less efficient and the oceans transitioned back to pre-OAE-2 like conditions.

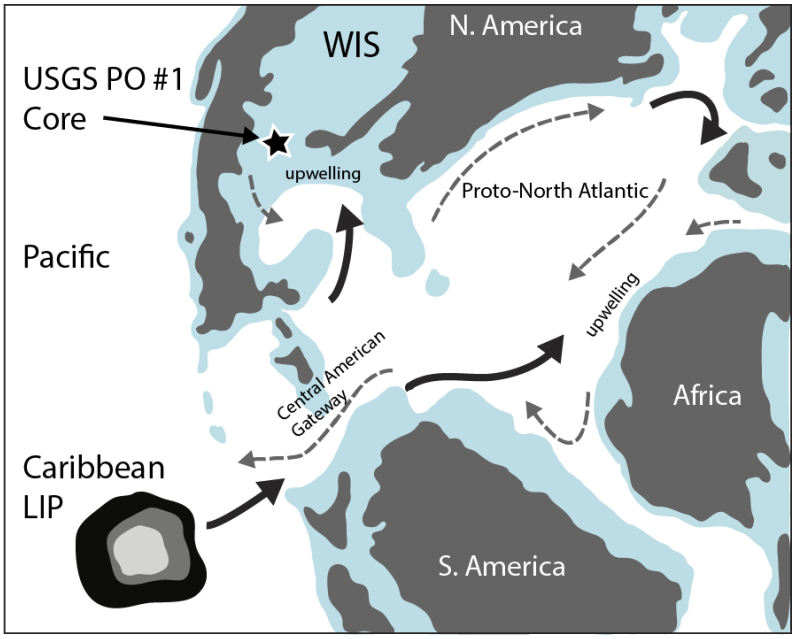

Figure 2.1 Paleogeographic map of the Proto-North Atlantic Ocean showing the location of the study area in reference to the Western Interior Seaway and Caribbean LIP. Modified from Trabucho Alexandre et al. (2010).

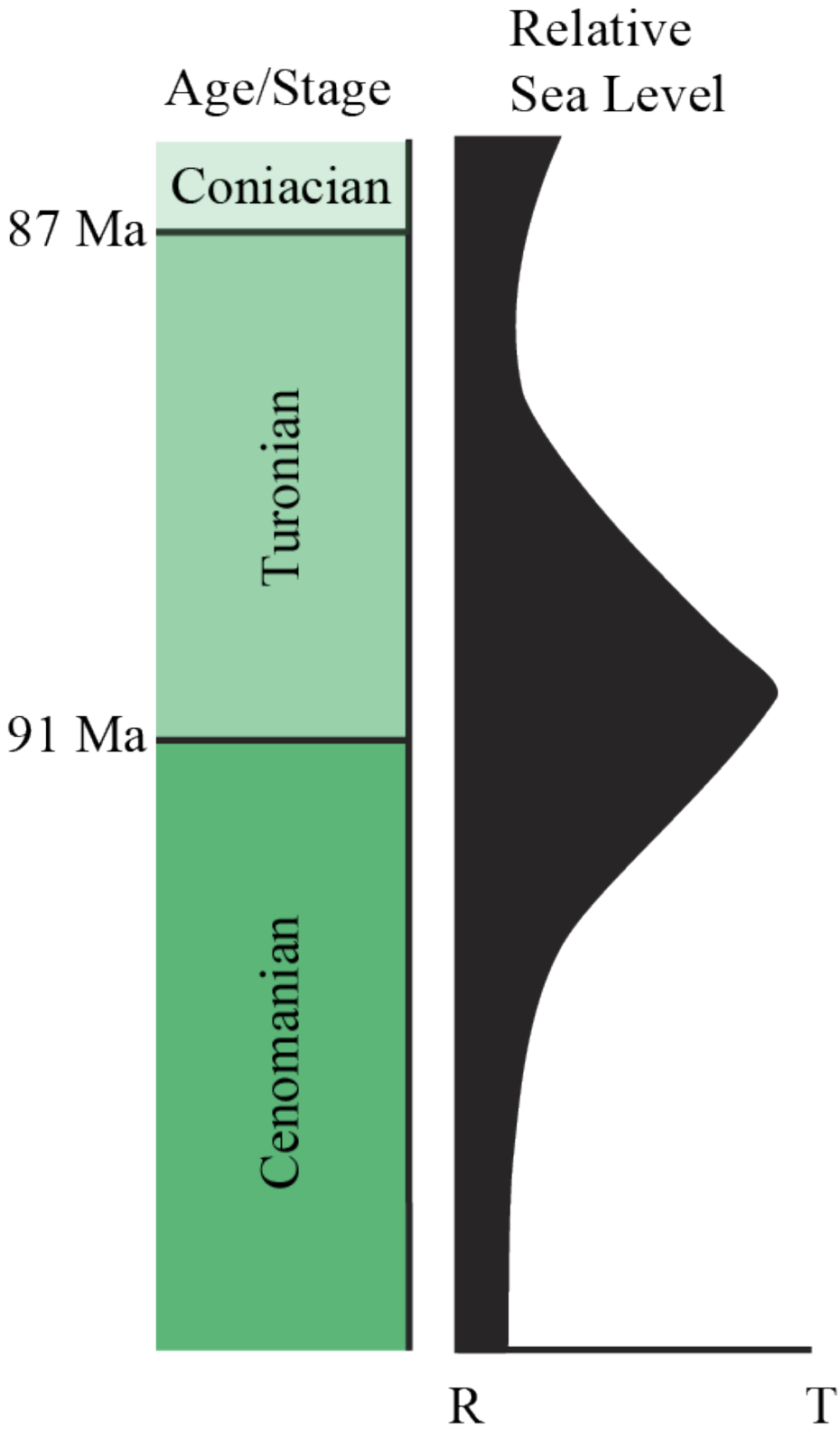

Figure 2.2 Relative seawater curve for the Cenomanian – Turonian boundary. T and R refer to transgression and regression, respectively. Modified from Miller et al. (2005).

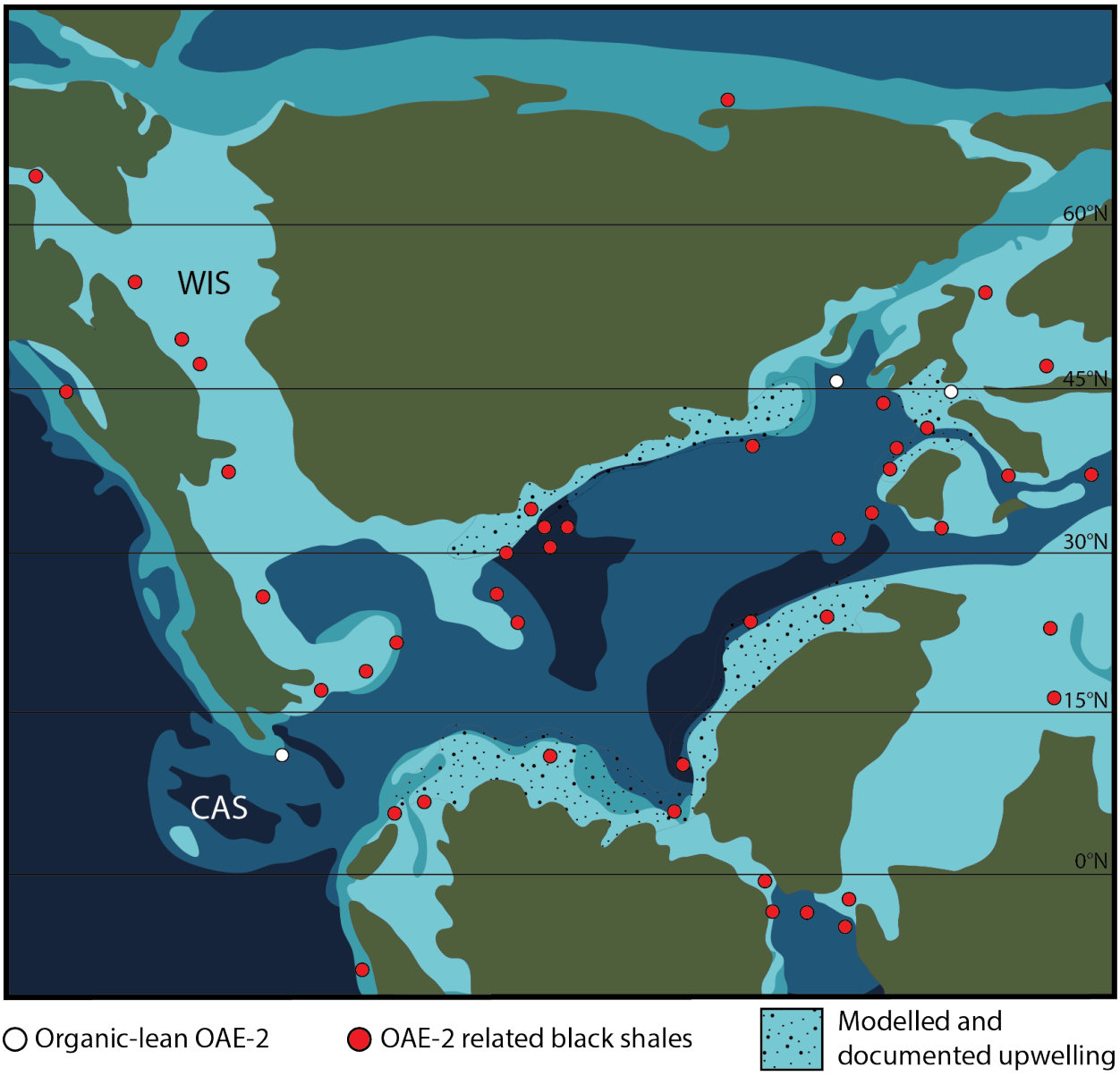

Figure 2.3 Paleogeographic map of the Proto-North Atlantic Ocean with locations of modeled and observed upwelling. CAS denotes the Central America Seaway and WIS denotes the Western Interior Seaway. From Topper et al. (2011).

2.2 The Caribbean Large Igneous Province

Large igneous province (LIP) events are geologically short periods of time in which massive amounts of magma is erupted or intruded because of early hot spot development (Snow et al. 2005). Unlike seafloor spreading or other plate derived movement, LIP events occur on a much shorter timescale and produce a much larger volume of lava, with the eruption lasting 100 to 1000 kyr. Multiple phases of submarine eruptions during the formation of the Caribbean plateau

closely coincide with the onset of major ocean anoxic events, including 1a, 1b, and 2 (Figure 2.4; Snow et al. 2005). This has led many studies (Turgeon and Creaser, 2008; Trabucho Alexandre et al., 2010; Holmden et al., 2016) to postulate that large scale hydrothermalism, at the scale of a LIP, might have been responsible for the abrupt change in ocean chemistry leading to OAE-2. But as Snow et al. (2005) pointed out, for a hydrothermal event such as the Caribbean LIP to be responsible for the changes in ocean chemistry during OAE-2, it must have occurred within the measurable uncertainty associated with the timing of the Cenomanian – Turonian boundary (93.9 Ma).

Orth et al. (1993) measured 28 samples associated with a possible extinction or migration event for elemental abundance anomalies from the WIS and the around the globe. They found significant metal enrichments (Sc, Ti, V, Cr, Mn, Co, Ni, Ir, Pt, and Au) within the 16 WIS samples, but found a significant drop in those abundances from the northern European localities. The authors attributed the source of the anomalies to hot spot development in the eastern Pacific Ocean. Sinton and Duncan (1997) later developed a model for the PNAO that considered the metals to be the result of an abrupt hydrothermal event linked to the Caribbean LIP and the metal rich, thermally buoyant plume. Snow et al. (2005) confirmed the spike in trace metal concentrations coincides with the LIP event. A negative $^{187}Os/^{188}Os$ and $^{87}Sr/^{86}Sr$ excursion corresponding to the start of OAE-2 further supports their conclusion (Figure 2.5).

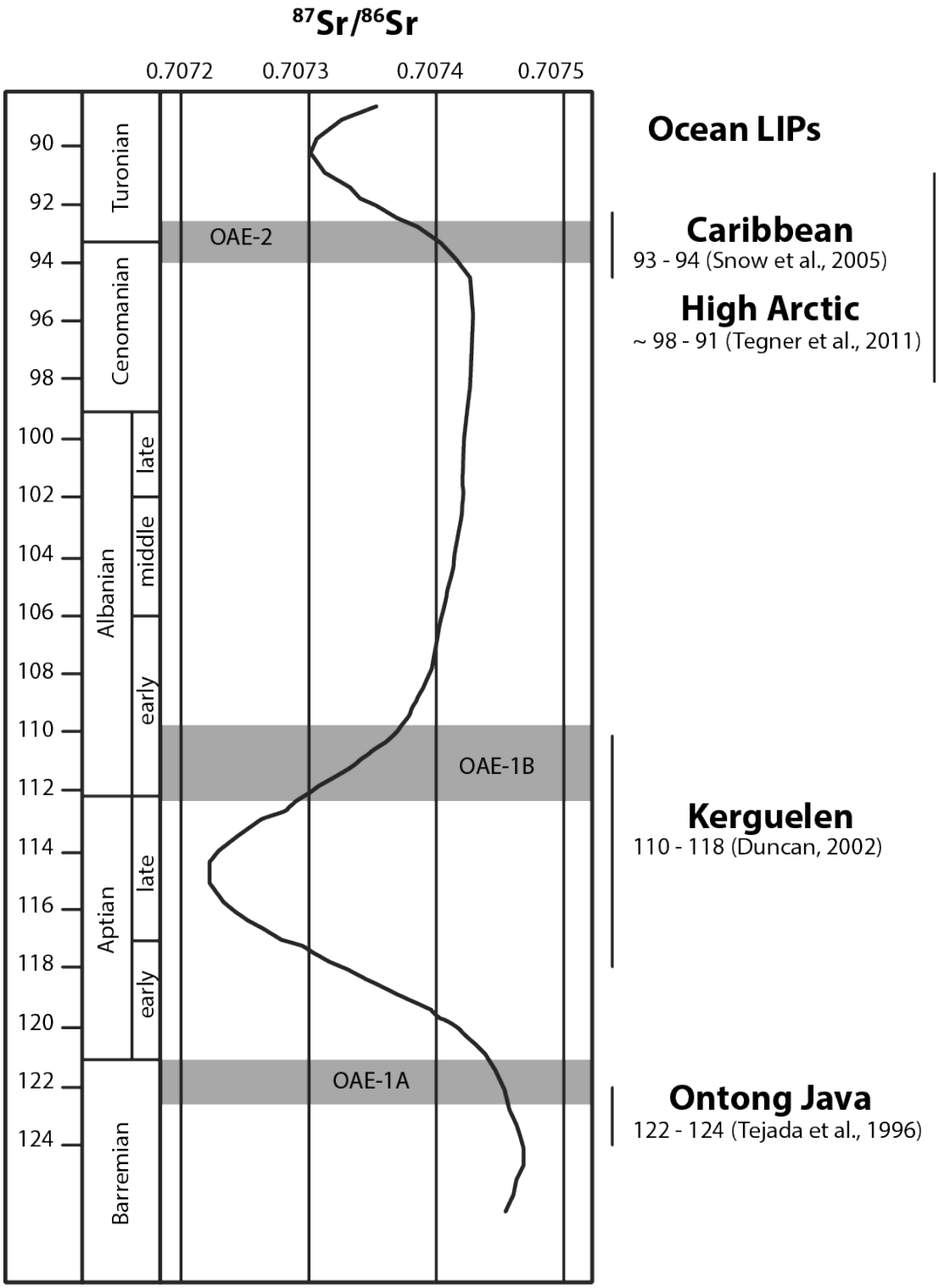

Figure 2.4 Mid-Cretaceous Sr isotope curve. Low points have been interpreted to be a result of large hydrothermal events such as the Ontong Java and Caribbean LIP supplying non-radiogenic Sr into the oceanic reservoir. Modified from Snow et al. (2005).

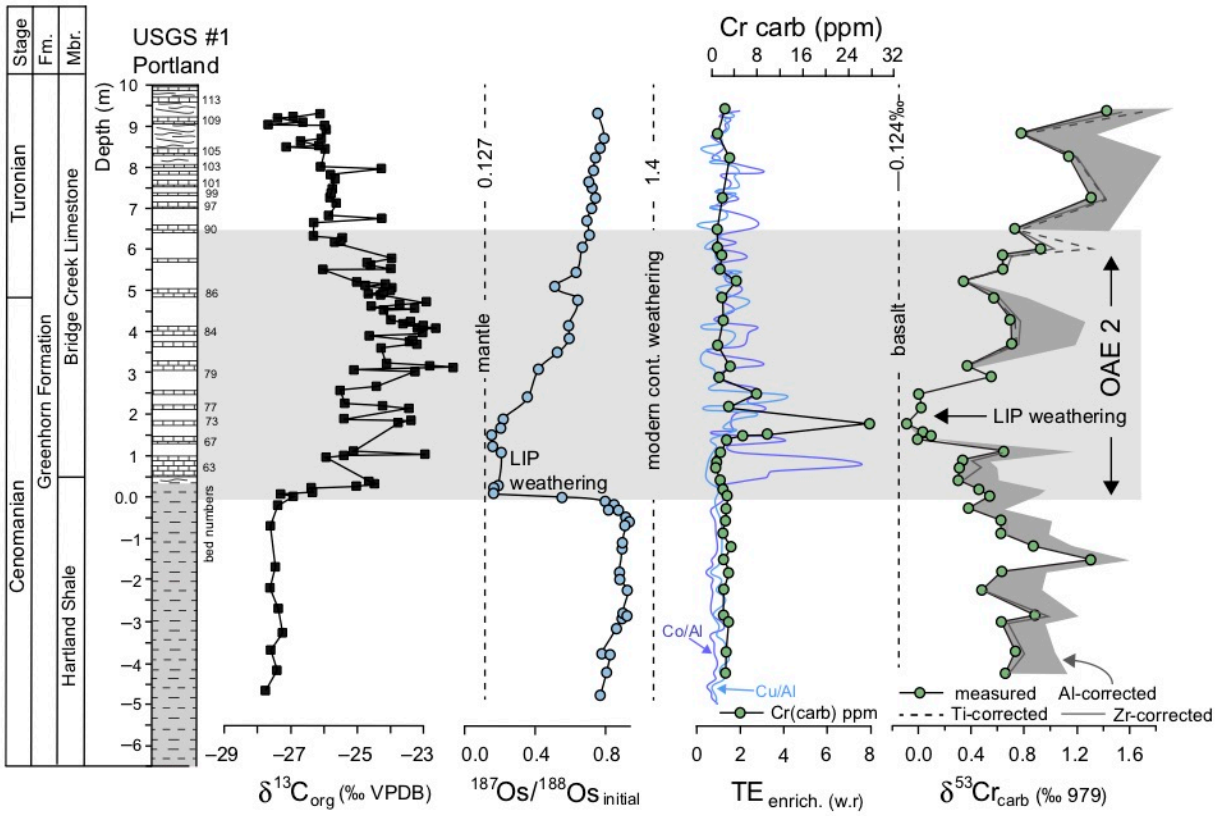

Figure 2.5 Chemostratigraphic profiles for the USGS PO #1 core from Holmden et al. (2016). $^{187}Os/^{188}Os$ profile decreases dramatically at the onset of OAE-2 and falls within the timeline of the Caribbean LIP indicating a possible connection to magmatic degassing and submarine weathering of the LIP. The carbonate $\delta^{53}Cr$ record also supports the timing of the Caribbean LIP. The record should show a positive excursion during increased anoxia but shows the opposite, suggesting the excess $\delta^{53}Cr$ comes from a hydrothermal source.

2.3 Plenus Cold Event

Although the Cretaceous was generally a warmer period relative to today (Figure 2.6), there is evidence for short-lived cooling events throughout the period. One such event occurred during the earliest stages of OAE-2 and is known as the Plenus Cold Event (PCE) from 94.7 to 94.35 Ma (Gale et al., 1996; Jenkyns et al., 2017). The initial discovery of the PCE comes from the work of Jefferies (1961, 1963) on the Plenus Marls, a series of hemi-pelagic marls from southeast France, as well as work done on pelagic chalks from southern England. Jefferies (1961, 1963) identified eight bed units within the Plenus Marls, based on unique faunal assemblages found within the marls. They determined that the type fauna, *Praeactinocamax plenus*, is not evident in Bed 3 and most concentrated in Bed 4 but ranges up to 8. Jefferies (1961, 1963)

acknowledged the likeness of *P. plenus* to assemblages found within mid-Cenomanian chalks considered to be of a "boreal type" affinity, able to adapt to cooler conditions quickly. The $\delta^{18}O$ records for this period support this claim with generally heavier values that align well with the beds above and below Bed 3 suggesting the PCE existed as two cooler periods punctuated with a warmer period (Jenkyns et al., 2017).

Evidence of the PCE within North American samples, particularly from the WIS have not been as easily identified as their counterparts within Europe. Jenkyns et al. (2017) suggest this to be due to the lack of belemnite preservation. However, rare cases of *Praeactinocamax* have been found within sediments deposited in the WIS have been referred to as "northern guest" that came south with the southern movement of a boreal water mass (Jenkyns et al., 2017). Although the identification of the PCE by the same metrics with the WIS may be difficult but evidence of a Plenus-like event has been found. Referred to as the Benthic Oxic Zone (BOZ), small boreal dinocysts have been found throughout the WIS, as far south as modern Texas. Evidence of the boreal dinocysts as far south as modern Texas suggests the southerly movement of cooler more oxygenated water masses throughout WIS at the start of OAE-2 (Figure 2.7). Additional evidence from paleo SST data from the Deep Sea Drilling Program and Integrated Ocean Drilling Program cores suggest a 4°C drop at the equator and a 5 to 11°C drop near the northern end of the PNAO (Forster et al., 2007; Sinninghe Damsté et al., 2010) during the same time. This implies that the cooler waters were also moving into the PNAO and even possibly wrapping around and into the southern end of the WIS. In either case it would be expected for the PCE to be recorded in the Portland core.

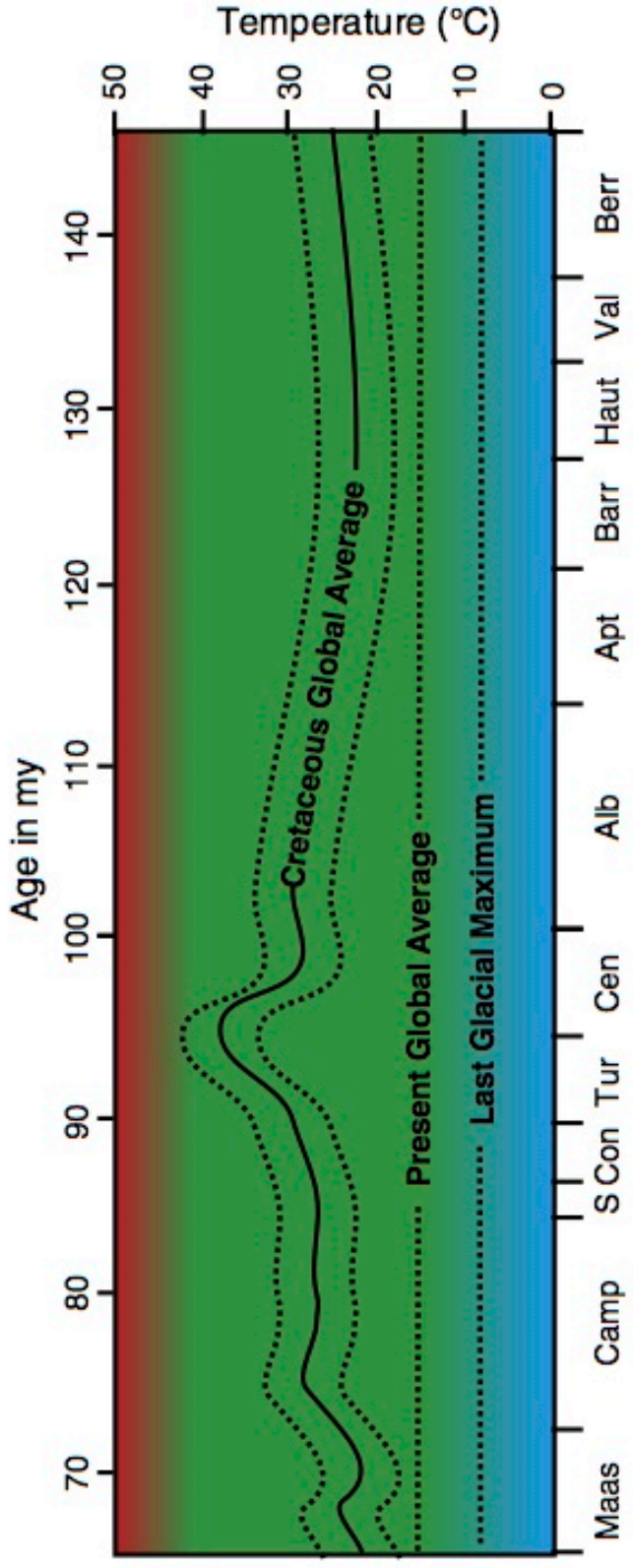

Figure 2.6 Average global temperatures during the Cretaceous Period compared to the present global average, from Hay and Floegel (2012).

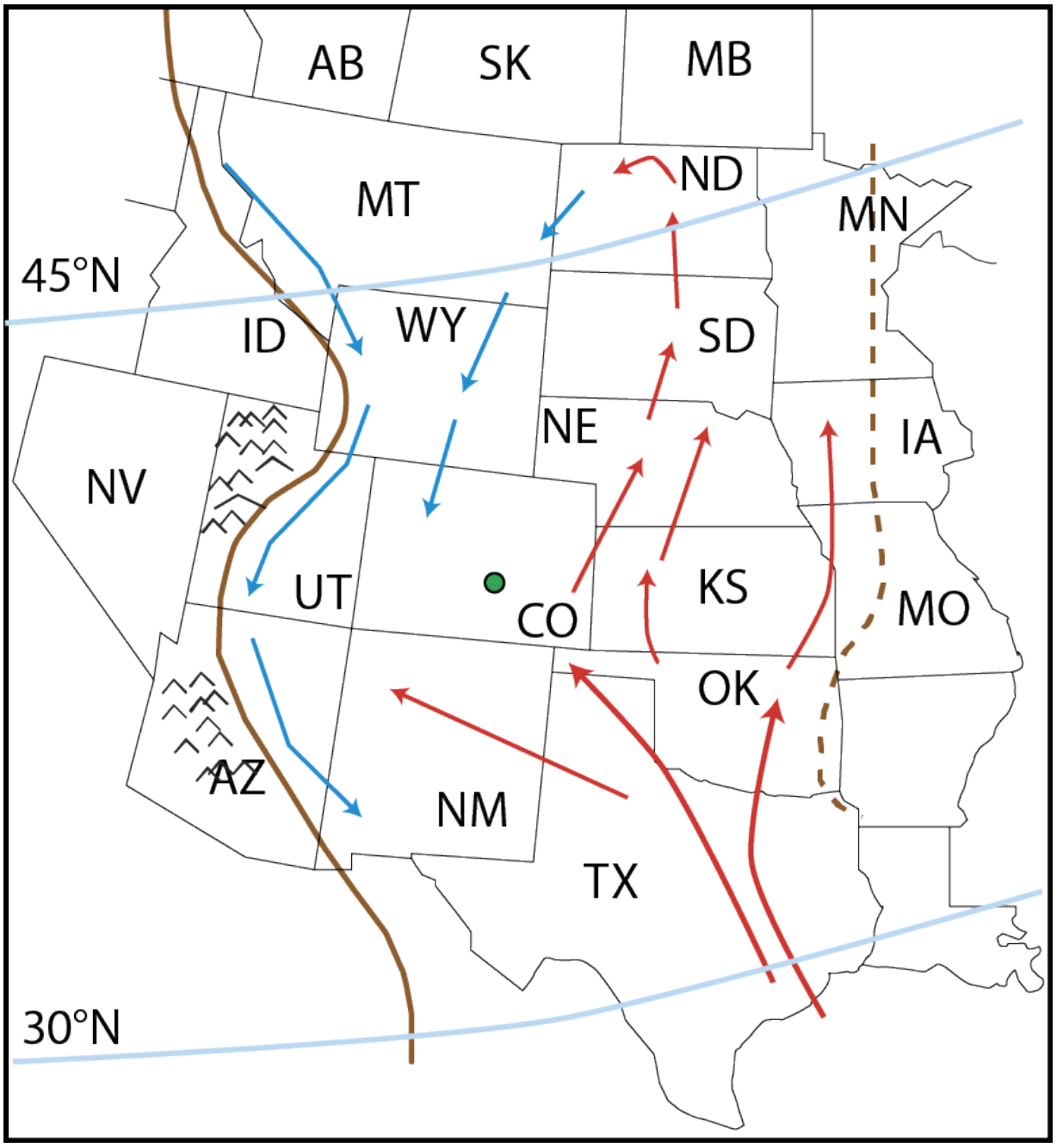

Figure 2.7 Surface circulation for the WIS during the Cenomanian-Turonian transition. The counter clockwise gyre would have pulled in the PNAO water along the eastern margins of the WIS and pulled down the cool waters from the north along the western edge of the seaway. Modified from Elderbak and Leckie (2016). Evidence of northern boreal dinocysts as far as modern Texas would be fall in line with the predicted circulation model for the WIS and it would not be unreasonable to capture the PCE in the Portland section (green circle).

2.4 Western Interior Seaway

The Western Interior Seaway (WIS), an epicontinental seaway, was at its largest during the Cenomanian-Turonian Transgression when it was approximately 1620 km across (Sageman, 1989) (Figure 2.8). Spanning from the southern edge of the United States to the northern tip of Canada, the seaway connected the northern boreal waters to the southern Tethys Sea. Tectonic subsidence from the Sevier Orogeny during the Late Jurassic and Cretaceous began forming the Western Interior Basin (WIB). Prior to the connection of the two water bodies, the WIB was characterized by several complex alluvial plains. Continued subsidence of the WIB during the Cenomanian-Turonian transgression led to widespread flooding and the eventual joining of the two water bodies. Bounded by the Sevier highlands to the west, the WIS slowly moved eastward reaching as far as modern-day Iowa and possibly Hudson Bay. The eventual erosion of the Sevier highlands is considered the dominant source of terrigenous material to the western edge of the WIS. The WIS experienced numerous episodes of transgressive – regressive sequences resulting in, at least along the western edge, thick units of siliciclastic sediments reflective of the dominant clastic input and to the east and central zones, sequences dominated by pelagic carbonates.

Unlike the PNAO, the WIS did not experience widespread anoxia. Lower levels of organic matter burial and increased diversification of both planktonic and benthic foraminifera suggests locally oxygenated environments throughout the WIS during OAE-2. Southward movement of well-oxygenated boreal waters likely spurred the abrupt rise of planktonic and benthic foraminifera diversity prior to OAE-2. However, the northward movement of poorly oxygenated southern waters from the Pacific, coincident with the positive $\delta^{13}C$ excursion at the onset of OAE-2, quickly took over. The abrupt rise of $\delta^{13}C$ values at the beginning of OAE-2 comes from increased burial of organic matter within the PNAO and is captured fully by the contemporaneous deposition of the Bridge Creek Limestone Member of the Greenhorn Formation within the WIS. The Bridge Creek Limestone is characterized by highly bioturbated limestone beds alternating with laminated marlstone beds, and frequent intervals of calcareous shales and bentonite layers in between.

Work done on the Rock Creek Anticline and the Pueblo section by Eicher and Worstell (1970) and Leckie et al. (1998) identified three distinct foraminiferal biofacies zones: (zone 1) supports the incursion of the Northern Boreal waters and the expansion of foraminifera diversity. (zone 2) a planktonic zone defined by decreased planktonic diversity and (zone 3) an increase biserial forms associated with the base of the uppermost *Neocardioceras juddii* ammonoid zone

and contemporaneous with a negative $\delta^{18}O$ excursion. The negative $\delta^{18}O$ excursion within the seaway suggests a higher riverine input and correlates to a decrease in planktonic diversity. Improved planktonic diversity correlates with a positive $\delta^{18}O$ excursion and the associated sea-level rise with incoming waters of the Tethyan waters into the PNAO and then into the WIS at the onset of OAE-2 (Keller and Pardo, 2004).

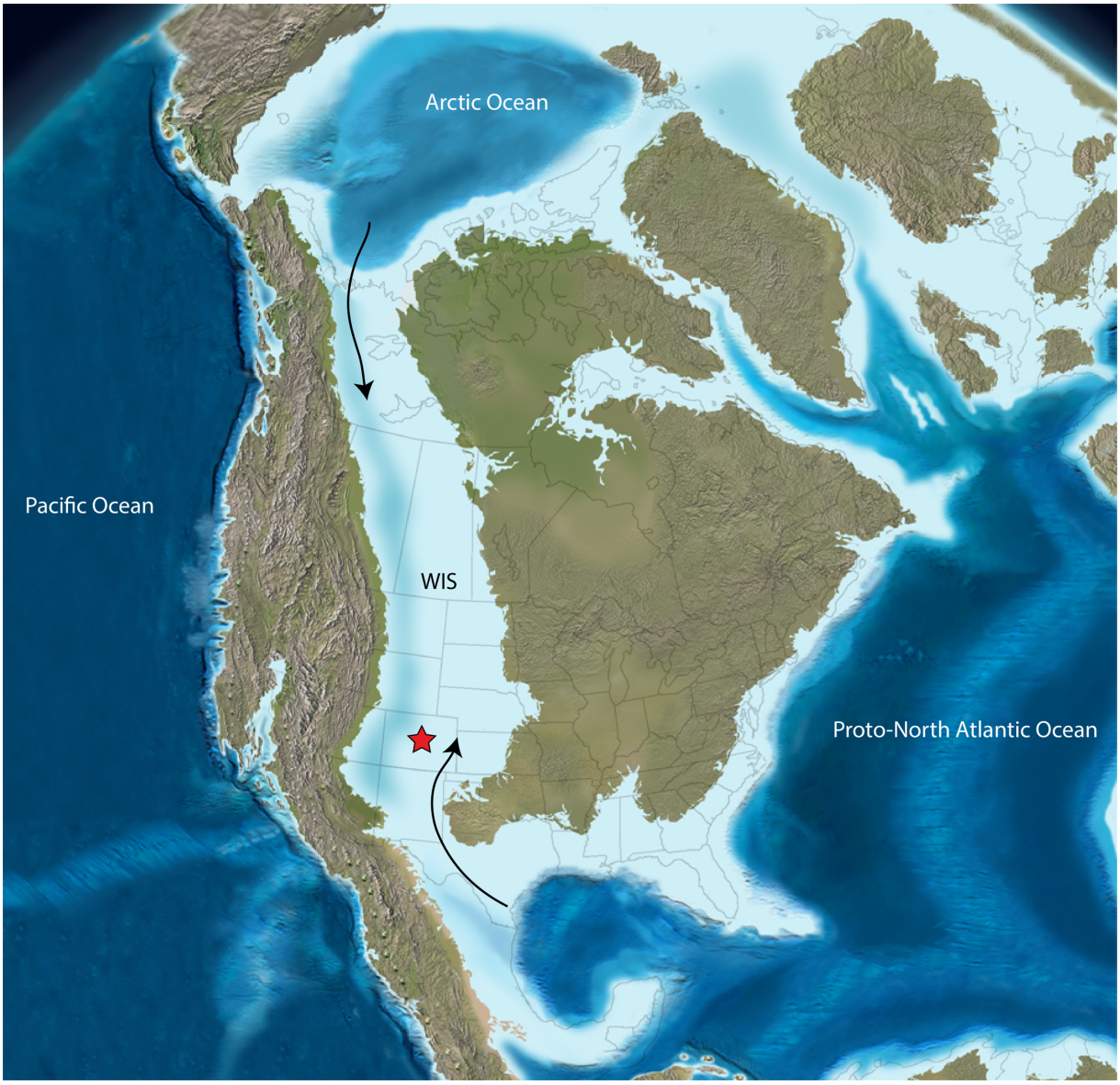

Figure 2.8 Paleogeographic map of the WIS during the mid-Cretaceous. Particular attention should be given to the connection of the WIS to both the southern PNAO waters and the northern boreal waters. This connection allowed the southern movement of boreal waters to invade the WIS. Red star denotes the location of the studied core, paleogeographic reconstructions place study area between ~35° to 40°N which are consistent with published estimates of 30° to 45°N (Kauffman, 1977; Trabucho Alexandre et al., 2010). Modified from Blakey (2011).

2.5 Research aim, hypothesis, and predictions

Considering the driving factors behind the cause of OAE-2, the geochemical state of the oceans, and the physical geometry of PNAO and WIS, this research aims to determine if the micritic limestone of the Bridge Creek Limestone and the calcareous shale of the Hartland Shale members, deposited in the Western Interior Seaway, record a similar stratigraphic variation in sedimentary $\delta^{238}U$ changes as previously published in Montoya-Pino et al. (2010) in black shales (~0.15‰) or Clarkson et al. (2018) in limestone (~0.47‰) in the Proto-North Atlantic Ocean. During periods of intense carbon production and sequestration, marine redox conditions can shift, resulting in the development and expansion of entirely new zones of marine anoxia. As this occurs, redox sensitive elements, such as uranium, are reduced and preferentially removed at a higher rate than before by anoxic marine sediment. Therefore, the hypotheses of this study are:

(1) If the size of the anoxic sink, relative to today, increased during OAE-2, then the $\delta^{238}U$ profile for the USGS Portland #1 Core will display a similar negative isotopic excursion to published results (either Montoya-Pino et al. (2010) or Clarkson et al. 2018) because the $\delta^{238}U$ signature of seawater is directly related to the size of the anoxic sink. The reduction of uranium into anoxic sediments is the greatest control on the seawater $\delta^{238}U$ value. Therefore, even a small increase in the anoxic sink will affect the $\delta^{238}U$ signature of seawater.
(2) If the $\delta^{238}U$ of seawater is truly susceptible to global scale perturbations, then the $\delta^{238}U$ record of the studied core should record evidence of the Plenus Cooling Event during the early stages of OAE-2.

If the $\delta^{238}U$ profile for the Portland core does display a similar trend to either published OAE-2 sections, then the viability of the uranium isotope system as a reliable indicator of marine anoxia appears to be true. However, if this is not the case then either the effects of carbonate diagenesis on the $\delta^{238}U$ record are poorly understood or our constraints on how the marine uranium isotope system operated in the past is not well defined. If either scenario is true or a combination of the two, then any attempt to quantify the extent of anoxia during OAE-2 or at any other time will be fundamentally flawed.

CHAPTER 3

Geological Background of the Study Area

Building off of the description of the WIS in Chapter 2, this section further describes the study location and lithology of the study core. Samples for this study are from the USGS Portland #1 core, drilled near Pueblo, Colorado, USA (38.2544°N, 104.6091°W) (Figure 3.1). The Portland core is divided into two stratigraphic units representing the two uppermost units of the Greenhorn Formation (Figure 3.2). The lower Hartland Shale Member sits upon the Lincoln Limestone and is capped by the Bridge Creek Limestone Member. Each member was deposited within the Cretaceous WIS and each member brackets OAE-2, with most of the event recorded in the upper Bridge Creek Limestone. The three units of the Greenhorn Formation represent a transgressive event known as the Greenhorn Cyclothem (Kauffman, 1977). Deposition of the Hartland shale occurred just prior to eustatic high-stand with maximum water depth around 200 m (Sageman, 1989). Whereas, deposition of the younger Bridge Creek Limestone marked the peak of the Greenhorn transgression with water depths varying somewhere between 600 and 900 m for the seaway (Eicher, 1967).

3.1 Hartland Shale Member

The lowest member, the Hartland Shale Member, is primarily characterized by large, meter scale beds containing thinly bedded calcarenite layers intermittently occurring within 30 to 100 cm thick gray shale layers (Keller and Pardo, 2004). The member itself ranges in thickness from south central Utah to northern Kansas, varying between ~7m to 35m thick (Figure 3.3). The Hartland shale was likely deposited close to the shoreline, where on occasion, it would receive an influx of freshwater and clastic sediments during the wet and humid climate conditions associated with the late Cretaceous.

3.2 Bridge Creek Limestone Member

The overlying Bridge Creek Limestone Member marks the transition from the Cenomanian into the Turonian. The bottom of the Bridge Creek consists of a 40-50 cm thick bioturbated micritic limestone (Bed 63). This bed has been previously interpreted as the type facies for the main sea-level transgression at the end of the Cenomanian (Keller and Pardo, 2004). Working up-section, the Bridge Creek transitions to thinner, 10-20 cm intermittently bedded thick bioturbated limestones, intercalated with thick, dark organic-rich shales, ranging between 10 to 60 cm in

thickness (Keller and Pardo, 2004). The alternating limestone beds align well with the ~ 41 ka obliquity cycle (Sageman et al., 2006).

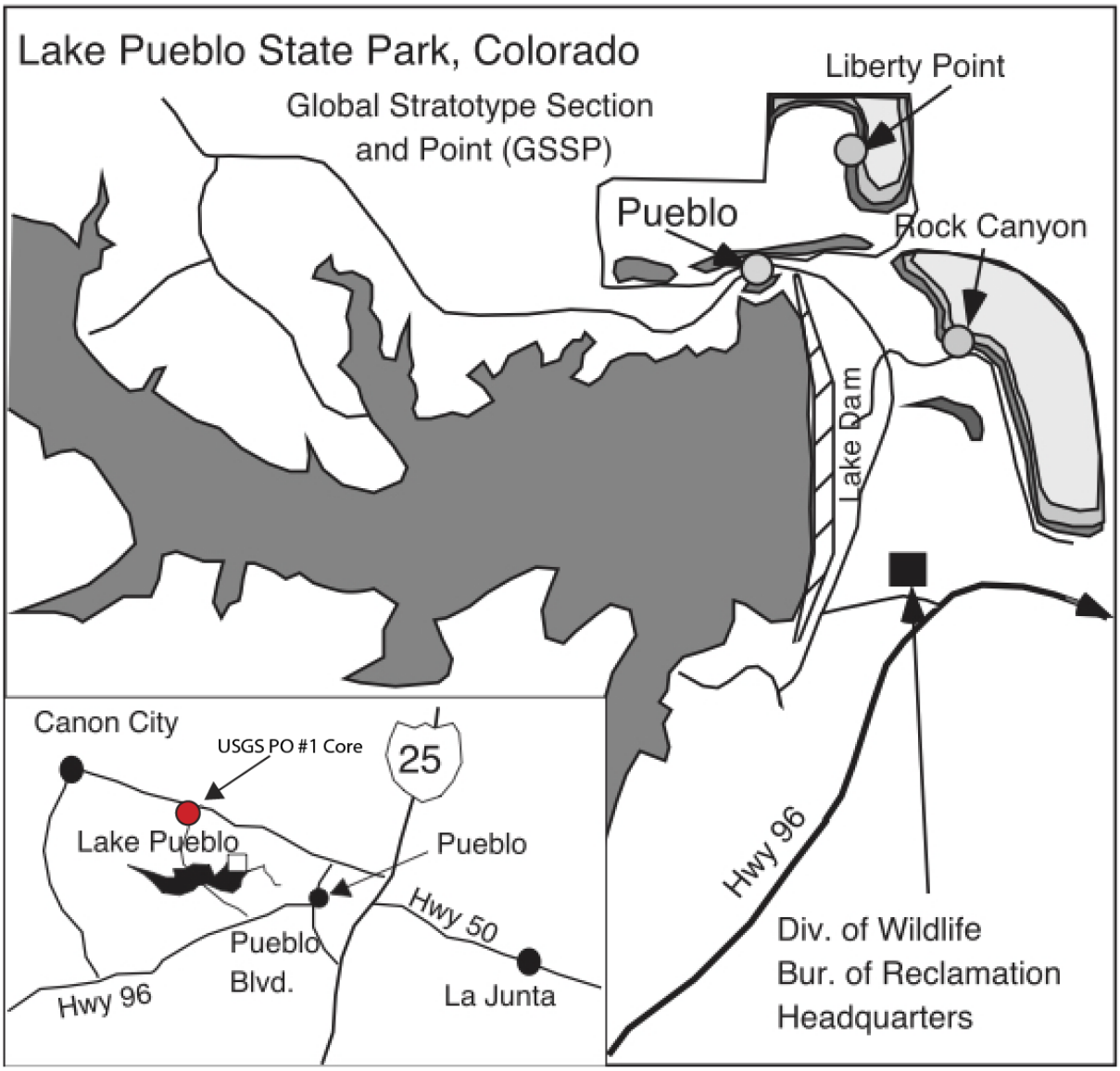

Figure 3.1 Location map of the USGS PO #1 Core. Located near Pueblo Colorado, USA. Modified from Keller and Pardo (2004).

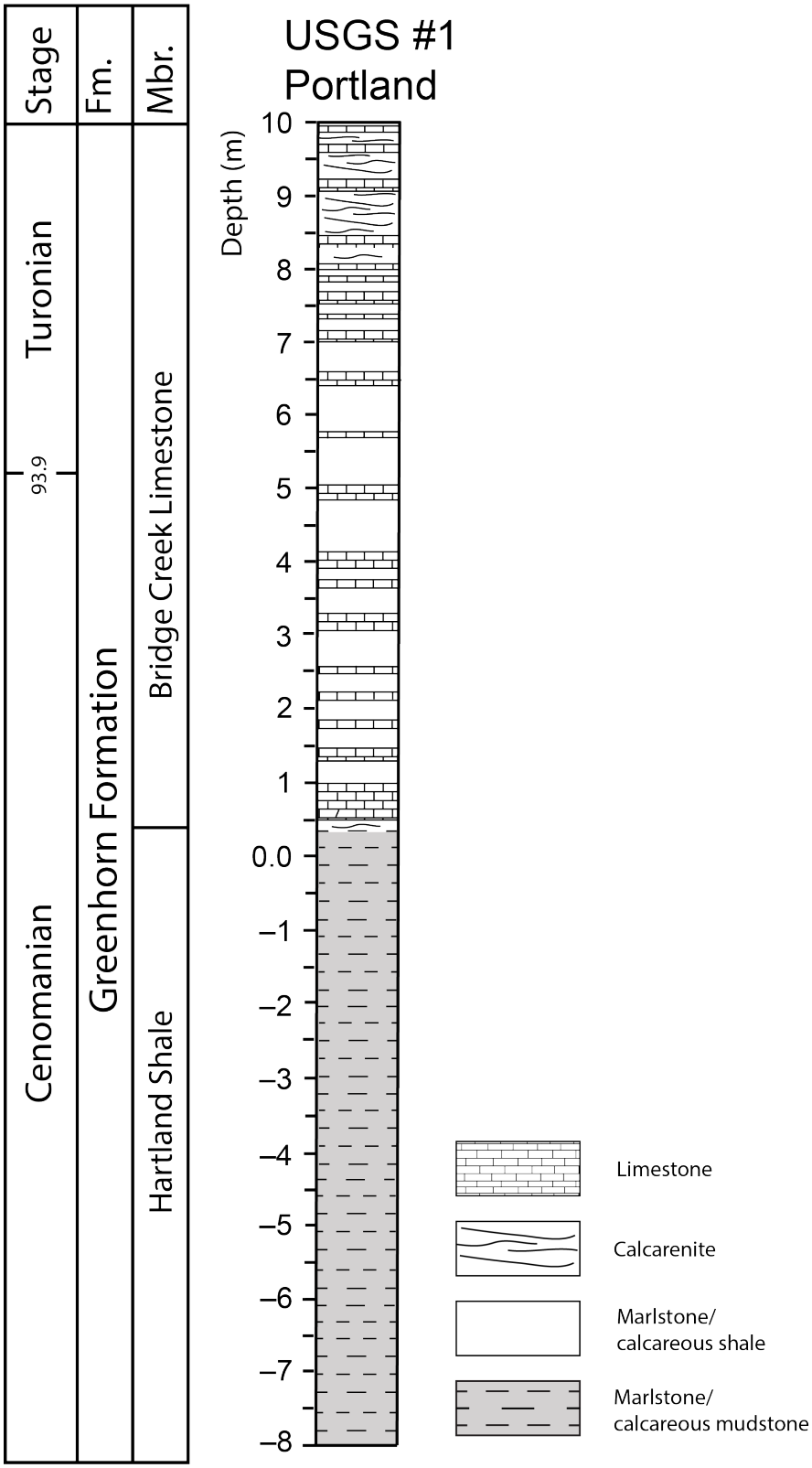

Figure 3.2 Stratigraphic column of the USGS PO #1 Core. Modified from Holmden et al. (2016).

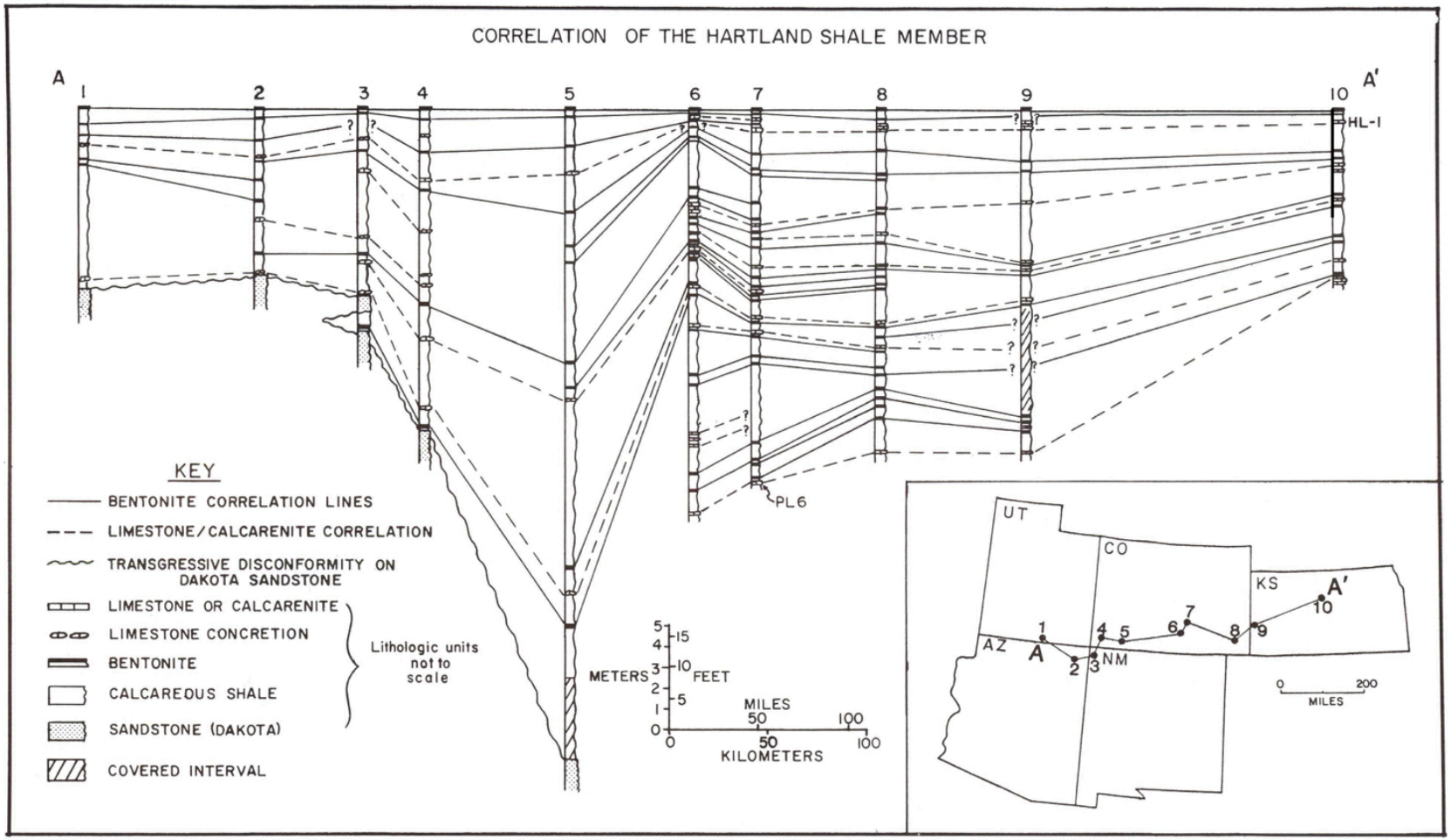

Figure 3.3 Stratigraphic correlation of Hartland Shale Member across a transect of the WIB (inset map). From Sageman (1985).

CHAPTER 4

Uranium Cycling in the Modern Ocean

Establishing a strong framework for uranium cycling in the modern ocean is crucial for the accuracy of the uranium isotope paleo-proxy and makes it possible to address fundamental questions about the co-evolution of Earth processes and life during Earth history. Studies in the last decade have contributed to better constraints on various aspects of the uranium isotope system (e.g. Stirling et al., 2007; Weyer et al., 2008; Brennecka et al., 2010, 2011; Holmden et al., 2015). Within this chapter, a breakdown of both the main sources and sinks for uranium is discussed, as well as the isotope systematics of the modern marine uranium cycle.

4.1 Sources and Sinks of the modern uranium budget

Uranium exists as one of two distinct geochemical states, either as the oxidized and highly soluble U^{6+} or as the reduced and immobile U^{4+} state. Unlike some redox proxies (Cr, Fe, etc.), hydrothermally sourced fluids are not a significant source of uranium (e.g. underwater vents and LIPs; German and von Damm, 2003). Under oxidizing conditions, immobile U^{4+} in continental rocks is released through chemical weathering processes and transported to the global oceans as the mobile U^{6+} phase. Under these oxic conditions, uranium exists as the stable, uranyl carbonate ion ($UO_2(CO_3)_3^{-4}$) within the oceans at a constant concentration of ~ 3 ppb (Ku et al., 1977). Based on the distribution of mass, more than 99% of the uranium within the modern oceans exists as the ^{238}U isotope and less than 1% as the ^{235}U isotope (Weyer et al., 2008). The hallmark of a reliable redox proxy is its ability to record any perturbations to a steady state system (where inputs are equal to the outputs). Based on U/Ca ratios from corals since the Pliocene, Dunk et al. (2002) assumed that the global reservoir of U appears to have been relatively stable over the last 4 Ma. This has led many to conclude that the marine uranium cycle is stable and at steady state (Barnes and Cochran, 1990; Morford and Emerson, 1999; Dunk et al., 2002; Henderson and Anderson, 2003). For the proxy to be robust and useful, a steady state system is required, but a detailed breakdown of the respective inputs and outputs is also needed. Based on work by Dunk et al., (2002) there are three pathways by which uranium can enter the ocean; aeolian dust (~2%), groundwater discharge (~18%), and river runoff (~80%), with river runoff representing the largest input (Figure 4.1). The largest sink of uranium from the oceans is the burial of U^{4+} within anoxic and suboxic marine sediments. The remaining uranium within the system is removed through

either complexation with carbonate minerals, submarine weathering, or incorporation into siliceous oozes. Under reducing marine conditions, soluble U^{6+} is reduced to the immobile U^{4+} and sequestered primarily into organic-rich shales (Anderson et al., 1989). The concentration of uranium within seawater is largely controlled by the extent of these reducing conditions. Today, the reducing sink (suboxic and anoxic sediments) represents between 55% and 80% of the total drawdown of uranium (Dunk et al., 2002). Due to the very small area of the seafloor that is anoxic (~ 0.3% of the seafloor), the majority of the drawdown by suboxic sediments (O_2 penetration depth <1 cm; Morford and Emerson, 1999; Dunk et al., 2002). However, due to the rate at which anoxic sediments sequester uranium (14x faster) the size of the anoxic sink can have a great effect on the uranium system. A smaller proportion of U is incorporated into biogenic carbonate (~28%) and a lesser amount into siliceous oozes (~4%). Adsorption onto iron oxyhydroxides during submarine weathering of basalts accounts for the remaining 12% (Dunk et al., 2002).

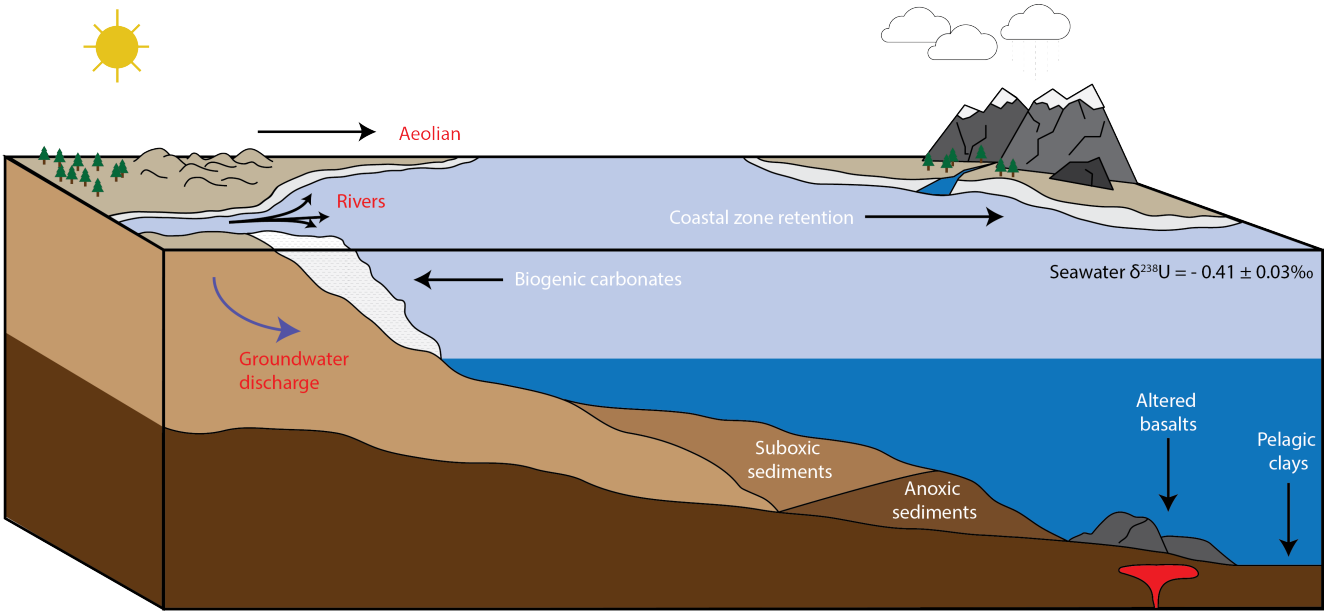

Figure 4.1 Source-sink block diagram for the modern uranium system. Red texts denotes input fluxes: Aeolian (1.8 ± 1.1 Mmol/year), groundwater (9.3 ± 8.7 Mmol/year), and riverine (42.0 ± 14.5 Mmol/year) for a total input of 53 ± 15 Mmol/year (Dunk et al., 2002). White text denotes major output fluxes: biogenic carbonates (13.3 ± 5.3 Mmol/year), suboxic sediments (15.3 ± 10.6‰), anoxic sediments (11.6 ± 6.0 Mmol/year), weathering of altered basalts (5.7 ± 3.3 Mmol/year), pelagic clays (0.4 ± 0.2 Mmol/year), and coastal zone retention (11.2 ± 5.6 Mmol/year).

4.2 Removal of uranium into biogenic carbonates

The magnitude of fractionation and the exact mechanisms that controls the reduction of U from solution and into the sediment is still somewhat unknown. This affects our ability to reliably use the isotopic signatures of these types of sediments as proxies for the geologic past. Fortunately, recent research has been focusing on the $\delta^{238}U$ record of biogenic carbonates as an alternative archive for seawater $\delta^{238}U$ values. According to work in the Bahamas by Romaniello et al. (2013), modern marine carbonates are likely recording the U isotopic signature of seawater. However, as Romaniello et al. (2013) state, carbonate-hosted proxies can face a number of complicating factors. They show that some carbonate precipitates were recording coeval seawater $\delta^{238}U$ values, while shallow sediments were not recording seawater $\delta^{238}U$ values, but rather heavier, more positive $\delta^{238}U$ values (**Figure 4.2**).

Romaniello et al. (2013) suggest that diagenesis may be responsible for the positive shift in the sediment $\delta^{238}U$ values. However, this is counter to the current understanding of the uranium-carbonate complexation mechanism. Uranium predominantly occurs as the uranyl carbonate ion in seawater and is readily incorporated into carbonate minerals. When binding with the aragonite crystal structure the uranyl carbonate is able to maintain its coordination and is likely incorporated directly (Reeder et al., 2000). Because there is no coordination or redox change required during the incorporation into aragonite, no fractionation of uranium is expected. However, when uranium is incorporated into the calcite structure, there is a coordination change in order to fit, implying some degree of fraction occurs (Reeder et al., 2000). However, like aragonite, no isotopic fractionation is observed during the incorporation of U into calcite.

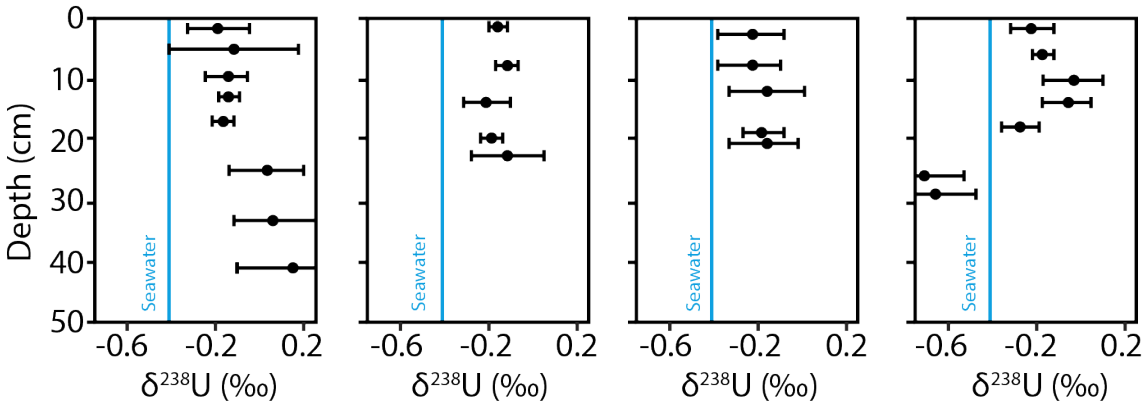

Figure 4.2 Schematic representation of $\delta^{238}U$ for modern Bahamian carbonates from Romaniello et al. (2013).

4.3 The effect of diagenetic alteration on carbonate hosted U

As is common within carbonate successions, the physical and chemical effects of diagenesis can be challenging to decipher. The effects of diagenesis on uranium isotopic composition of carbonates are not fully understood. Recent work measured modern day Bahamian carbonates and found no inherent fractionation of uranium during the complexation to carbonates (Romaniello et al., 2013). However, in the same study, they found that at shallow burial depths (1 to 3 cm) the $\delta^{238}U$ value migrates away from that of seawater, by up to + 0.4‰, indicating early stage diagenetic alteration. Quantifying the effects of diagenesis on U isotopes then becomes paramount to the success of the proxy because the carbonate $\delta^{238}U$ record offers the best chance to measure the $\delta^{238}U$ of paleo seawater. However, if we are unable to account for the effects of syndepositional diagenesis or post depositional alteration, then the carbonate $\delta^{238}U$ record is of little value.

Hood et al. (2016) argues that the effects of diagenesis cannot be accounted for unless detailed petrographic work with careful sample selection is done. They analyzed a number of Neoproterozoic carbonate reef samples from the Balcanoona Reefs that have undergone recrystallization. Values of $\delta^{238}U$ was measured for unaltered marine cements and found little variation between samples, though $\delta^{238}U$ variability was measured between different carbonate components, even in the same hand sample (Hood et al., 2016). Although sample to sample variation was minimal, compared to modern seawater $\delta^{238}U$, the unaltered cements were found to be significantly heavier (-0.23 ± 0.16‰). $\delta^{238}U$ and trace element concentrations (Fe, Th, and Zr) measurements were also done on deeper water carbonates. Both a heavily altered carbonate cement and a "pristine" cement was measured. The $\delta^{238}U$ values were found to be similar between the two samples, but element concentrations were found to be much heavier for the altered cement. They propose the heavier $\delta^{238}U$ values could be due to reducing pore fluid, as suggested by Romaniello et al. (2013) but discount the idea due to a lack of sulfide minerals within the carbonate reef (Hood et al., 2016). This considered, Hood et al. (2016) suggests the effect of diagenesis needs to be addressed on a sample per sample basis for any carbonate based redox proxy.

Lau et al. (2017) addressed possible issues facing the use of the carbonate hosted $\delta^{238}U$ seawater record for a suite of limestone samples from the Neoproterozoic Tashir Formation in Mongolia. They determined the effects of diagenesis to be statistically insignificant through a

simple model for seawater-derived diagenetic fluids modelled after the work of Banner and Hanson (1990). The model predicts the order in which elemental concentrations and isotopic compositions reset. They determined $\delta^{18}O$ values are reset initially, followed by Sr and U concentrations and finally, $\delta^{238}U$ and $\delta^{13}C$ values. Lau et al. (2017) found evidence for resetting in the $\delta^{18}O$ record of their samples. However, the $^{87}Sr/^{86}Sr$ ratios for the samples where well within the range of typical seawater for that time. They state that lithological changes can be a factor in how readily sediment can alter due to the varying pore size and resulting penetration depth of the overlying seawater. However, within their section they found little variation in the [U] and $\delta^{238}U$ profile, despite multiple facies changes throughout. In addition to the original sampling location, sections ~75 km away were measured for $\delta^{238}U$ values. They recorded a similar shift in the mean $\delta^{238}U$ values which Lau et al. (2017) interpreted as a feature of a primary signal.

Based on the results from Hood et al. (2016) and Lau et al. (2017), the effects of diagenesis appear to be minimal or non-existent in samples with no recrystallization. Hood et al. (2016) does imply that different $\delta^{238}U$ values can be found between carbonate components due to the differing diagenetic histories. In the three examples above, each studied a fully carbonate succession. The samples of this study are dominantly a mix of non-recrystallized micritic limestone with a siliceous component. The effects of diagenesis for the samples of the Portland core are likely minimal and are postulated here to have not affected our samples (see chapter 7 for further discussion).

CHAPTER 5

Analytical methods

5.1 Sample preparation and digestion

A total of 29 samples were processed through an agate ball mill at the University of Saskatchewan to achieve a consistent size prior to digestion. Samples were chosen based on their position relative to the OAE-2 interval and $\delta^{13}C$ curve. Each sample was loaded into an agate bowl, which was then run through three to five, three minute, cycles. Samples were then cleaned out and the agate bowls were cleaned with a mixture of Alconox®, water and then dried. After drying, the agate bowls were cleaned with two rinses of 90% ethanol and loaded with the next sample.

The chromatography procedures used were developed in the Saskatchewan Isotope Lab with the addition of adding oxalic acid (C_2H_2O) to elute Th. Prior to elution of the samples themselves, three seawater samples; a 20 ml loading volume control, a 40 ml loading volume, and a 10 ml loading volume with oxalic acid were spiked with ^{233}U-^{236}U and ^{230}Th spikes to determine the proper elution scheme for the samples. The 10 ml control was processed using a 20 ml 5N HNO_3 rinse followed by a 10 ml rinse of 5N HCL to elute Th. This was then followed by a 10 ml rinse with 0.5N HNO_3 to elute U (Table 5.1 and Figure 5.1). The second column was loaded with 40 ml of sample and processed exactly the same way as the control (Table 5.2 and Figure 5.1). Finally, the third column was loaded with 10 ml sample and rinsed with 20 ml of 5N HNO_3. Following the initial rinse, the column was rinsed with a mixture of 5N HCL and 1N oxalic acid to elute Th. This was followed by a 10 ml rinse with 0.5N HNO_3 to remove U (Table 5.3 and Figure 5.1). Based on the results of the three experiments, we determined that loading volume did not affect the Th or U elution, and that the addition of oxalic acid to the second rinse did remove Th earlier, but not enough so to warrant further use. As a result, samples were processed using a 20 ml 5N HNO_3 rinse, followed by a 10 ml rinse of 5N HCL and then a final rinse of 10 ml of 0.5N HNO_3.

Table 5.1 Elution behaviour for isotope chromatography experiment 1: control.

Load	Load (ml)		Th	U
Load sample - HNO3 5N	10	0-10	0.0000	0.0000
Rinse - HNO3 5N	20	11-20	0.0000	0.0000
HCL 5N	1	20-21	0.0320	0.0010
HCL 5N	2	21-22	0.0030	0.0020
HCL 5N	3	22-23	0.0380	0.0020
HCL 5N	4	23-24	9.5000	0.0020
HCL 5N	5	24-25	5.8000	0.0020
HCL 5N	6	25-26	0.1300	0.0020
HCL 5N	7	26-27	0.0300	0.0020
HCL 5N	8	27-28	0.0160	0.0020
HCL 5N	9	28-29	0.0160	0.0020
HCL 5N	10	29-30	0.0150	0.0020
HCL 0.05N	11	30-31	0.0233	1.8167
HCL 0.05N	12	31-32	0.0033	116.6670
HCL 0.05N	13	32-33	0.0033	1.4500
HCL 0.05N	14	33-34	0.0033	0.8833
HCL 0.05N	15	34-35	0.0033	0.1833
HCL 0.05N	16	35-36	0.0033	0.2000
HCL 0.05N	17	36-37	0.0033	0.0233
HCL 0.05N	18	37-38	0.0033	0.1167
HCL 0.05N	19	38-39	0.0033	0.0833
HCL 0.05N	20	39-40	0.0033	0.0833
		Sum =	15.6330	121.5259
		Yield =	99%	99%

Table 5.2 Elution behaviour for isotope chromatography experiment 2: 40 ml load.

Load	Load (ml)		Th	U
Load sample - HNO3 5N	40	0-40	0.0000	0.0000
Rinse - HNO3 5N	20	41-60	0.0000	0.0000
HCL 5N	1	60-61	0.1100	0.0050
HCL 5N	2	61-62	0.5900	0.0050
HCL 5N	3	62-63	0.3700	0.0050
HCL 5N	4	63-64	5.7000	0.0050
HCL 5N	5	64-65	19.0000	0.0050
HCL 5N	6	65-66	0.2100	0.0050
HCL 5N	7	66-67	0.0450	0.0050
HCL 5N	8	67-68	0.0150	0.0050
HCL 5N	9	68-69	0.0100	0.0300
HCL 5N	10	69-70	0.0150	0.0250
HCL 0.05N	11	70-71	0.0367	1.1000
HCL 0.05N	12	71-72	0.0050	55.0000
HCL 0.05N	13	72-73	0.0150	48.3333
HCL 0.05N	14	73-74	0.0150	0.2667
HCL 0.05N	15	74-75	0.0150	0.1333
HCL 0.05N	16	75-76	0.0150	0.0667
HCL 0.05N	17	76-77	0.0150	0.0667
HCL 0.05N	18	77-78	0.0150	0.0667
HCL 0.05N	19	78-79	0.0150	0.0667
HCL 0.05N	20	79-80	0.0150	0.0667
		Sum =	26.2267	105.2618
		Yield =	99%	99%

Table 5.3 Elution behaviour for isotope chromatography experiment 3: oxalic acid.

Load	Load (ml)		Th	U
Load sample - HNO3 5N	10	0-10	0.0000	0.0000
Rinse - HNO3 5N	20	11-20	0.0000	0.0000
HCL 5N + oxalic 1N	1	20-21	0.0550	0.0050
HCL 5N + oxalic 1N	2	21-22	60.0000	0.0100
HCL 5N + oxalic 1N	3	22-23	86.6667	0.0100
HCL 5N + oxalic 1N	4	23-24	3.6667	0.0100
HCL 5N + oxalic 1N	5	24-25	0.8000	0.0060
HCL 5N + oxalic 1N	6	25-26	0.0700	0.0060
HCL 5N + oxalic 1N	7	26-27	0.0475	0.0060
HCL 5N + oxalic 1N	8	27-28	0.0223	0.0060
HCL 5N + oxalic 1N	9	28-29	0.0250	0.0060
HCL 5N + oxalic 1N	10	29-30	0.0150	0.0060
HCL 0.05N	11	30-31	0.0233	2.0000
HCL 0.05N	12	31-32	0.0233	80.0000
HCL 0.05N	13	32-33	0.0233	15.0000
HCL 0.05N	14	33-34	0.0233	0.3000
HCL 0.05N	15	34-35	0.0233	0.0007
HCL 0.05N	16	35-36	0.0233	0.0002
HCL 0.05N	17	36-37	0.0233	0.0002
HCL 0.05N	18	37-38	0.0233	0.0002
HCL 0.05N	19	38-39	0.0233	0.0002
HCL 0.05N	20	39-40	0.0233	0.0002
		Sum =	151.6012	97.3727
		Yield =	100%	100%

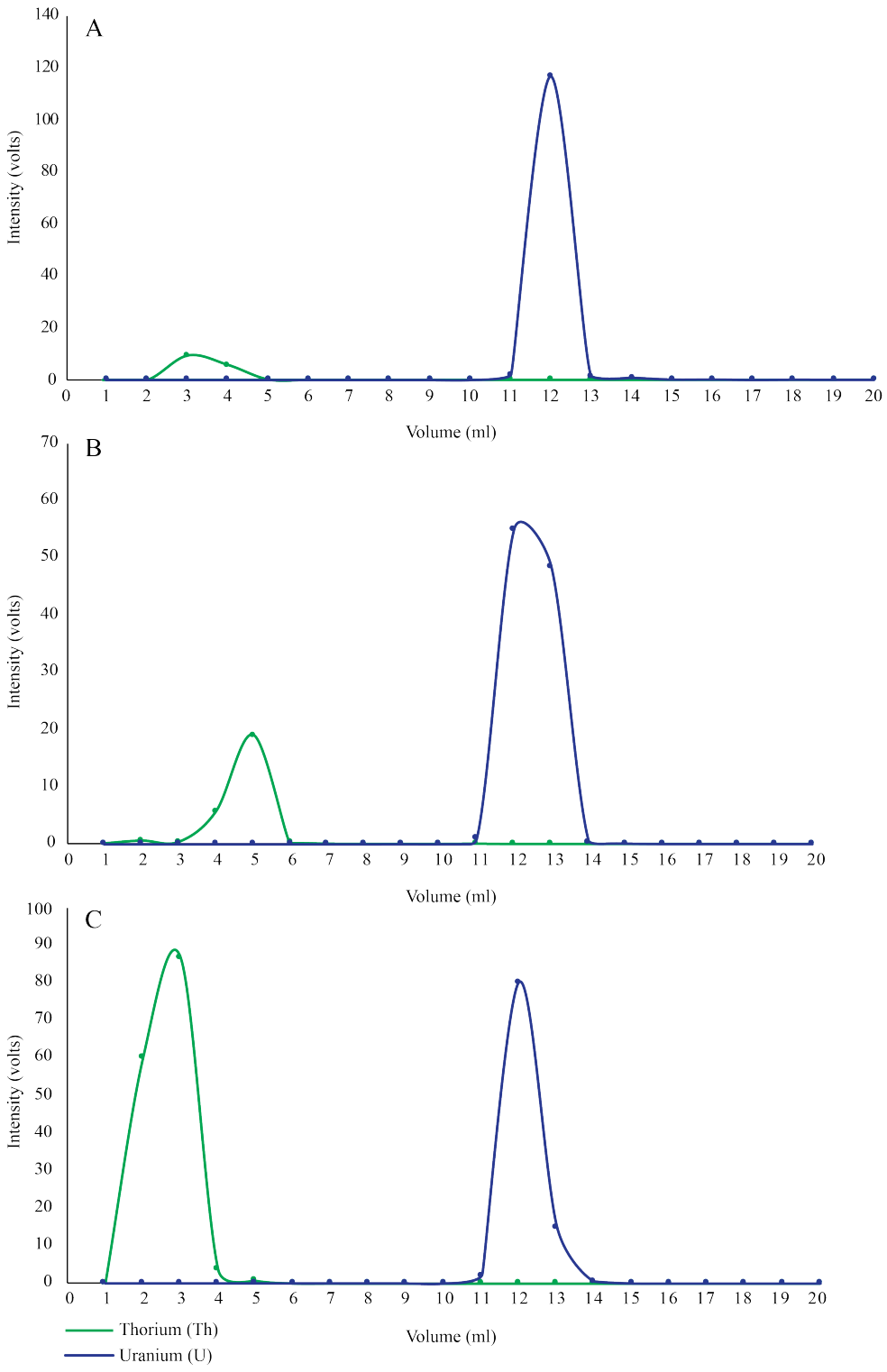

Figure 5.1 Measurement intensity vs. volume (ml) sampled. The three graphs depict when elution occurred of either Th (green) or U (blue) for the 3 experiments. Graph A represents the control experiment, while B is representative of the larger sample volume, and finally C shows experiment results when oxalic acid is added to the 5N HCL rinse. Although beam intensity was higher in C, for the purpose of this study it did not matter. In all cases Th and U eluted from the resin at essentially the same point.

Complete whole rock acid digestion was used in lieu of selective leaching of the carbonate component only. Leaching ideally targets the carbonate component, relying on a calculated mass to ensure the desired components are dissolved. Possible contamination can occur if the non-carbonate component is also dissolved. The uncertainty associated with this method introduces possible error and may produce results not truly representative of the desired component. Instead, whole rock acid digestion provides a result representative of the whole rock, which can be corrected for detrital components later. As such, three separate whole-rock digestion methods were used for the digestion of samples in preparation for chromatography. Method one measured a portion (0.1 g) of each sample and ashed each at 600°C for 18 to 20 hours to remove residual organic matter. Samples then underwent a multi-step acid digestion of HCL-HF-HNO_3 in 20 ml Savillex Teflon beakers. After the initial acid attack by HCL samples where centrifuged at 3200 rpm for 15 minutes, the supernatant (Ca-rich component) was decanted in a 15 ml acid leached Savillex container, dried on a hotplate and re -solubilized in 5N HNO_3. The remaining solids were then transferred to a larger Savillex container where they were dried down and treated with a 1:2.5 volume of concentrated HNO_3 and concentrated HF. Once sealed, the containers were placed in 180°C oven for 72 hours to digest the remaining solids. Once cooled, the samples were dried down on a hotplate and slowly diluted with 3 ml of concentrated HNO_3, and then dried down again. The Ca-rich supernatant was then recombined with the other half, refluxed overnight, and dried down. Each sample was then brought up in 45 ml of 0.5 HNO_3 as a stock solution. Samples were then aliquoted as 1 g amounts and spiked with a ^{233}U-^{236}U and ^{230}Th spike for U and Th concentration measurements. The samples were then processed through the column chemistry procedure discussed above to elute the U and Th. The columns utilized Eichrom® UTEVA resin.

The second method utilized the same ashing and digestion procedure as method one but differed by not bringing the samples up into a stock solution. Instead samples were spiked with a predetermined ^{233}U-^{236}U and ^{230}Th spike and brought up in 5ml of 5N HNO_3 and loaded into the column. Method 3 follows the same protocol as method 2 but the spike is introduced prior to digestion. Possible fractionation can occur during the separation process and spiking prior to that corrects for this possibility.

5.2 Uranium isotope analysis

Isotope dilution mass spectrometry using the double spike method is the most effective way to account for machine induced bias and unintended isotope fractionation during elution chemistry. To account for any fractionation, sample specific aliquots of stock solution were measured and spiked with a ^{233}U-^{236}U spike before elution. Before elution, the 3 ml gravity-flow columns with the Eichrom® UTEVA resin underwent cleaning and equilibration and like the previous elution scheme for the U and Th concentrations, the samples were processed and purified from the matrix elements. About 120 ng of U from each sample was mixed with sufficient spike to achieve a $(^{233}U)_{spike}$ / $(^{235}U)_{sample}$ ratio of ~ 2.4. Uncertainties associated with fractionation of Th as well as lost sample in the form residues left behind within the first run experiments required a new approach. Isotope dilution was still used however, samples were spiked directly after ashing. After spiking the samples were processed the same as way as the previous samples.

U isotope ratios were measured using a Thermo Scientific Neptune MC-ICP-MS at the University of Saskatchewan. Samples were dissolved in 0.50 M HNO_3 and introduced into the machine through an Aridus desolvation sample introduction system. U isotopic compositions are reported in the δ notation relative to the standard NBL CRM 112-A (formerly NBS SRM 960 and CRM-145) (equation 5.1**)** where $(^{238}U/^{235}U)_{sample}$ and $(^{238}U/^{235}U)_{std}$ are the U isotope ratio of the sample and standard, respectively.

$$\delta^{238}U = \left[\frac{(^{238}U/^{235}U)_{sample}}{(^{238}U/^{235}U)_{standard}} - 1\right] x\ 1000 \quad \text{.....(5.1)}$$

CHAPTER 6

Results

6.1 Uranium and thorium concentrations

Data presented in this section and the following sections represents values after ashing and are not corrected for mass loss during the ashing process. The authigenic seawater U concentrations calculated show a total range of 0 to 9.77 (n = 19) during the OAE-2 interval. This is considerably lower than the pre-OAE ($[U_a]$ = 5.53 to 9.09 ppm, n = 7) and post-OAE ($[U_a]$ = 4.40 to 8.15 ppm, n = 3) intervals. Thorium concentrations ($[Th_m]$ = 0.26 to 20.4, n = 29) show no observable correlation to U concentration or U isotopes. The Th/U ratios were calculated from the measured whole rock concentration (Table 6.1 & 6.2).

6.2 Lithogenic U contribution

The $\delta^{238}U$ values (and U concentration) were corrected for detrital U released from lithogenic material during whole rock digestion. Thorium was used for this correction due to its low solubility in seawater. The lithogenic $\delta^{238}U$ was estimated by averaging the data from two samples with the largest Th/U ratio (PO 486.7 and PO 479.2), yielding Th/U = 2.86, $\delta^{238}U$ = -0.46‰ in Experiment 1 and Th/U = 3.43, $\delta^{238}U$ = -0.59‰ in Experiment 2. Samples with the largest Th/U ratio are assumed to be primarily continentally-derived and therefore representative of the lithogenic component. The correction tends to decrease U concentration and increase $\delta^{238}U$ for samples that display an isotopic signature greater than that of the lithogenic $\delta^{238}U_l$ value. Authigenic U was determined through equation 6.1, where U_a is the authigenic (seawater derived) component, U_m is the measured U concentration, Th_m is the measured Th concentration, and U/Th_D is the U/Th ratio for the detrital end member.

$$[U_a] = [U_m] - [Th_m] \left(\frac{U}{Th}\right)_D \quad (6.1)$$

A correction for $\delta^{238}U$ can be determined using equation 6.2, where $\delta^{238}U$ is the corrected value, $\delta^{238}U_m$ is the measured value, $\delta^{238}U_l$ is the reference crustal value (Experiment 1: $\delta^{238}U_l$ = -0.46‰; Experiment 2: $\delta^{238}U_l$ = -0.59‰) determined from the $\delta^{238}U$ vs. Th/U plot (Figure 6.1), and F_l is the fraction of lithogenic U. These two values fall well within a reasonable range when compared to published $\delta^{238}U$ values for bulk continental crust ($\delta^{238}U$ = -0.28 ‰, Th/U = 3.87; Taylor and McLennan, 1995; Tissot and Dauphas, 2015)

$$\delta^{238}U = \frac{\delta^{238}U_m - (\delta^{238}U_l)(F_l)}{1 - F_l} \quad \text{.....(6.2)}$$

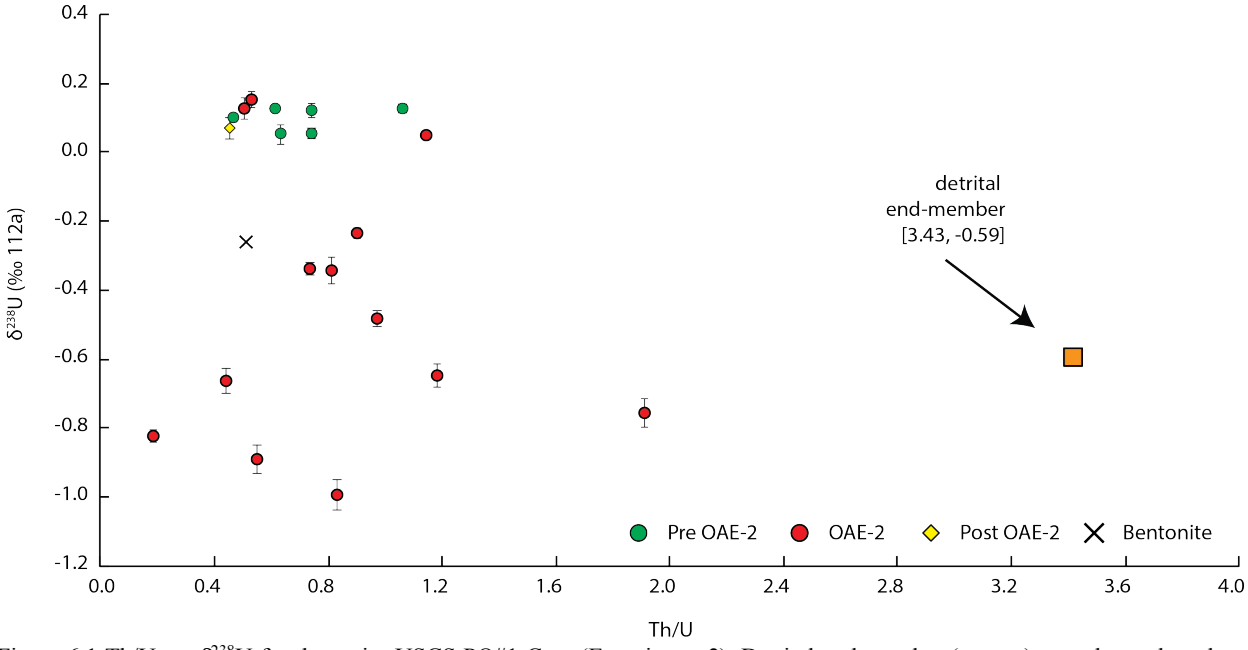

Figure 6.1 Th/U vs. $\delta^{238}U$ for the entire USGS PO#1 Core (Experiment 2). Detrital end-member (orange) was chosen based on measured Th/U ratios. Samples with the highest Th/U are assumed to be continentally derived. Symbols: X represents a bentonite layer from within the study core. Red circles denote OAE-2 samples. Green circles denote pre OAE-2 samples and the yellow diamonds are post OAE-2 samples. Each measured sample defines a point mixing line with the detrital end-member. The y-intercept of the mixing line is the seawater-derived $\delta^{238}U$ value corrected for detrital U for that sample.

6.3 Uranium isotope data

The $\delta^{238}U$ data for the two separate experiments is displayed in figure 6.2. Slight variations in the Th/U ratios between the two experiments can be seen in their respective tables (Table 6.1 and 6.2) however negligible variation can be found in the $\delta^{238}U$ values between the two. Due to sample volume restriction, Experiment 2 had fewer measurements, as such figure 6.3 contains measurements from both experiments. The $\delta^{238}U$ isotope date can be separated into three distinct intervals (Figure 6.3). The lowest interval represents pre-OAE background conditions and is

characterized by stable $\delta^{238}U$ values for both experiments. Experiment 1 (spiking before digestion) had a mean $\delta^{238}U$ value of 0.10 ± 0.06‰, while Experiment 2 (spiking after digestion) had a $\delta^{238}U$ of 0.09 ± 0.02‰. This was interpreted to mean there was no significant fractionation induced by the dissolution and storage of the purified U samples that were not spiked at the beginning of the purification procedure. The $\delta^{238}U$ values for the middle interval of the core representing OAE-2 are shifted to negative values with a men $\delta^{238}U$ value of -0.48 ± 0.07‰ and -0.52 ±0.04‰, respectively, for the two dissolution protocols. The $\delta^{238}U$ values for the post-OAE-2 upper core interval shifts back to pre-OAE-2 baseline values (Experiment 1 = 0.10 ± 0.07‰; Experiment 2 = 0.12 ± 0.02‰). Seawater standards were measured to ensure accuracy throughout sample runs (Table 6.3).

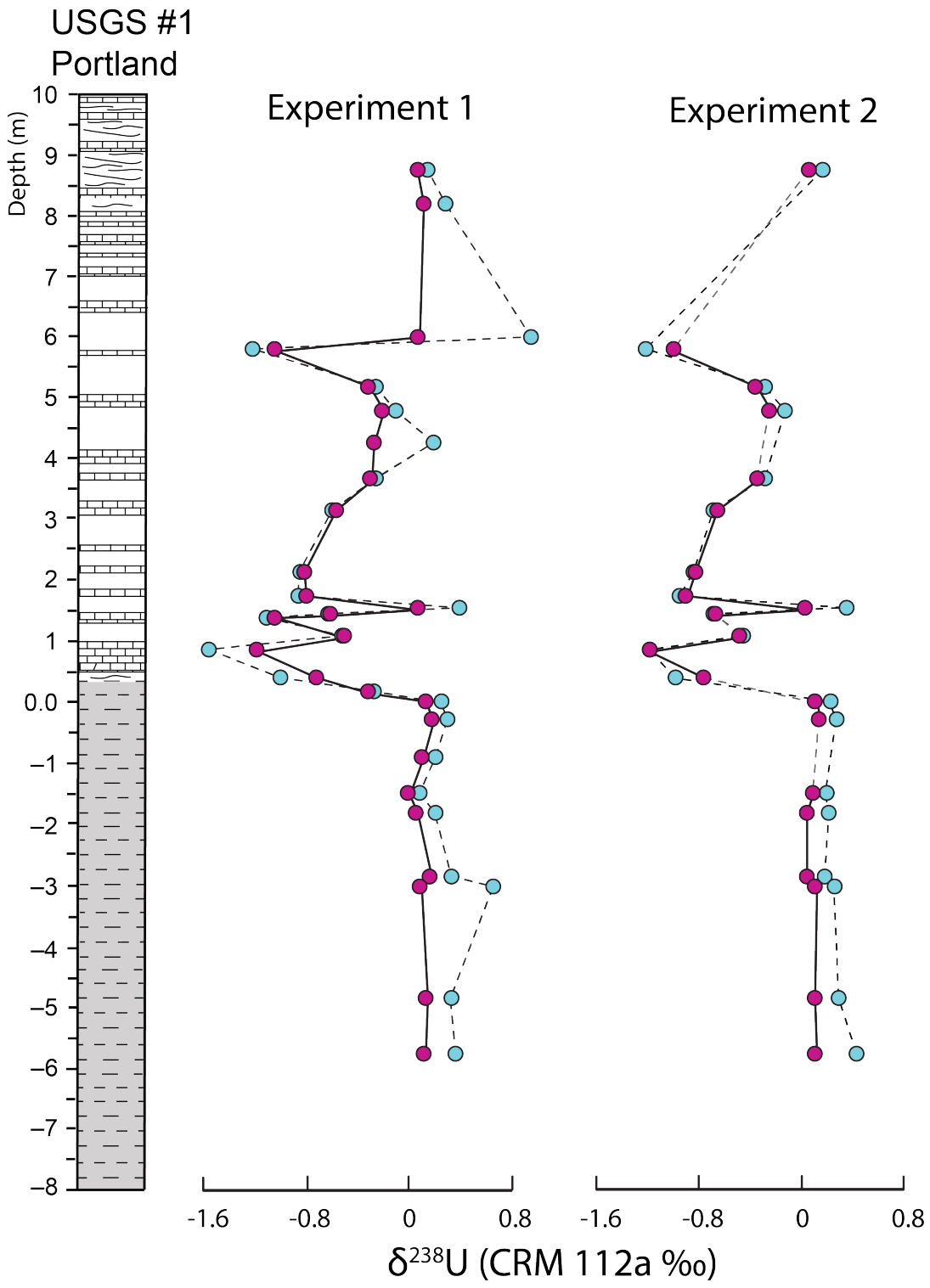

Figure 6.2 Uranium isotopic profile for Experiment 1 and 2. Purple circles denote measured isotopic values; blue circles represent corrected $\delta^{238}U$ values.

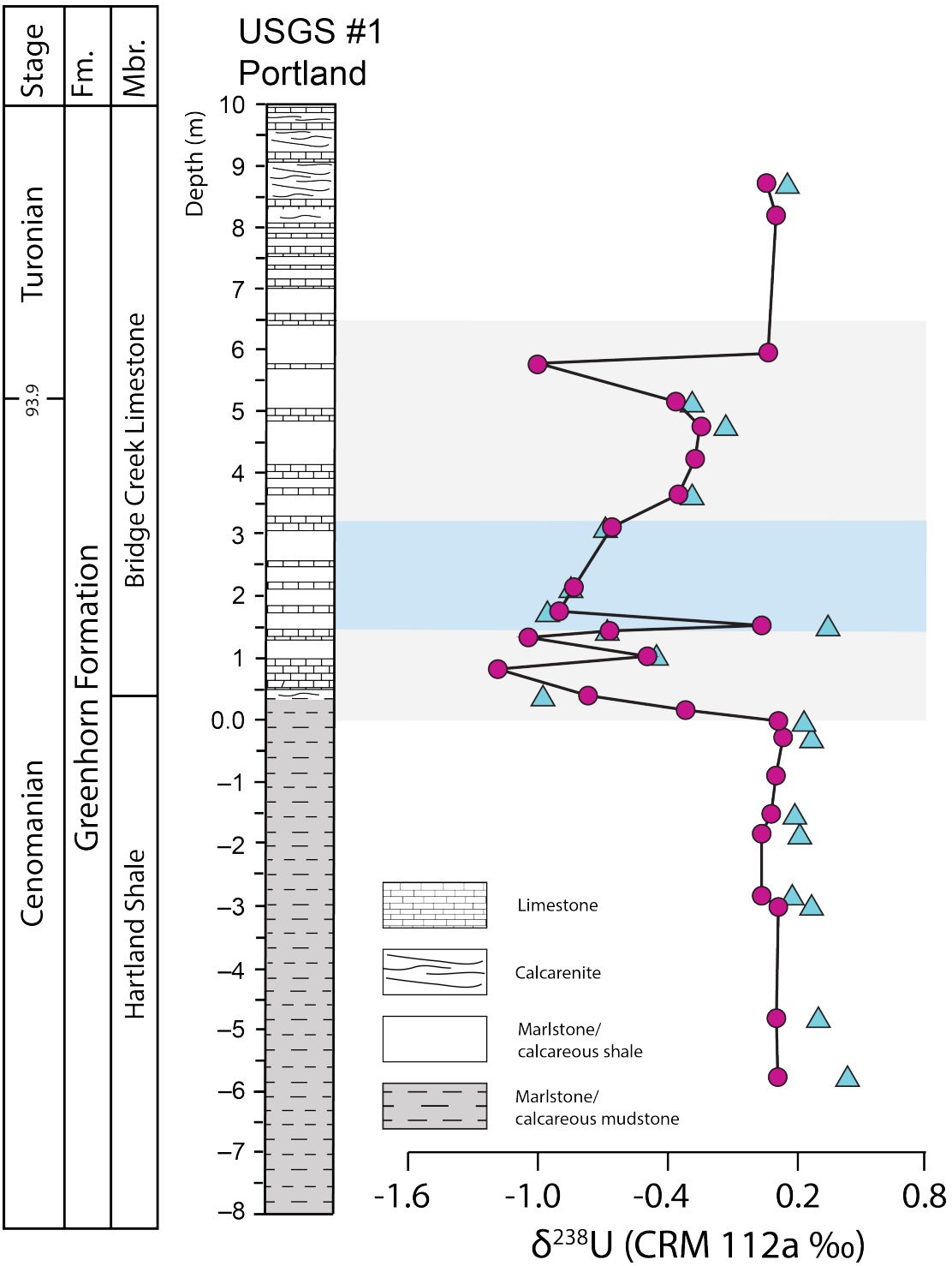

Figure 6.3 Uranium isotopic record for USGS PO#1 Core. Purple circles denote measured isotopic values; blue triangles represent corrected $\delta^{238}U$ values. Grey box denotes the extent of OAE-2 with the blue box representing the Plenus Cold Event.

Table 6.1 Geochemical data for experiment 1 from USGS PO #1 Core.

	Sample ID	Serial	Depth (m)	U (ppm)	Th (ppm)	Th/U	U (ppm)		$\delta^{238}U$ (s.e.)	Th corrected
							Lithogenic	Authigenic		$\delta^{238}U$ (‰)
Post	PO 458+26	PO 102	8.75	9.38	3.5	0.37	1.23	8.15	0.07	0.15
OAE-2	PO 461-10	PO 103	8.20	10.47	6.7	0.64	2.34	8.12	0.12	0.29
	PO 467+28	PO 106	6.01	11.55	20.4	1.77	7.15	4.40	0.08	0.95
	PO 469	PO 107	5.80	1.70	1.12	0.66	0.39	1.30	-1.04	-1.21
	PO 471	PO 109	5.19	1.72	1.3	0.76	0.46	1.26	-0.31	-0.25
	PO 472.29	PO 110	4.80	1.87	1.4	0.76	0.50	1.37	-0.20	-0.10
	PO 474+(1-2)	PO 111	4.26	4.48	9.1	2.02	3.17	1.30	-0.27	0.20
	PO 475.98	PO 112	3.67	3.19	2.0	0.62	0.69	2.50	-0.29	-0.25
	PO 478.13	PO 113	3.16	2.59	1.3	0.51	0.46	2.13	-0.57	-0.59
	PO 481.42	PO 116	2.15	1.44	0.26	0.18	0.09	1.35	-0.82	-0.84
	PO 482.71	PO 117	1.76	0.94	0.42	0.45	0.15	0.80	-0.80	-0.86
OAE-2	PO 484	PO 118	1.54	4.60	5.07	1.10	1.78	2.82	0.07	0.41
	PO 484.31	PO 119	1.44	2.43	0.91	0.38	0.32	2.11	-0.61	-0.63
	PO 484+15	PO 120	1.39	2.46	0.70	0.28	0.24	2.21	-1.04	-1.10
	PO 485+15	PO 121	1.08	2.01	1.53	0.76	0.53	1.48	-0.50	-0.52
	PO 486.26	PO 122	0.85	0.30	0.29	0.97	0.10	0.20	-1.18	-1.55
	PO 487.69	PO 124	0.41	0.94	1.40	1.49	0.49	0.45	-0.72	-1.00
	PO 488.5	PO 125	0.17	8.31	4.67	0.56	1.64	6.67	-0.31	-0.27
	PO 489	PO 126	0.01	10.46	5.11	0.49	1.79	8.67	0.14	0.26
	PO 490	PO 127	-0.29	11.56	5.10	0.44	1.79	9.77	0.19	0.31
	PO 492	PO 129	-0.90	10.79	4.87	0.45	1.71	9.09	0.11	0.22
	PO 494	PO 131	-1.51	6.80	2.85	0.42	1.00	5.80	0.00	0.08
	PO 495	PO 132	-1.82	9.99	6.18	0.62	2.16	7.82	0.06	0.21
Pre	PO 498.45	PO 134	-2.87	9.30	5.48	0.59	1.92	7.39	0.17	0.34
OAE-2	PO 499	PO 135	-3.04	11.21	16.21	1.45	5.68	5.53	0.10	0.67
	PO 505	PO 138	-4.86	8.96	6.46	0.72	2.26	6.70	0.14	0.34
	PO 508	PO 139	-5.78	8.92	7.55	0.85	2.64	6.27	0.13	0.38
	PO 479.2	PO 114	2.87	1.75	5.0	2.84	1.74	0.01	-0.43	-0.60
	PO 486.7	PO 123	0.71	0.22	0.62	2.87	0.22	0.00	-0.49	-0.60
	Detrital				Average	2.86		Average	-0.46	

[a] delta values relative to CRM 112a

Table 6.2 Geochemical data for experiment 2 from USGS PO #1 Core.

	Sample ID	Serial	Depth (m)	U (ppm)	Th (ppm)	Th/U	U (ppm)		$\delta^{238}U$ (s.e.)	Th corrected
							Lithogenic	Authigenic		$\delta^{238}U$ (‰)
Post OAE-2	PO 458+26	PO 102	8.75	8.337	3.79	0.45	1.11	7.23	0.07	0.17
OAE-2	PO 469	PO 107	5.80	1.507	1.26	0.84	0.37	1.14	-1.00	-1.21
	PO 471	PO 109	5.19	1.663	1.36	0.82	0.40	1.27	-0.35	-0.28
	PO 472.29	PO 110	4.80	1.771	1.60	0.90	0.47	1.30	-0.24	-0.12
	PO 475.98	PO 112	3.67	2.913	2.14	0.74	0.63	2.29	-0.34	-0.27
	PO 478.13	PO 113	3.16	1.156	1.37	1.19	0.40	0.76	-0.65	-0.68
	PO 481.42	PO 116	2.15	1.639	0.31	0.19	0.09	1.55	-0.83	-0.84
	PO 482.71	PO 117	1.76	0.987	0.54	0.55	0.16	0.83	-0.89	-0.95
	PO 484	PO 118	1.54	4.672	5.35	1.15	1.56	3.11	0.04	0.36
	PO 484.31	PO 119	1.44	2.514	1.11	0.44	0.33	2.19	-0.67	-0.68
	PO 485+15	PO 121	1.08	2.115	2.06	0.97	0.60	1.12	-0.49	-0.44
	PO 487.69	PO 124	0.41	0.810	1.55	1.92	0.45	0.36	-0.76	-0.98
	PO 489	PO 126	0.01	9.840	5.02	0.51	1.47	1.12	0.12	0.25
Pre OAE-2	PO 490	PO 127	-0.29	10.872	5.82	0.53	1.70	9.17	0.15	0.29
	PO 494	PO 131	-1.51	6.751	3.18	0.47	0.93	5.82	0.09	0.20
	PO 495	PO 132	-1.82	7.592	5.68	0.75	1.66	5.93	0.05	0.23
	PO 498.45	PO 134	-2.87	8.112	5.16	0.64	1.51	6.60	0.05	0.19
	PO 499	PO 135	-3.04	9.794	6.04	0.62	1.76	8.03	0.12	0.28
	PO 505	PO 138	-4.86	10.090	7.54	0.75	2.20	7.89	0.11	0.31
	PO 508	PO 139	-5.78	7.714	8.20	1.06	2.39	5.32	0.12	0.44
	PO 479.2	PO 114	2.87	1.402	5.01	3.58	1.46	-0.06	-0.49	0.00
	PO 486.7	PO 123	0.71	0.223	0.73	3.27	0.21	0.01	-0.69	0.00
	Detrital				Average	3.42		Average	-0.59	

[a] U isotope data corrected to CRM 112a

Table 6.3 Seawater $\delta^{238}U$ measurements

Sample ID	$\delta^{238}U$	s.e.
OSIL-1	-0.43	0.04
OSIL-1	-0.30	0.06
OSIL-1	-0.42	0.09
OSIL-1	-0.37	0.10
OSIL-1	-0.48	0.06
OSIL-1	-0.41	0.03

CHAPTER 7

Discussion

The results from the Portland core show a distinct negative $\delta^{238}U$ excursion that correlates with uranium concentrations in the study section, but also with all previous uranium studies on the Cenomanian-Turonian OAE (Figure 7.1). The negative shift meets expectation for the behaviour of a redox sensitive proxy during a period of increased anoxia in the oceans. Because there is a fractionation of U isotopes that occurs during reduction and removal into anoxic marine sediment a change in the output flux of U will cause a change in the $\delta^{238}U$ and U concentration of seawater. The direction of the fractionation factor is such that an expansion of anoxic sediment in the oceans will preferentially draw down heavy isotopes of U, thus leaving the residual pool of U in seawater with a lighter $\delta^{238}U$ value. Indeed, the studied section shows that there is a shift to lower [U] and lighter $\delta^{238}U$ values at the onset of OAE-2. The negative shift in $\delta^{238}U$ occurs at the same stratigraphic level as the positive shift in $\delta^{13}C_{org}$, which is traditionally taken as marking the beginning of OAE-2. The negative excursion in $\delta^{238}U$ values during OAE-2 is in agreement with previously published $\delta^{238}U$ profiles from two locations in the proto-North Atlantic region (Montoya-Pino et al., 2010; Clarkson et al., 2018), but there are differences as well. The main one relates to the magnitudes of the excursions (Figure 7.2). The sedimentary $\delta^{238}U$ profile excursion is just 0.15‰ (Montoya-Pino et al., 2010) in the succession of organic-rich black shales at Demerara Rise. Clarkson et al. (2018) studied a pelagic carbonate succession at Eastbourne, UK, and found a 0.47‰ negative excursion. The negative excursion recorded in the WIS in this study is nearly 1.0‰, recorded in a pelagic succession of argillaceous limestone and intercalated shale. The $\delta^{238}U$ excursion in the Portland core is more than 2x the size of excursion in the Eastbourne section (Clarkson et al., 2018) and just under 6.5x the size of the $\delta^{238}U$ excursion in the core collected from Demerara Rise (Montoya-Pino et al., 2010). In the following sections, I will discuss possible explanations for the different magnitudes of the excursions in the three $\delta^{238}U$ profiles, and the implications for the magnitude of expanded ocean anoxia during OAE-2.

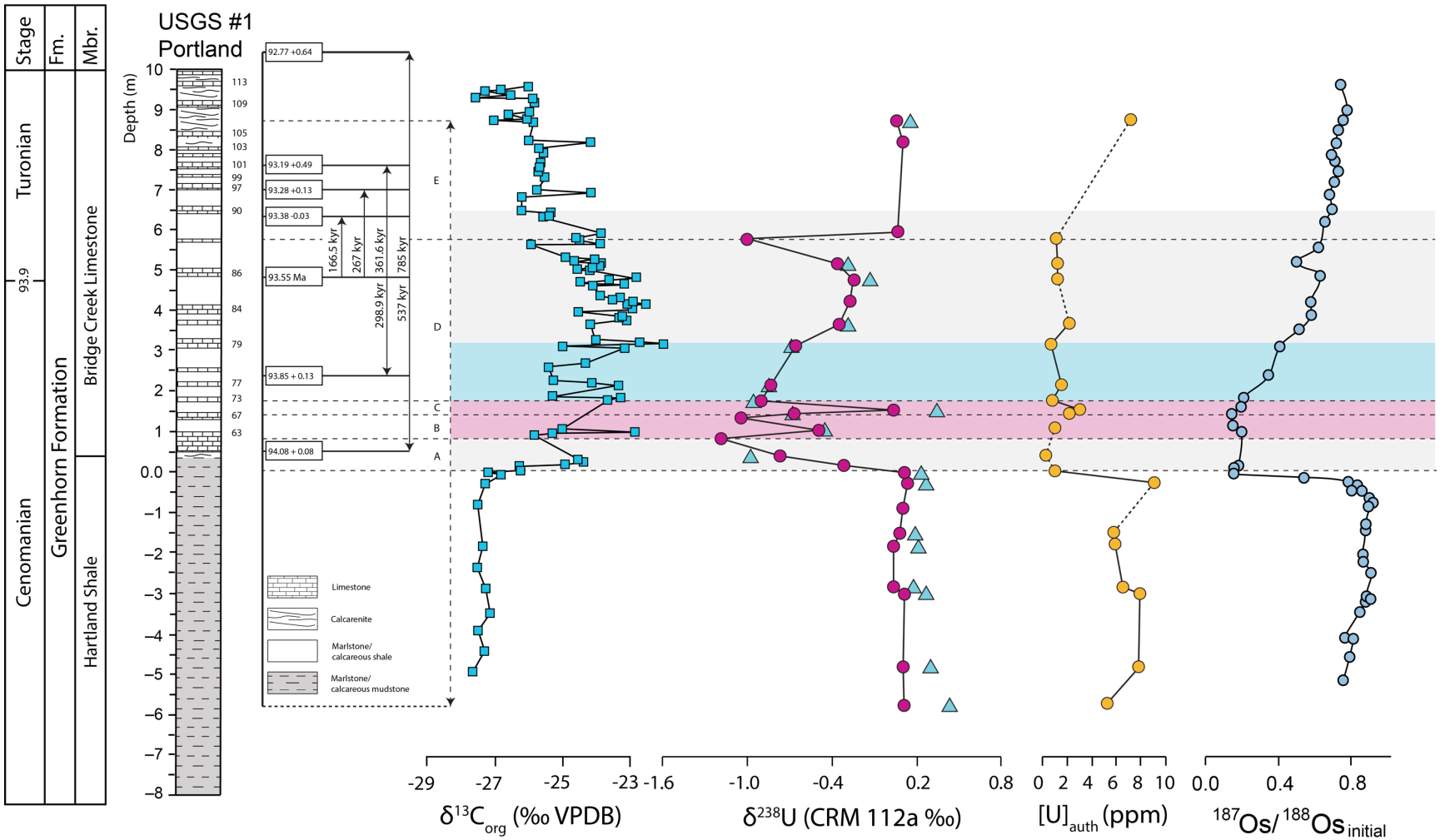

Figure 7.1 $\delta^{13}C$, $\delta^{238}U$, authigenic [U], and $^{187}Os/^{188}Os$ vs. depth for the Portland core. Grey band defines the OAE-2 interval, while the blue bar denotes the Plenus Cold Event and the pink bar the Benthic Oxic Zone. Blue triangles are the corrected $\delta^{238}U$ values from experiment 2, while the pink circle is the measured $\delta^{238}U$ values. A systematic shift towards negative $\delta^{238}U$ values occurs at the onset of the positive $\delta^{13}C$ excursion and negative $^{187}Os/^{188}Os$ excursion as would be predicted during expansion of marine anoxia. A short re-oxygenation event and brief return to positive $\delta^{238}U$ values suggests the $\delta^{238}U$ profile from the Portland section does capture both the PCE and BOZ. Orbital timescale information comes from Sageman et al. (2004) and is indicated by the solid lines. Interpreted dates and timing are indicated by dashed lines. Intervals A through E are estimates based on the interpreted time line. Interval A represents 140 kyr long interval and the time from the onset of OAE-2 and the start of the BOZ. Interval B covers the initial rise of $\delta^{238}U$ values (10 kyr long). C interval covers the major reoxygenation and positive $\delta^{238}U$ excursion associated with the PCE (30 kyr). Interval D is the interval after the PCE and the slow return to pre-OAE-2 conditions (500 kyr). $\delta^{13}C$ and $^{187}Os/^{185}Os$ profiles come from Holmden et al. (2016).

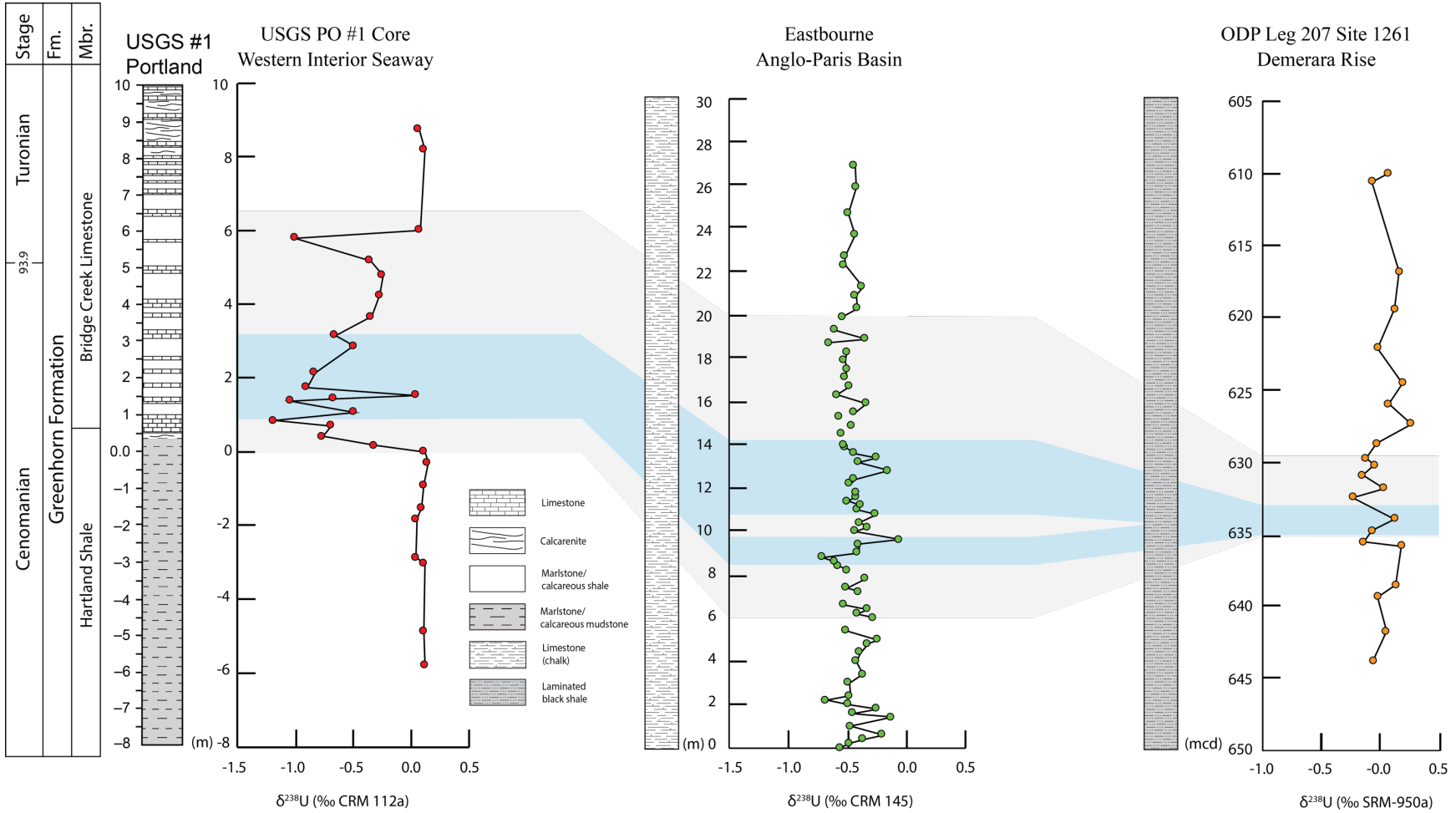

Figure 7.2 $\delta^{238}U$ vs depth profiles for the Portland core, Eastbourne section (Clarkson et al., 2018), and ODP site 1261 (mcd = meters composite depth; Montoya-Pino et al., 2010). Grey band represents the OAE-2 interval in the respective core and the blue band represents the PCE interval through each core. Correlations are based on the placement of the OAE-2 interval in the corresponding publications.

7.1 Marine redox conditions during the rise and fall of OAE-2

It is clear that the $\delta^{238}U$ record from the Portland section records a major change to the anoxic sink. It is particularly gratifying to see that the pre-excursion and post-excursion background $\delta^{238}U$ values are very uniform. It is an indication that seawater had a similar $\delta^{238}U$ value before and after OAE-2, and a similar uptake-related U isotope fractionation factor (Figure 7.1). However, at the onset of OAE-2, which is denoted by a positive carbon isotope excursion, the $\delta^{238}U$ values plummet well below the pre-OAE-2 average sedimentary $\delta^{238}U$ value (0.10‰). Based on an orbital time scale from Sageman et al. (2004), the drop from pre- OAE-2 $\delta^{238}U$ values took about 140 kyrs or just over a third of one residence time of U in the modern oceans. After the initial drop in stage A, there is an almost immediate return to pre OAE-2 like sedimentary $\delta^{238}U$ values (stages B and C), coinciding with the onset of the Plenus Cold Event (PCE) in Europe and the Benthic oxic zone (BOZ) in North America. The short-lived positive excursion took about ten thousand years to return to the positive $\delta^{238}U$ values of the pre-OAE-2 baseline. The PCE was characterized by two cooler periods punctuated by a brief warming period (Jenkyns et al., 2017; see also Chapter 2). The decreased atmospheric temperatures compared to the relatively high temperatures at the time were accompanied by a southward movement of well-oxygenated waters into the PNAO and the WIS. The injection of oxygenated water back into the PNAO would have minimized the effect of the anoxic sink and allowed for the brief return of pre-OAE-2 like conditions in the water column. The $\delta^{238}U$ record displays a two-peaked excursion that aligns well with the two pulses of the cooler, more oxygenated, water (Figure 7.1). The [Mo] profile and evidence of bioturbation throughout the Bridge Creek Limestone suggest that the transition from suboxic conditions characteristic of the Hartland shale water column to one more sustaining of benthic life occurred prior to the Benthic Oxic Zone. Oxygenation of the water column prior to the to the Benthic Oxic Zone suggests the excursion is not a function of the local re-oxygenation event, but rather a representation of the global redox conditions. Continuing up-section, the end of the Benthic Oxic Zone is defined by a less extreme drop of the sedimentary $\delta^{238}U$ values. Considering the overall length of the PCE, it would be reasonable to assume that the return to light $\delta^{238}U$ values may also have been controlled by the reworking of anoxic sediments. Re-oxidation of anoxic sediment would have released massive amounts of the heavier ^{238}U back into the oceans, quickly driving the $\delta^{238}U$ of seawater to a lighter value. Assuming ocean turnover times were similar to

today (~1500 years; Döös et al.2012) then the ten thousand-year reoxygenation event could have easily been long enough to allow the new U to become conservatively mixed. Continuing up-section, the end of the PCE is defined by a less extreme drop of the $\delta^{238}U$ values. The smaller magnitude of the decrease is likely a relict feature of the initial expansion of anoxia. Because the size of the anoxic sink is increasing, uranium concentration within the oceans is expected to be lower than at the start of the excursion (**Figure 7.3**). The fourth stage (stage D) is characterized by a slow return to pre-OAE-2 conditions.

Clarkson et al. (2018) offered a similar interpretation of the $\delta^{238}U$ profile for the Eastbourne section. At the onset of the carbon isotope excursion, which defines the start of OAE-2, the $\delta^{238}U$ values decrease, which Clarkson et al. (2018) interpreted to reflect the expansion of ocean anoxia. Sedimentary $\delta^{238}U$ values shift from -0.24 ± 0.09‰ to a minimum of -0.71 ± 0.06‰, which defines a –0.47‰ excursion. A similar drop occurs in the redox sensitive trace metal profiles in the two other sections studied by these authors (Raia del Pedale and South Ferriby). After the initial decline in $\delta^{238}U$, the Eastbourne section records a rapid return to more positive $\delta^{238}U$ values (-0.41 ± 0.07‰). The shift back to heavier sedimentary $\delta^{238}U$ values implies that the extent of ocean anoxia globally decreased. Clarkson et al. (2018) noted that the shift to heavier more positive values occurred during the Plenus Cold Event, which is correlative with the Benthic Oxic Zone in the Portland Core. The end of the Plenus Cold Event interval in the Eastbourne section is associated with a decrease in $\delta^{238}U$ values. The tail end of the OAE-2 interval in the Eastbourne section is represented by a gradual return to pre-OAE-2 $\delta^{238}U$ values. Unlike the Eastbourne section, the $\delta^{238}U$ profile for the Portland core records an abrupt rise to pre-OAE-2 sedimentary $\delta^{238}U$ values. Similar measurements of that single data point all fall between the two experiments fall within error of each other implying the value is not an anomaly. However, if we remove the single data point from the $\delta^{238}U$ profile, the return to pre- OAE-2 values is much more gradual and similar to the Eastbourne section (Clarkson et al., 2018). Clarkson et al. (2018) suggested the gradual return may be a lingering effect of the receding anoxia. A possible explanation for the difference may then be a result of ocean circulation or even simpler, due to the proximity of the sample site to areas of widespread anoxia.

Organic-rich shales were thought to contain the most promising record of the changing redox conditions in the global ocean, at least with regards to the U isotope record (e.g., Montoya-Pino et al. 2010). Unlike both the Portland core and Eastbourne study, Montoya-Pino et al. (2010)

sampled organic-rich siliciclastic sediments from ODP (leg 207) site 1261, at Demerara Rise. Demerara Rise is a ~380 km long, ~220 km wide plateau off the coast of modern day Venezuela. Water depths are relatively shallow (~700 m) for most of the plateau but the northwest margin deepens to 3000 to 4000 m below sea level. Redox sensitive trace element (TE) concentrations for the black shale units show considerable enrichment prior to OAE-2, particularly molybdenum (Figure 7.4), suggesting the existence of a euxinic depositional environment prior to OAE-2. Molybdenum concentrations depict a significant drop in concentrations during OAE-2, signifying the drawdown of redox elements from the oceanic reservoir because of the expanding anoxic sink. Due to the sensitivity of molybdenum to local redox conditions, the drastic drop in Mo may also indicate a change in the redox environment at the local scale. Post-OAE-2 TE concentrations show a similar signature to the pre-OAE-2 interval implying the return to an H_2S-dominated environment. Shelf margins with evidence for intense upwelling, including Demerara Rise (Trabucho Alexandre et al., 2010), have the potential to limit bottom water renewal resulting in permanently anoxic or euxinic environments. In the case of the Namibian shelf in the modern ocean, low dissolved oxygen is not controlled by topographic barriers, such as the Black Sea or Cariaco Basin, but rather the combination of intense upwelling and the resulting oxygen demand by settling organic matter from high productivity (Algeo and Lyons, 2006). As a result of poor bottom water renewal, there is potential for isotopic signatures to be muted. As a result, the $\delta^{238}U$ profile from Montoya-Pino et al. (2010) presents a greater challenge to interpret. It is only recently that research focusing on U reduction into anoxic sediments is beginning to understand the processes at hand. Montoya-Pino et al. (2010) measured $\delta^{238}U$ values through a complex redox interval, possibly altering the global signal to reflect the local redox environment. The additional task of interpreting the $\delta^{238}U$ profile with few samples and a barely discernable $\delta^{238}U$ excursion (Figure 7.2) challenged the interpretation of global redox conditions. Despite the challenges, the $\delta^{238}U$ excursion recorded still displays a systematic shift towards heavier $\delta^{238}U$ values and follows the expected trend if anoxia did increase during OAE-2. Except, unlike the other two profiles above, the $\delta^{238}U$ profile from Montoya-Pino et al. (2010) does not appear to record the PCE or BOZ, even though evidence for a re-population event due to surface-water cooling correlated to the PCE exists in other Demerara rise cores (Friedrich et al., 2006). The additional lack of a positive $\delta^{238}U$ excursion during the PCE or BOZ in the Montoya-Pino et al. (2010) study suggests the profile may not be as globally significant as the other two profiles.

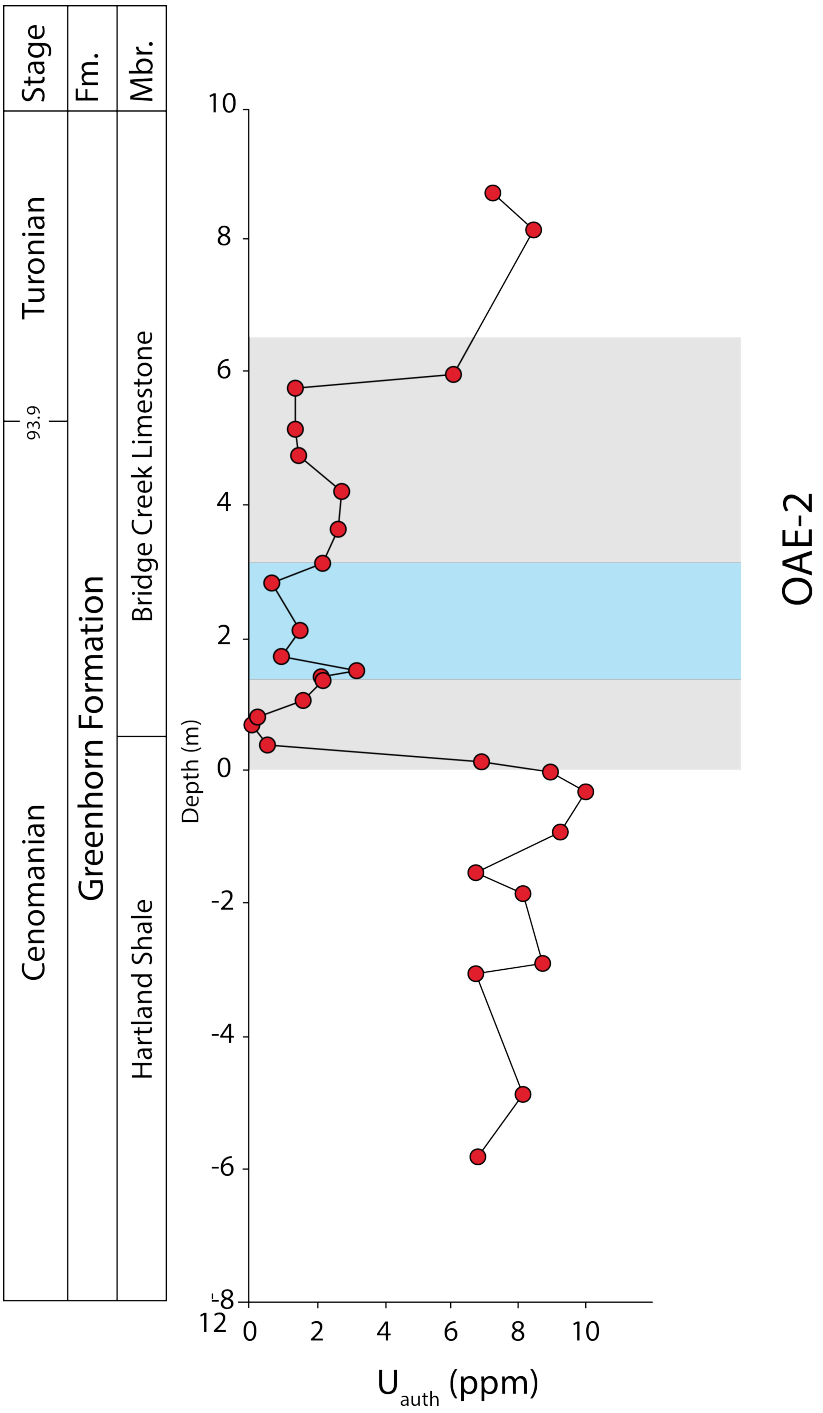

Figure 7.3 Authigenic U concentration profile for the studied section of the Portland core. Grey represents the OAE-2 interval. Similar to the $\delta^{238}U$ profile, the authigenic [U] goes down during the event. This is a result of the increased size of the anoxic sink throughout the event. Small increases in authigenic [U] correspond with the PCE (blue bar) and the short return of oxygenated waters.

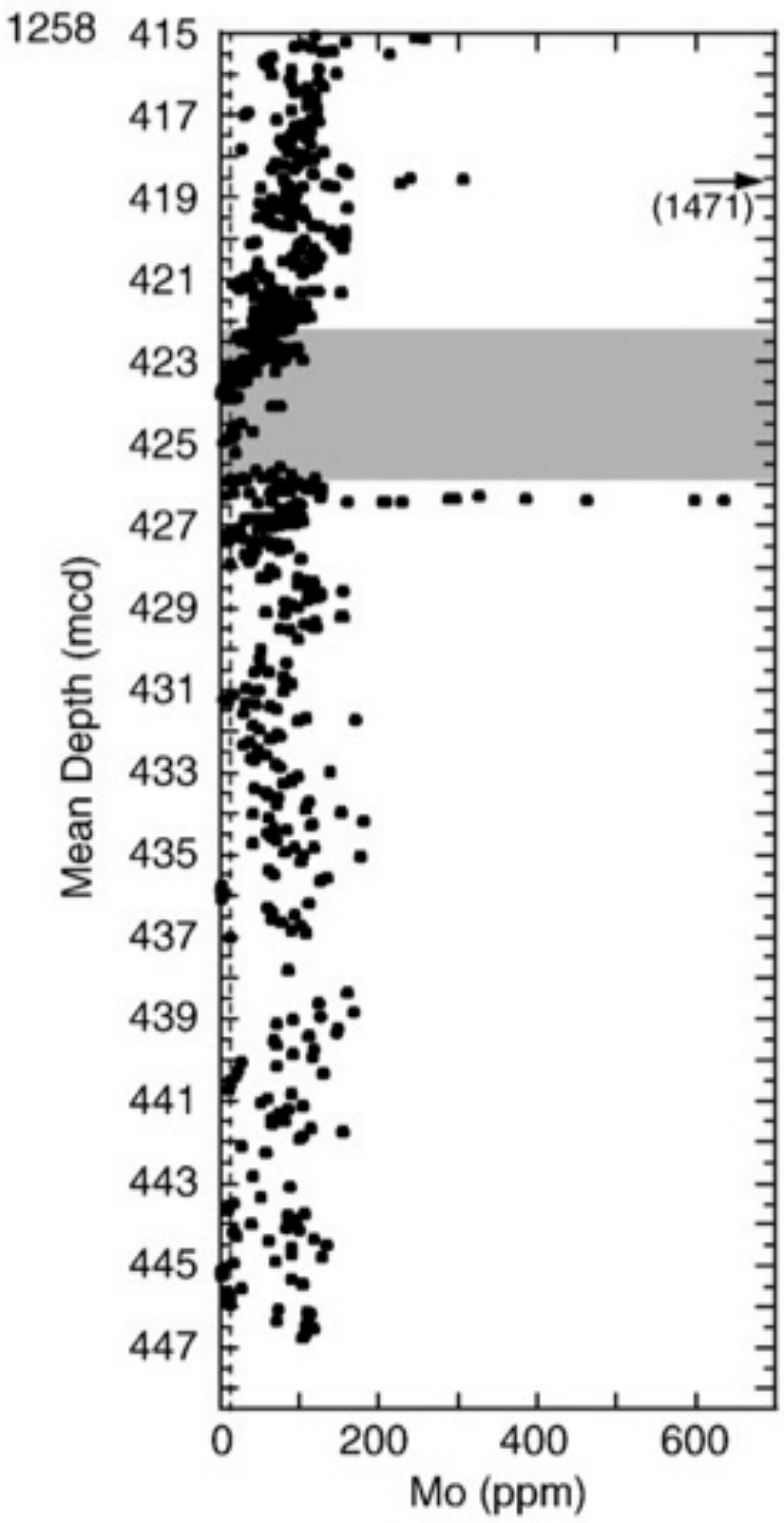

Figure 7.4 [Mo] vs. depth profile for ODP Leg 207, site 1258 (Demerara Rise) from Hetzel et al. (2009). Grey band represents the OAE-2 interval.

7.2 Reconciling the marine $\delta^{238}U$ profile from the Portland core and Eastbourne section

Although the interpretations of the sedimentary $\delta^{238}U$ values for the redox state of the oceans during OAE-2 in both the Portland core and the Eastbourne section agree regarding the timing of changes in relative anoxia during OAE-2, there is still the difference in the magnitudes of the excursions to consider. The Clarkson et al. (2018) $\delta^{238}U$ profile is based on measurements of relatively pure calcium carbonate sediment. Despite the lithological purity, they leached their samples in buffered acetic acid to ensure that U from detrital sources would not be dissolved. Reeder et al. (2000) determined that the complexation of uranium to either calcite or aragonite was not associated with any fractionation, therefore carbonates are able to retain primary seawater $\delta^{238}U$. This was more recently tested by Romaniello et al. (2013), who measured both carbonate sediments and primary carbonate precipitates (PCP). They found the primary carbonate precipitates recorded coeval seawater $\delta^{238}U$ values (Figure 4.2) but that carbonate sediments recorded a $\delta^{238}U$ that was 0.2 to 0.4‰ heavier. Apparently, there is additional uptake of U into carbonate after the primary carbonate precipitates are released from their mostly biological producers to form a sediment. In other words, there are two sources of U in carbonate sediment. First, there is seawater-derived uranium that is sequestered by biological producers of carbonate sediment, which has the same $\delta^{238}U$ as seawater. Second, there is seawater-derived U that diffuses into the pore fluids of carbonate sediment if the pore fluids are anoxic. The diffusion-driver is reduction of U(VI) to particle reactive U(IV) in the anoxic sedimentary pore fluids. This secondary source of seawater-derived U in marine carbonate sediment is fractionated in the manner observed by Romaniello et al. (2013), i.e., towards heavier isotope values. Accordingly, carbonate sediment $\delta^{238}U$ values are mixtures of fractionated and unfractionated seawater derived U, with the net result being that the seawater-derived U becomes isotopically heavier if the pore fluids are anoxic.

Clarkson et al. (2018) were concerned that their sedimentary $\delta^{238}U$ profile from Eastbourne may be susceptible to this type of syndepositional diagenesis or perhaps later diagenetic fluids during burial, and that the sedimentary record of $\delta^{238}U$ values deviate from changes in seawater $\delta^{238}U$ during OAE-2 by a constant or variable fractionation factor. Clarkson et al. (2018) plotted $\delta^{238}U$ vs. Mg/Ca, Sr/Ca, Mn/Ca, and U/Ca (Figure 7.5) to look for potential diagenetic effects. The assumption is that the stable low-Mg calcite of pelagic carbonates is resistant to

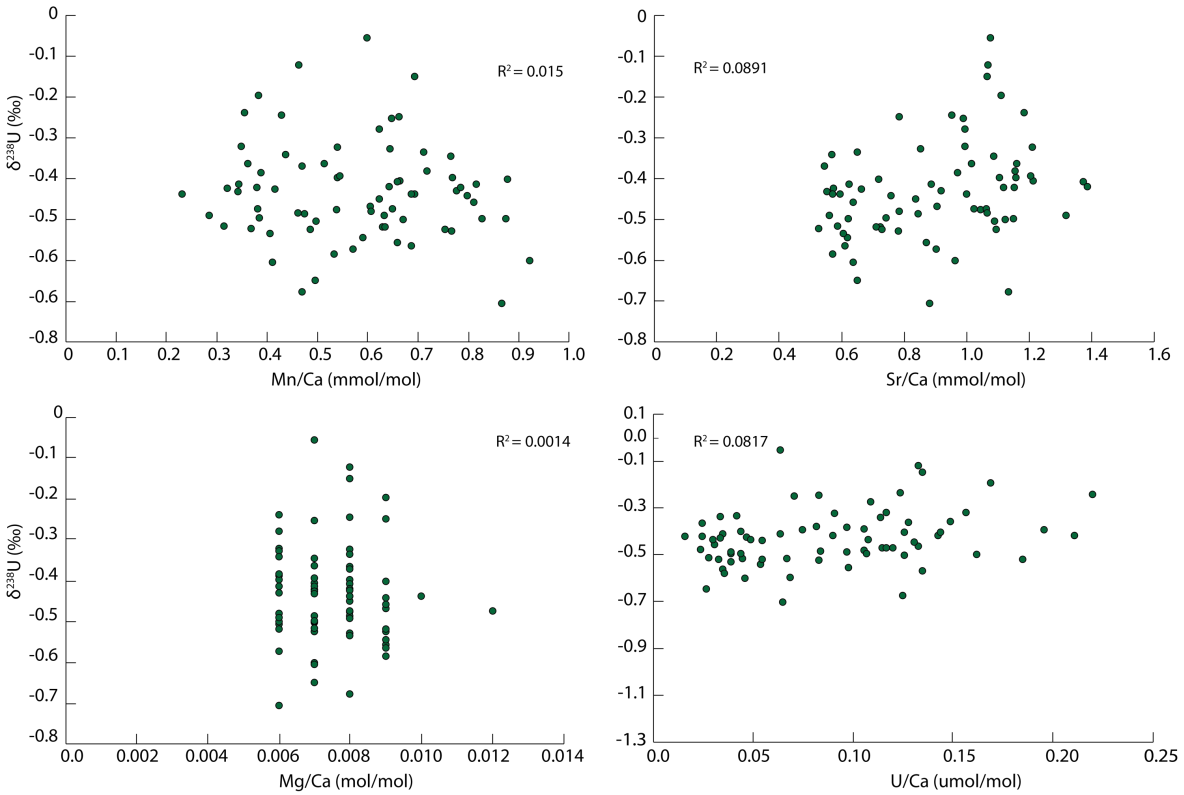

Figure 7.5 δ^{238}U vs. Mn/Ca, Sr/Ca, Mg/Ca, and U/Ca for Eastbourne (Clarkson et al., 2018). Plots are used to determine effects of diagenesis on carbonate δ^{238}U measurements. Unlike the Eastbourne section, the samples of the studied core have a higher clay and silt content than a chalk and as a result may affect the ratios. Eastbourne samples were better constrained due to their high $CaCO_3$ and low detrital content.

diagenetic alteration. Therefore, if the samples were altered, then a sample with a lighter or more positive δ^{238}U value should also have a higher Mg/Ca ratio. They also cite the lack of correlation of the δ^{238}U values with Sr/Ca and Mn/Ca as evidence of no alteration. Clarkson et al. (2018) also measured δ^{238}U values from two additional sites and found higher Mg/Ca ratios with heavier δ^{238}U values in Raia del Pedale, which they present as evidence for carbonate recrystallization in those sections. The heavier δ^{238}U values for the three high Mg/Ca values are consistent with the negative excursion in the Eastbourne section and appear to be unaffected by diagenesis. The lack of correlation between high Mg/Ca and δ^{238}U values in the highly altered Raia del Pedale section confirmed their confidence in the δ^{238}U profile of Eastbourne is unaltered by late stage diagenesis. However earlier in section 4.3, it was argued that the effects of diagenesis may be less important to the interpretation of sedimentary δ^{238}U profiles than the syndepositional uptake of fractionated U isotopes during diffusion-related uptake of seawater-derived U at the sediment water interface,

because the fractionation factor can vary from zero to 0.6‰ depending on the oxygen penetration depth into the sediment (Figure 7.6).

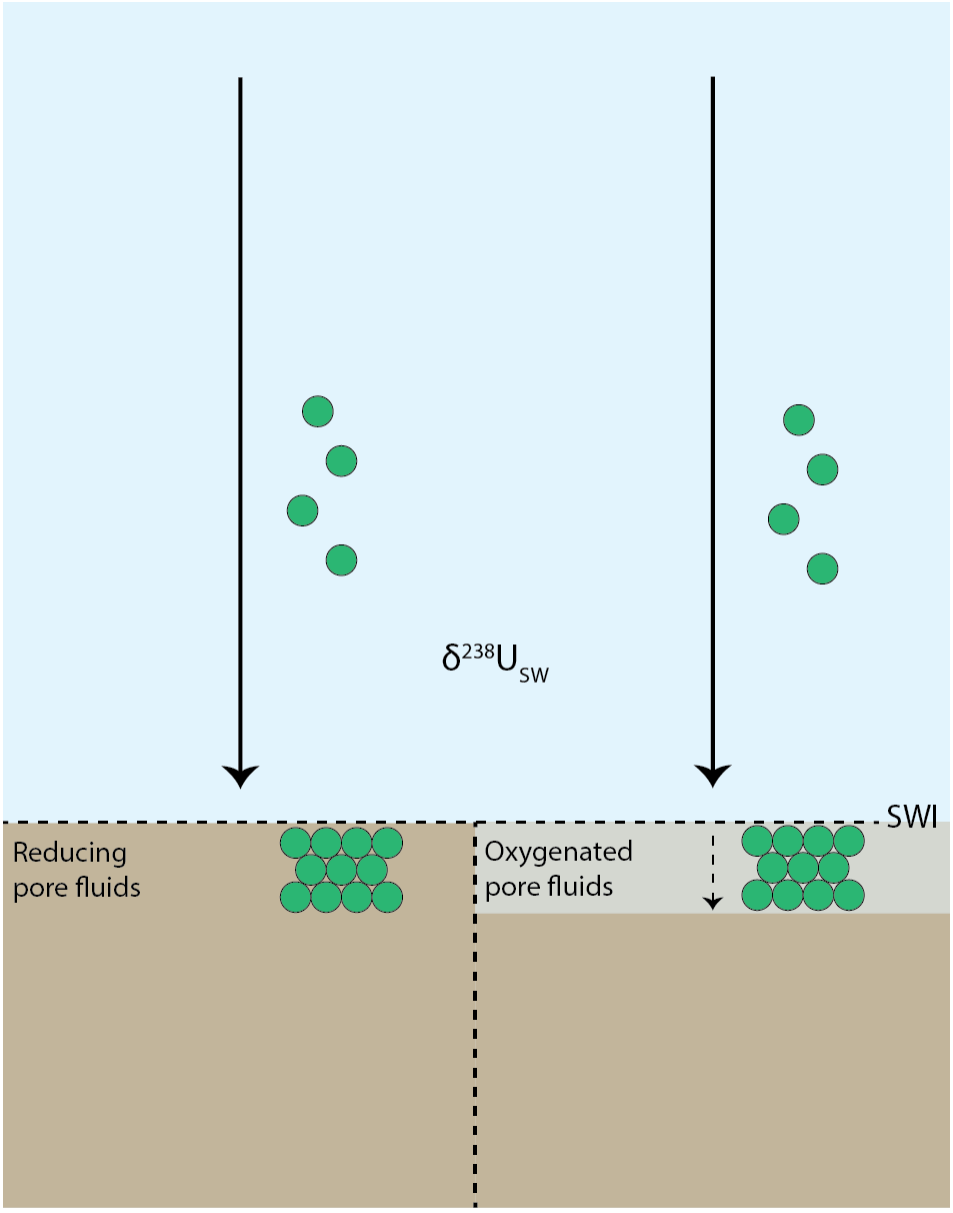

Figure 7.6 Schematic diagram depicting the role of pore fluid chemistry on the reduction of U during carbonate deposition. The left diagram displays the precipitation of primary carbonates (green circles) retaining seawater $\delta^{238}U$. Additional reduction occurs when these carbonates are deposited if the pore fluids are reducing, imparting an additional fractionation of 0.2 to 0.4‰ (Romaniello et al., 2013). The right side depicts the same carbonate precipitation and deposition, however pore fluids in this scenario are oxygenated. This imparts no additional fractionation and extends the reduction pathway, resulting in carbonate sediments that retain the primary $\delta^{238}U$ value of the fluid in which they formed.

The $\delta^{238}U$ of any sediment is controlled by the reduction pathway uranium travels as it works its way down into the sediment. In the case of anoxic sediment and an oxic water column, reduction of U begins at the sediment water interface. As a result, the effective fractionation factor for U reduction in these sediments is ~0.6‰ or about half the full equilibrium isotope fraction factor of 1.2‰ based on ab initio modeling (Fujii et al., 2006; Abe et al., 2008), due to the preferential reduction of heavy isotopologues of U(VI) compared to the light isotopologues (Clark and Johnson, 2008; Bura-Nakić et al., 2018). However, if the overlying water column is oxygenated, and the sediment pore fluids do not become anoxic immediately below the sediment-water interface, but rather at a deeper level in the sediment column, then the fractionation factor decreases until it becomes zero (Clark and Johnson, 2008). This means that sediment with oxygen penetration depths deep enough will record the $\delta^{238}U$ of seawater directly without fractionation. Returning to the study of Romaniello et al. (2013), coupled with the knowledge that sediment pore fluids on the Bahamas Bank are characteristically anoxic (Romaniello et al., (2013) the heavier-than-seawater $\delta^{238}U$ values measured in carbonate sediment reflects diffusion-related post-depositional uptake of U(VI) from seawater into anoxic pore fluids.

Differences in oxygen penetration depth offers a way to reconcile the differences in the magnitudes of sedimentary $\delta^{238}U$ excursions recorded in the Eastbourne section, UK, and the Colorado core in the Western Interior Seaway reported in this study. Clarkson et al. (2018) proposed that the sedimentary $\delta^{238}U$ profile for the Eastbourne section records seawater, directly, without any fractionation, implying that the oxygen penetration depth was deep enough to allow no fractionation to occur. I suggest instead, that during OAE-2, pore fluids became anoxic at Eastbourne, and as a result the magnitude of the actual change in seawater $\delta^{238}U$ is larger than the shift in the sediment would suggest. By contrast, I interpret the negative $\delta^{238}U$ excursion in the Portland core as being larger than the excursion in seawater because the pre- and post-excursion baseline $\delta^{238}U$ values are too heavy, due to the likelihood of persistent pore fluid anoxia at these times. As a result, applying a net shift of -0.6‰ to the entire $\delta^{238}U$ profile should account for the fractionation of U during reduction in anoxic sediments. Prior to the adjustment, both pre and post OAE-2 intervals averaged a $\delta^{238}U$ of 0.10‰, which is ~0.50‰ heavier than the average for modern seawater $\delta^{238}U$ (-0.41‰). After correction, the pre- and post- OAE-2 $\delta^{238}U$ values fall more in line with the modern seawater average as well as the pre- and post- OAE-2 $\delta^{238}U$ averages from Clarkson et al. (2018) and even the pre and post OAE-2 $\delta^{238}U$ average from Montoya-Pino et al.

(2010). However, the issue of the $\delta^{238}U$ profile for the OAE-2 interval was not that it was too positive compared to the Eastbourne section, instead it was too negative. This means when the 0.6‰ shift is applied to the OAE-2 interval, the negative most values recorded become -1.78 ± 0.17‰ and -1.60 ± 0.04‰. However, applying a shift of -0.6‰ to account for reduction into anoxic sediments during the OAE-2 interval does not agree with the ichnological data from the Bridge Creek limestone (Figure 7.7).

The OAE-2 interval in the Portland core begins just before the deposition of the Bridge Creek limestone. The transition from the lower Hartland shale into the younger Bridge Creek was accompanied by a major marine transgression worldwide and an overall shift in bottom water oxygen conditions in the WIS. The Hartland shale is documented as a well-laminated calcareous shale succession containing up to 10% total organic carbon (TOC) and interpreted as likely deposited under anoxic to low oxygen conditions (Sageman, 1989). Conversely, the younger Bridge Creek limestone unit is dominated by highly bioturbated beds within the lowermost section (Savrda, 1998), suggesting a significant increase in bottom water oxygenation. Trace element profiles of Mo through the Portland core exhibit a systematic shift at the Hartland Shale-Bridge Creek contact (Figure 7.2). Additional evidence from ichonological work by Savrda (1998) identified *Planolites*, *Chondrites*, and *Zoophycos* trace fossils through the early Bridge Creek limestone implying both bottom water sediments were oxygenated.

Instead of adjusting the $\delta^{238}U$ profile for the Portland core, if the same 0.6‰ shift would be applied to the Eastbourne section, the two $\delta^{238}U$ profiles become equally hard to reconcile. Therefore, I suggest a combination of adjustments is needed to reconcile the two $\delta^{238}U$ profiles. It appears that a shift of 0.6‰ for both the pre and post-OAE-2 intervals is an appropriate value to use. If there is any agreement between all studies focusing on the $\delta^{238}U$ record in the past, it is that the $\delta^{238}U$ of modern seawater is the best constrained measurement we have. Both Montoya-Pino et al. (2010) and Clarkson et al. (2018) refer back to the $\delta^{238}U$ of modern seawater as the likely value for seawater prior to OAE-2. For consistency, the shift of 0.6‰ is then reduced to 0.5‰ to reflect the necessary shift required to move both the pre- and post-OAE-2 $\delta^{238}U$ values of the Portland core to modern seawater $\delta^{238}U$. This appears to best represent the depositional environments and redox conditions during the pre and post interval in the Portland core. The 0.5‰ is easily justified for the pre OAE-2 interval due to evidence of a poorly oxygenated water column

from TE data, evidence of anoxic pore fluids due to high TOC, and lithological difference to the Bridge Creek limestone. The OAE-2 interval is not as easily explained because it occurred within the same unit as the OAE and evidence of an overall oxygenated water column come from TE data (Figure 7.8). However, Savrda (1998) interpreted oxygenation curve (IOC) for the Bridge Creek depicts a decrease in benthic oxygenation following the OAE-2 interval. Additionally, they determine an almost 50% decrease in bioturbation occurred throughout the middle Bridge Creek and lower yet for the uppermost section. Increased [Mo] after the OAE-2 also interval supports the shift to lower levels of bottom water O_2 (Figure 7.8). Therefore, it is assumed that the post OAE-2 interval underwent similar reductive processes as the pre-OAE-2 interval and a shift of 0.50‰ is not unreasonable. As for the OAE-2 interval itself, it appears that no shift is needed to reconcile the $\delta^{238}U$ profile of the Portland core, implying that the $\delta^{238}U$ profile through the OAE-2 interval is directly recording the $\delta^{238}U$ of coeval seawater. TE data and ichnological data from Savrda (1998) **(**Figure 7.7) all suggest bottom water and pore fluid conditions were conducive to capturing the $\delta^{238}U$ of seawater during OAE-2. Evidence for extensive bioturbation within the Bridge Creek Limestone (Figure 7.7) supports the possibility of a deeper oxygen penetration depth. As discussed, a longer reductive pathway due to deeper oxygen penetration would in theory prevent the alteration of the PCP $\delta^{238}U$ value during deposition. In addition to bioturbation, the connection of the WIS to both the PNAO and to Boreal waters in the north and evidence of increased benthic foraminiferal diversity during the OAE suggests the existence of a well-established bottom water renewal system during the event (Elderbak and Leckie, 2016), which would not have been conducive to allowing anoxic conditions to establish within the water column. Whole rock geochemistry also supports the apparent re-oxygenation of the upper Bridge Creek Limestone (Figure 7.8) through the interval. Mo concentrations depict a drastic change in the amount of available oxygen at the transition shifting from an average [Mo] of 20 ppm through the Hartland Shale to an average of 3.7 ppm for the Bridge Creek Limestone. Based on the trend, the [Mo] data does appear to exhibit a relative increase of dissolved oxygen within the water column during deposition of the Bridge Creek Limestone.

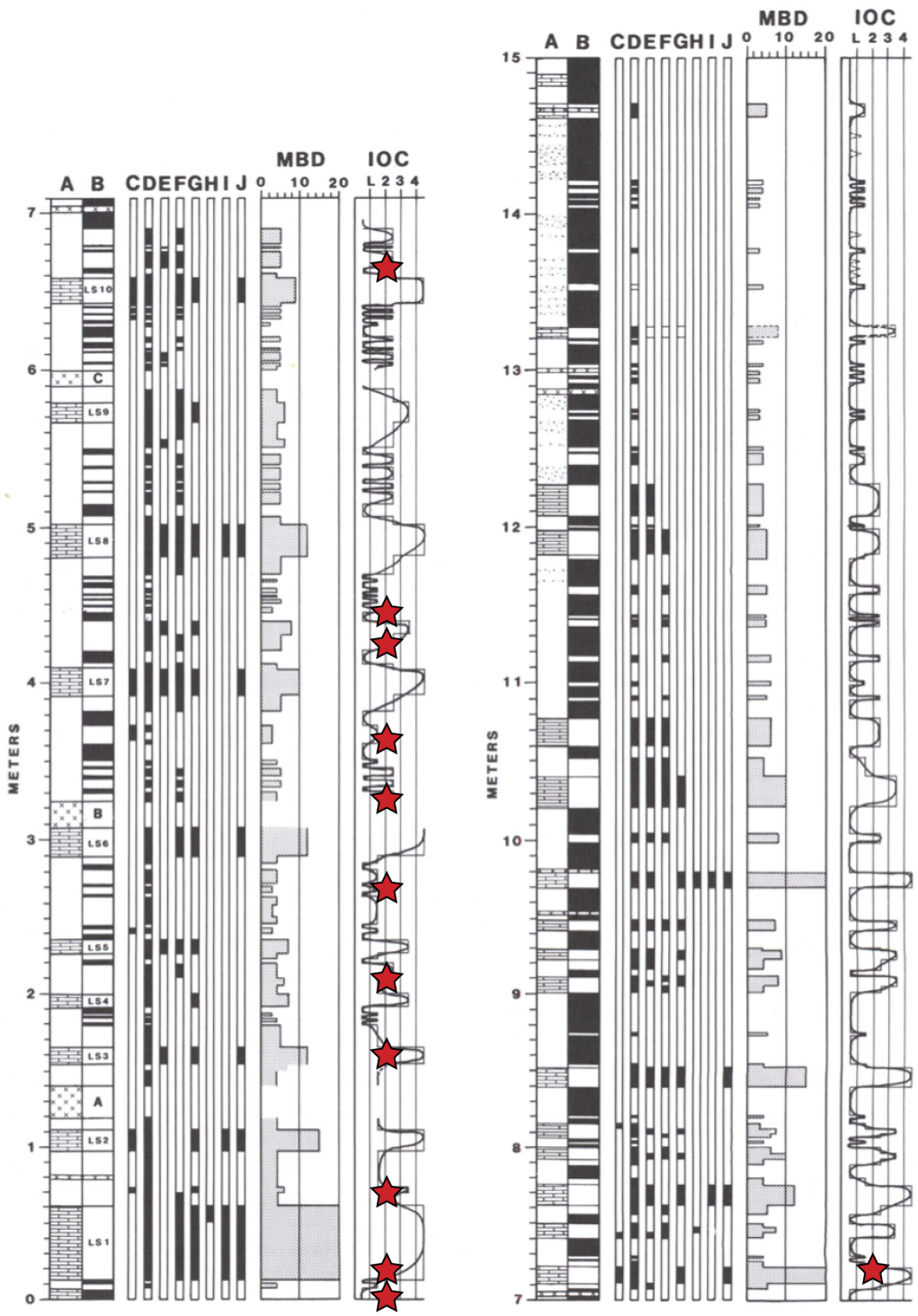

Figure 7.7 Maximum burrow diameter (MBD) and interpreted oxygen content (IOC) for the entire Bridge Creek Limestone from Savrda (1998). MBD is used as an interpretation of the amount of available oxygen. The larger the burrow diameter, the deeper the oxygen penetration zone. As such, evidence of bioturbation and increased burrow diameter suggests deposition of the Bridge Creek Limestone occurred under generally well-oxygenated conditions. IOC is inferred as the level of oxygen required for individual ichnocoenoses (ichnofossil communities) to exist. Ichnocoenoses were erected based on interpreted oxygen content (Savrda, 1998). Red stars denote sample locations.

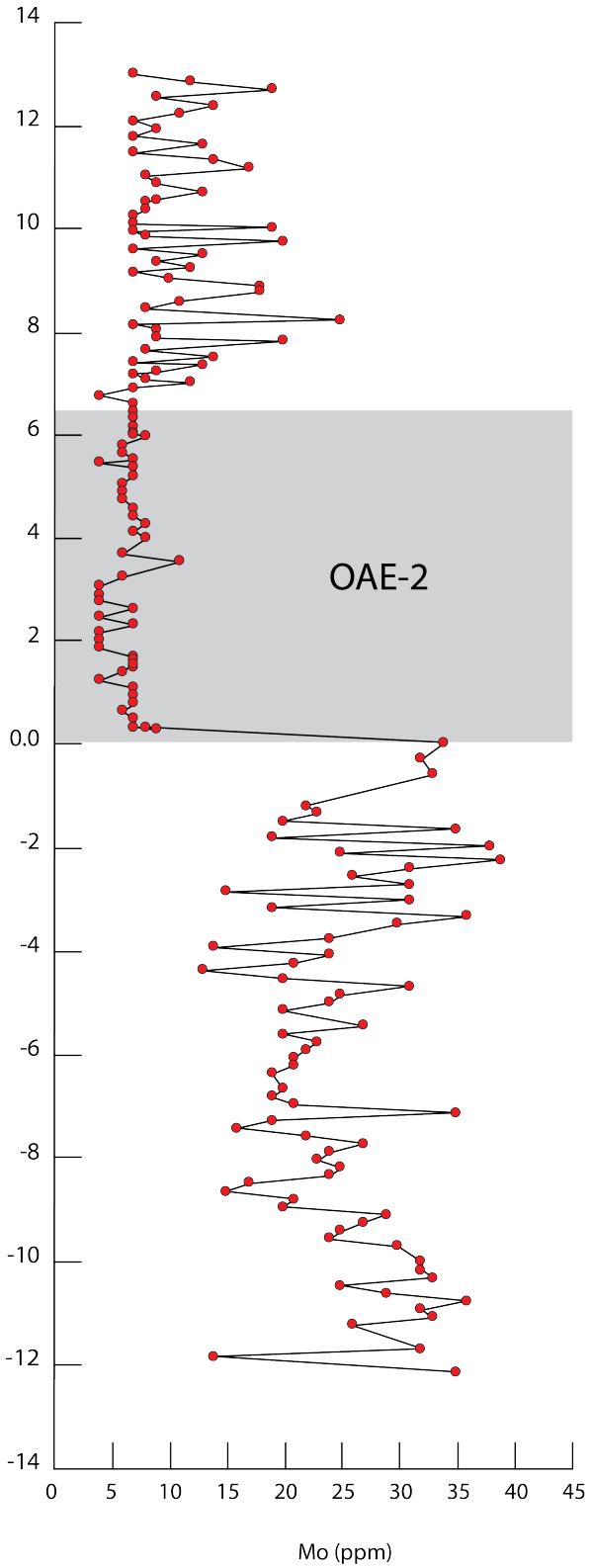

Figure 7.8 [Mo] profile for the USGS PO #1 Core. Grey box denotes the OAE-2 interval for the core.

Despite correcting the two intervals to reflect seawater a difference of -0.64‰ still exists between the two $\delta^{238}U$ profiles. If a correction is applied to the Eastbourne section as well, then it is possible to reconcile the two profiles. Adjusting the OAE-2 interval to account for reduction due to syndepositional diagenesis (0.2 to 0.4‰; Romaniello et al. 2013) the heaviest $\delta^{238}U$ value shifts somewhere between -1.11‰ and -0.91‰ from an original measurement of -0.71‰. This new range of $\delta^{238}U$ values aligns well within error of the two heaviest $\delta^{238}U$ values from the Portland core (-1.18 ± 0.17 ‰ and -1.00 ± 0.04‰) (Figure 7.9).

This interpretation is not without complications. Much of the work done on the Eastbourne section suggests that the effects of diagenesis are minimal throughout the section. Pearce et al. (2009) points to the existence of many bioturbated zones throughout the Eastbourne section and low TOC values (<0.2%) as reasons for little to no alteration of the carbonate sediments. Well ventilated bottom waters throughout the Anglo-Paris Basin (Gale et al., 2000; Keller et al., 2001) and evidence for high concentrations of Mn within the sediments suggested deposition under an oxic water column (Jarvis et al., 2001; Clarkson et al., 2018). The lack of proxy evidence for pore fluid anoxia within any part of the Eastbourne section poses a problem for this interpretation. Although, Gale et al. (2000) and Keller et al. (2001) measured low TOC values for the Eastbourne section, Gale et al.'s (2000) TOC profile depicts the highest concentration of organic matter during the latest stages of the Plenus Cold Event and upper beds of the Plenus Marls. A slight increase in TOC is explained by an increase in paleoproductivity throughout the latter half of the Plenus Cold Event by the incursion of well oxygenated boreal waters (Jenkyns et al., 2017). However, it must be considered that the organic carbon preserved in sediment is only a fraction of the original carbon that was originally deposited, the rest having been re-mineralized at the sediment water interface and within the sediment itself (Figure 7.10).

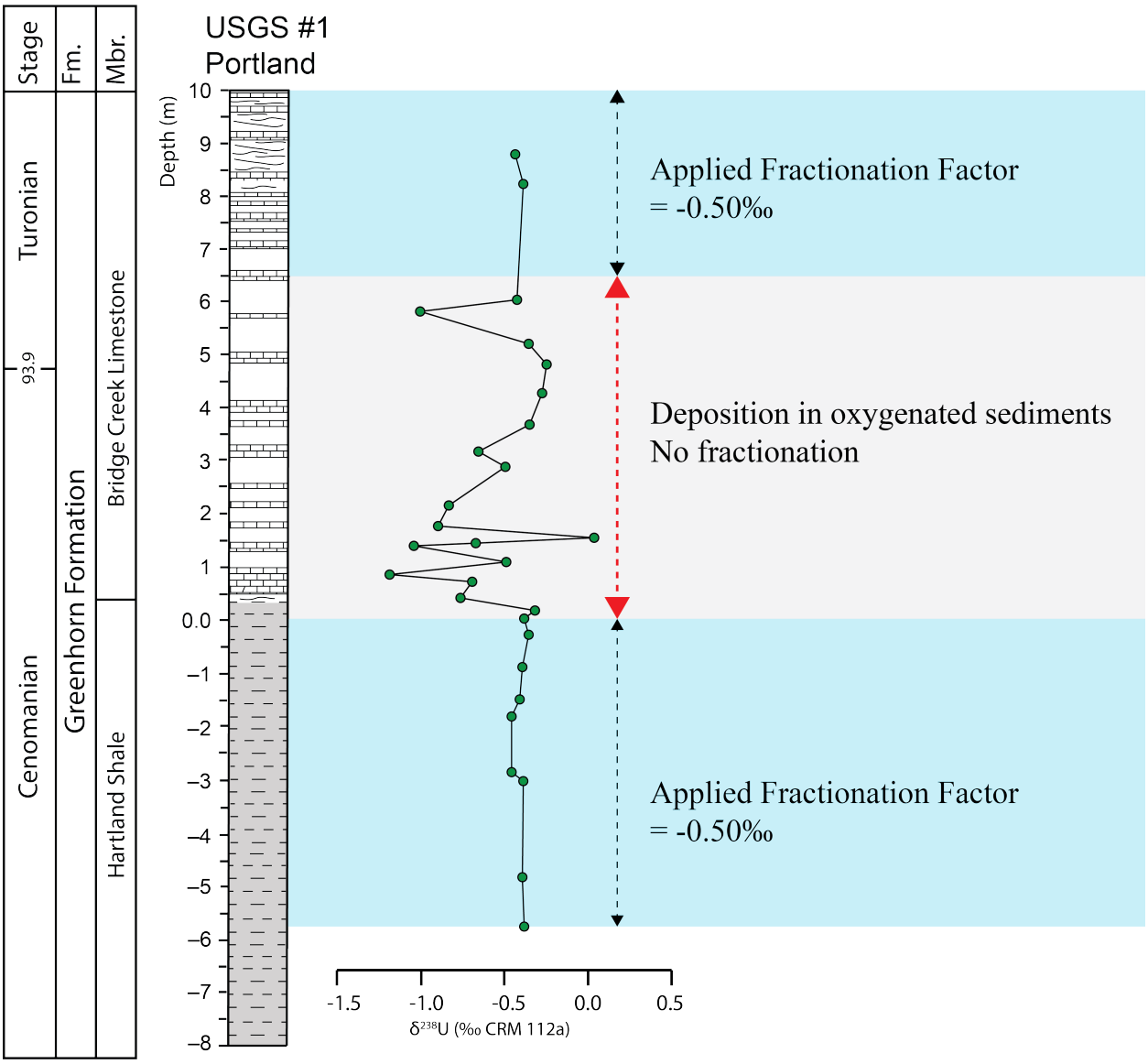

Figure 7.9 The adjusted $\delta^{238}U$ profile for the Portland core. Blue boxes indicate samples that were shifted by -0.50‰ due to reduction in anoxic sediments. The grey box in between represents the entire OAE-2 interval in the Portland core and the section that is interpreted to be unaffected by reduction under anoxic sediments or by syndepositional diagenesis. The now abnormally positive $\delta^{238}U$ value associated with the peak of the PCE is likely the effect of reoxygenation of anoxic sediments during the event. The event would have liberated ^{238}U heavy uranium from the sediment and into the water column driving the $\delta^{238}U$ of seawater to a more positive value. A similar data point can be found in the Eastbourne section during the peak PCE interval.

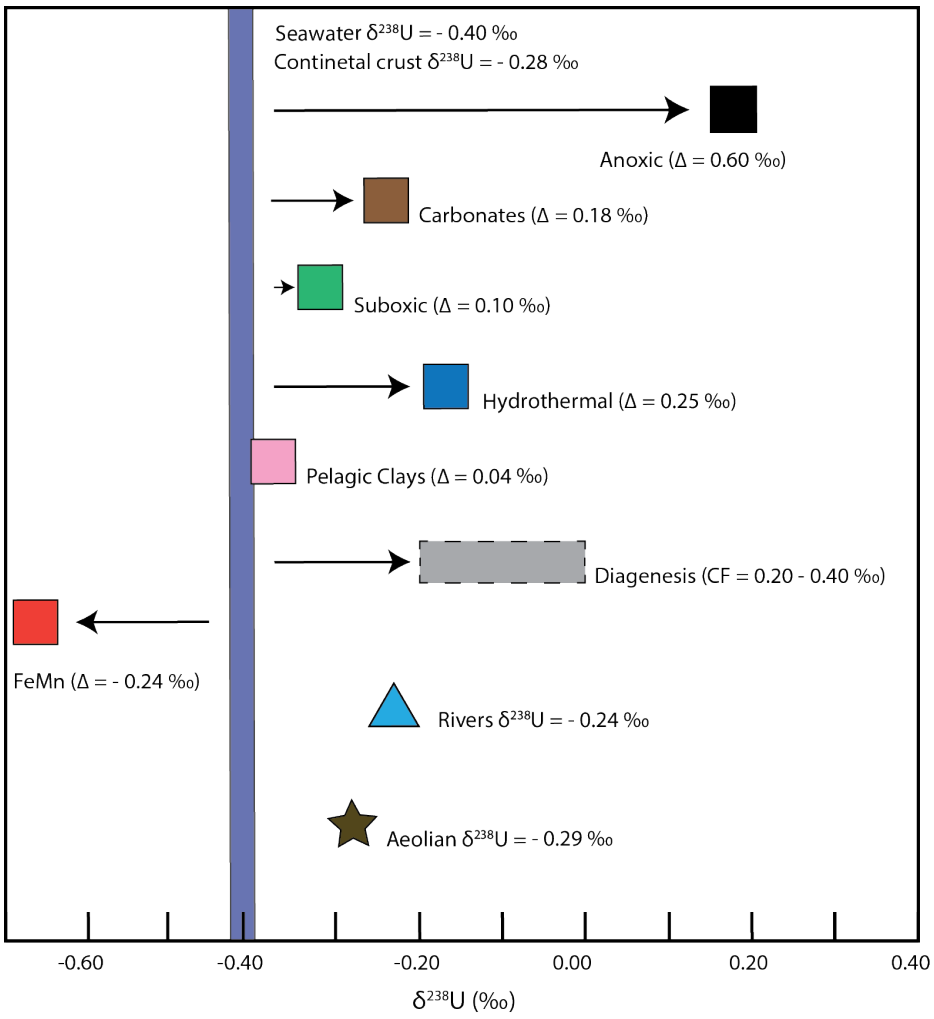

Figure 7.10 Modern U sources and sinks and their associated fractionation factors. Alteration due to diagenesis is accounted for as a correction factor (CF). Fractionation factors illustrate the lack of mechanisms available to justify the difference between this studies $\delta^{238}U$ curve and the Eastbourne section. No mechanism, other than adsorption to FeMn under oxygenated waters can shift the $\delta^{238}U$ profile of the Eastbourne section to a more negative value. Values come from Table 6.3 and references within.

7.3 Alternative explanations for the multiple $\delta^{238}U$ profiles

An alternative explanation may come from the rapid removal of uranium from seawater. The expectation is that $\delta^{238}U$ signature of seawater should be uniform throughout. Depending on the sediment type and the redox conditions of those sediments, the seawater $\delta^{238}U$ profile should easily be resolved from the measured profiles. The only caveat to that principle is whether or not the water the sediment deposited in is reflective of global seawater. Meaning, a $\delta^{238}U$ profile may not be representative of the global oceans, instead it reflects the water from which it is reduced. This may explain the differences between all three studies (Figure 7.2). Instead of each capturing

seawater $\delta^{238}U$, they all reflect a separate reservoir value. It may be possible that global circulation models for OAE-2 are wrong and seaways and oceans we understood to be well connected were actually more restricted. The negative $\delta^{238}U$ excursion at the onset of OAE-2 and positive excursion during the PCE occurred in 140,000 and 30,000 years, respectively. These timelines are significantly shorter than the residence time of U in modern oceans (400,000 years) and may reflect limited ocean mixing for the study area. As a result, the difference in the $\delta^{238}U$ profiles may reflect a reservoir effect.

7.4 Implications of OAE-2 ocean redox conditions

Recently Clarkson et al. (2018) approached the issue of quantifying the extent of the increase in anoxia during OAE-2 using the uranium isotope proxy coupled with biogeochemical modeling of the C, P, and U cycles, proposing that between 8% and 15% of the global seafloor was overlain by anoxic waters during OAE-2. Montoya-Pino et al. (2010) estimated the extent of anoxia during OAE-2 was much smaller, around 1 to 2%. Using the same approach as Montoya-Pino et al. (2010) the $\delta^{238}U$ excursion from the Portland core can be modelled and an estimate for marine anoxia can be calculated.

Based on the uranium mass balance model presented from Dunk et al. (2002) and the assumption that the marine U isotope cycle is in steady state (a system where the total inputs, concentration and isotopic signature, are equal to the total outputs of the system) the following mass balance equation can be used:

$$\delta^{238}U_{sw} = [(\delta^{238}U_{river}\, F_{river}) + (\delta^{238}U_{a}\, F_{a})] - \sum \Delta^{238}U_{sink}\ J_{sink} \quad \text{(6.3)}$$

where $\delta^{238}U_{sw}$ is equal to the predicted $\delta^{238}U$ seawater value, $\delta^{238}U_{river}$ is equal to the $\delta^{238}U$ of the riverine input, $\delta^{238}U_{a}$ is equal to the aeolian input. F_{river} and F_{a} are the respective fractions of the total flux associated with two inputs. The $\Delta^{238}U_{sink}$ is equal to the fractionation factor associated with the particular sink (e.g., the anoxic sink has a fractionation factor of 0.60‰), and finally J_{sink} is the flux associated with a particular sink. When modern values are substituted in for the sources and sinks, as well as their respective fractionation factors (Table 7.1), a predicted $\delta^{238}U$ for seawater of -0.40‰ is calculated, which matches measured $\delta^{238}U$ seawater values from around the world (-0.41 to -0.39‰). As discussed above, for the Cenomanian-Turonian the $\delta^{238}U$ of seawater

is assumed to be equal to the modern value.

Using the Montoya-Pino et al. (2010) equation, it becomes obvious that the measured $\delta^{238}U$ OAE-2 values from this study (i.e., -1.04 ± 0.04‰) are not within the realm of possibility (Table 7.2). The heaviest $\delta^{238}U$ value calculated by the model (i.e., -0.83‰) would require complete ocean floor anoxia. Not only is this unrealistic for this time period, but also highlights a major misstep in previous $\delta^{238}U$ studies. The uranium mass balance budget is a complicated system that still has many unanswered questions. The process of diffusive transport is a perfect example of how complicated the U isotope system is and how little is still known about the redox change uranium is subjected to during sequestration. Until these details are addressed, it is limiting to model $\delta^{238}U$ excursions. Even the approach taken by Clarkson et al. (2018) is limited in what it can achieve, for example, their model benefits from additional constraints put in place by carbon and phosphorus cycles. However, this improvement does not explain the larger $\delta^{238}U$ excursion recorded in the Portland section. Nevertheless, results from $\delta^{238}U$ modeling do seem to guide the direction of future research, but at its current state there are several unknowns that reduce the reliability of interpretations that come from modeling $\delta^{238}U$ values.

Table 7.1 Table of variables for both the steady state and non-steady state models.

Source	$\delta^{238}U$ (‰)		Flux (Mmol/yr)[1]	(+/-)	Fraction	FF x Fract.
Riverine	-0.24[2,8]	-	42	14.5	96%	-0.23
Aeolian	-0.29[8]	-	1.8	1.1	4%	-0.01
Sink	$\Delta_{reservoir-SW}$ (‰)	$\delta^{238}U$ (‰)	Flux (Mmol/yr)[1]	(+/-)	Fraction	FF x Fract.
Anoxic	0.60[6]	0.18	11.6	6	21%	0.13
Carbonate	0.18[9]	-0.24	13.3	5.6	24%	0.04
Sub oxic	0.10[3,8]	-0.32	15.3	10.6	28%	0.03
Hydrothermal	0.25[7]	-0.17	1.9	3.3	3%	0.01
FeMn	-0.24[2,3,4,8]	-0.66	1	0.8	2%	0.00
Pelagic clays	0.04[7]	-0.38	0.4	0.2	1%	0.00
Coastal Zone retention	-0.24[8]	-0.18	11.2	5.6	20%	-0.05

(1) Dunk et al. (2002); (2) Stirling et al. (2007); (3) Weyer et al. (2008); (4) Brennecka et al. (2011); (5) Romaniello et al. (2013); (6) Andersen et al. (2014); (7) Andersen et al. (2015); (8) Tissot and Dauphas (2015); (9) Chen et al. (2017)

Table 7.2 Steady state mass balance model results.

Modern	% seafloor anoxic	Anoxic Flux (Mmol/yr)	% Total output	$\delta^{238}U_{sw}$ predicted
Based on Dunk et al. (2010) outputs	0.35%	11.6	21%	-0.40
Based on Dunk et al. (2010) inputs	0.35%	11.6	27%	-0.50
Montoya-Pino et al. (2010)	% seafloor anoxic	Anoxic Flux (Mmol/yr)	% Total output	$\delta^{238}U_{sw}$ predicted
	1.00%	33.1	43%	-0.53
	2.00%	66.2	61%	-0.62
Clarkson et al. (2018)	% seafloor anoxic	Anoxic Flux (Mmol/yr)	% Total output	$\delta^{238}U_{sw}$ predicted
	8.00%	265.0	86%	-0.76
	10.00%	331.2	88%	-0.78
	12.00%	397.4	90%	-0.79
	14.00%	463.7	91%	-0.79
	15.00%	496.8	92%	-0.80
Owens et al. (2013)	% seafloor anoxic	Anoxic Flux (Mmol/yr)	% Total output	$\delta^{238}U_{sw}$ predicted
	2.50%	82.8	66%	-0.65
	3.00%	99.4	70%	-0.67
	3.50%	115.9	73%	-0.69
	4.00%	132.5	75%	-0.70
	4.50%	149.0	78%	-0.72
	5.00%	165.6	79%	-0.73
This Study	% seafloor anoxic	Anoxic Flux (Mmol/yr)	% Total output	$\delta^{238}U_{sw}$ predicted
	50%	1656	97%	-0.83
	75%	2484	98%	-0.83
	100%	3312	99%	-0.83

7.5 Implications for the U Isotope Proxy

The continued use of the uranium isotope proxy seems promising. It reacts as expected to major changes in the redox state of the oceans. As such, it allows the ability for reliable, albeit broad scale interpretations to be made. Although the three $\delta^{238}U$ profiles presented in this paper record excursions of differing magnitudes, the somewhat similar profiles of Clarkson et al. (2018) and this study suggests we are close to a singular $\delta^{238}U$ profile for OAE-2. Unlike similar redox proxies, such as molybdenum, U appears to be susceptible to minute changes in the redox state of a system and it appears to dependably record these changes making it an ideal tool to study the complex redox history of the Earth's oceans. Yet our ability to interpret the $\delta^{238}U$ record is dependent on our capability to quantify the chemical changes uranium is subjected to during reductive processes. The work done by Montoya-Pino et al. (2010) and this research highlights the difficulties of interpreting the paleo-seawater $\delta^{238}U$ record. Researching modern environments is a huge step towards understanding the uranium isotope system. Establishing how the system operates in modern oceans allows us to define a baseline for comparison. Once understood, research studying ancient oceans will be more capable of drawing realistic conclusions for how an event such as OAE-2 was able to develop and its long-lasting effects. A substantial part of the present and ongoing research being produced is looking at the effects of post depositional alteration in marine carbonates (Romaniello et al., 2013; Hood et al., 2016; Lau et al., 2017; Clarkson et al., 2018; Chen et al., 2017). The differences between the $\delta^{238}U$ profile for the USGS Portland #1 core and the potentially diagenetically unaltered profile from Eastbourne is an example of the gap that still exists in our understanding.

CHAPTER 8

Conclusions

The U isotope proxy is a promising tool to decipher the redox state of the ancient oceans. This research analyzed a suite of samples from the Bridge Creek Limestone and Hartland Shale located in WIS, deposited during OAE-2 for U isotopes, [U] and [Th]. The data capture the rise and fall of OAE-2 within the $\delta^{238}U$ profile. There are only two publications that investigate the effects of an expanding anoxic sink during OAE-2 to the seawater $\delta^{238}U$ profile; Montoya-Pino et al. (2010) and Clarkson et al. (2018). By analyzing and comparing the $\delta^{238}U$ profiles of each publication to the studied core, it becomes clear that the U isotope system can reliably record changes to the relative extent of anoxia in the oceans.

The Portland core exhibits a large negative $\delta^{238}U$ excursion equal to 1.19‰ during OAE-2. An excursion of this magnitude cannot be explained by any one process, but rather it requires combining multiple processes to account for the large offset. Considering the depositional environment and the redox setting during deposition of the Hartland Shale and Bridge Creek Limestone, one can offset the $\delta^{238}U$ signal by accounting for the magnitude of fractionation associated with the different processes making it possible to reduce the size of the excursion. Assuming deposition before and after the OAE occurred under more reducing conditions (Δ = +0.5 to +0.6‰), the $\delta^{238}U$ seawater average for those times would not be ~ 0.1‰ but rather -0.40‰, or similar to the modern seawater $\delta^{238}U$ value. Lithological evidence, ichnofossil evidence, and other research (Clarkson et al., 2018) all support a $\delta^{238}U$ of seawater for the pre and post-OAE intervals to be similar to the modern oceans, leaving the size of the negative $\delta^{238}U$ excursion in the Portland core to be 0.64‰. Adjusting the $\delta^{238}U$ profile from the Eastbourne section (Clarkson et al., 2018) accounts for syndepositional diagenesis due to pore fluid reduction during the OAE-2 interval. With this adjustment, it becomes possible to resolve the two differing $\delta^{238}U$ profiles. As a result, the $\delta^{238}U$ profile for the OAE-2 interval as recorded in the USGS #1 Portland Core is representative of the coeval seawater $\delta^{238}U$ value during the event.

8.1 Suggestions for future work

Deciphering the $\delta^{238}U$ profile for OAE-2 would benefit from more sampling within the WIB. Targeting sample sites along the long axis of the WIS would be an interesting addition to the research. It may provide insight on how the $\delta^{238}U$ profile evolves as the overlying water column shifts to reflect the water chemistry of the nearest open water source. It would also confirm one way or another the $\delta^{238}U$ profile from the Portland core. The usefulness of Savrda (1998) IOC profiles and field observations to this research suggests future studies should be done in conjunction with comprehensive ichnological work. The addition of an experienced ichnologist identifying the exact level where the sediments transferred to and from anoxic and oxic conditions would add significant value to the research in sediment. Additional suggestions include dealing with differences in $\delta^{238}U$ between samples of carbonate cements, and within different growth zones (Hood et al., 2016). Future work would benefit from testing the degree of alteration (e.g., petrographic analysis and cathodoluminescence) on a sample by sample basis, as well as, considering the use of other well-established geochemical proxies to help contextualize water column redox dynamics, possible detrital influences and any other complicating factor as a way of improving estimates of diagenetic resets, when working on a smaller scale.

References

Abe, M., Suzuki, T., Fujii, Y., Hada, M., and Hirao, K., 2008, An ab initio molecular orbital study of the nuclear volume effects in uranium isotope fractionations: The Journal of chemical physics, v. 129, p. 164309.

Algeo, T.J., and Lyons, T.W., 2006, Mo–total organic carbon covariation in modern anoxic marine environments: Implications for analysis of paleoredox and paleohydrographic conditions: Paleoceanography, v. 21.

Andersen, M.B., Elliott, T., Freymuth, H., Sims, K.W.W., Niu, Y., and Kelley, K.A., 2015, The terrestrial uranium isotope cycle: Nature, v. 517, p. 356–359, doi: 10.1038/nature14062.

Andersen, M.B., Romaniello, S., Vance, D., Little, S.H., Herdman, R., and Lyons, T.W., 2014, A modern framework for the interpretation of 238 U/235 U in studies of ancient ocean redox: Earth and Planetary Science Letters, v. 400, p. 184–194.

Anderson, R.F., Fleisher, M.Q., and LeHuray, A.P., 1989, Concentration, oxidation state, and particulate flux of uranium in the Black Sea: Geochimica et Cosmochimica Acta, v. 53, p. 2215–2224.

Arthur, M.A., Schlanger, S.O., and Jenkyns, H.C., 1987, The Cenomanian-Turonian Oceanic Anoxic Event, II. Palaeoceanographic controls on organic-matter production and preservation: Geological Society, London, Special Publications, v. 26, p. 401–420, doi: 10.1144/GSL.SP.1987.026.01.25.

Banner, J.L., and Hanson, G.N., 1990, Calculation of simultaneous isotopic and trace element variations during water-rock interaction with applications to carbonate diagenesis: Geochimica et Cosmochimica Acta, v. 54, p. 3123–3137, doi: 10.1016/0016-7037(90)90128-8.

Barnes, C.E., and Cochran, J.K., 1990, Uranium removal in oceanic sediments and the oceanic U balance: Earth and Planetary Science Letters, v. 97, p. 94–101.

Bekker, A., Holland, H.D., Wang, P.-L., Rumble, D., Stein, H.J., Hannah, J.L., Coetzee, L.L., and Beukes, N.J., 2004, Dating the rise of atmospheric oxygen: Nature, v. 427, p. 117–120, doi: 10.1038/nature02260.

Berner, R.A., and Canfield, D.E., 1989, A new model for atmospheric oxygen over Phanerozoic time: American Journal of Science, v. 289, p. 333–361.

Blakey, R., 2011, Paleogeography and geologic evolution of North America: On-line Accesible: http://jan. ucc. nau. edu/~ rcb7/nam. html [Acceso: 30/05/2011],.

Bralower, T.J., and Thierstein, H.R., 1984, Low productivity and slow deep-water circulation in mid-Cretaceous oceans: Geology, v. 12, p. 614–618, doi: 10.1130/0091-7613(1984)12<614:LPASDC>2.0.CO;2.

Brennecka, G.A., Borg, L.E., Hutcheon, I.D., Sharp, M.A., and Anbar, A.D., 2010, Natural variations in uranium isotope ratios of uranium ore concentrates: Understanding the 238U/235U fractionation mechanism: Earth and Planetary Science Letters, v. 291, p. 228–233, doi: 10.1016/j.epsl.2010.01.023.

Brennecka, G.A., Wasylenki, L.E., Bargar, J.R., Weyer, S., and Anbar, A.D., 2011, Uranium Isotope Fractionation during Adsorption to Mn-Oxyhydroxides: Environmental Science & Technology, v. 45, p. 1370–1375, doi: 10.1021/es103061v.

Bura-Nakić, E., Andersen, M.B., Archer, C., de Souza, G.F., Marguš, M., and Vance, D., 2018, Coupled Mo-U abundances and isotopes in a small marine euxinic basin: Constraints on processes in euxinic basins: Geochimica et Cosmochimica Acta, v. 222, p. 212–229, doi: 10.1016/j.gca.2017.10.023.

Chen, X., Romaniello, S.J., and Anbar, A.D., 2017, Uranium isotope fractionation induced by aqueous speciation: Implications for U isotopes in marine CaCO3 as a paleoredox proxy: Geochimica et Cosmochimica Acta, v. 215, p. 162–172, doi: 10.1016/j.gca.2017.08.006.

Clark, S.K., and Johnson, T.M., 2008, Effective Isotopic Fractionation Factors for Solute Removal by Reactive Sediments: A Laboratory Microcosm and Slurry Study: Environmental Science & Technology, v. 42, p. 7850–7855, doi: 10.1021/es801814v.

Clarkson, M.O., Stirling, C.H., Jenkyns, H.C., Dickson, A.J., Porcelli, D., Moy, C.M., Strandmann, P.A.E.P. von, Cooke, I.R., and Lenton, T.M., 2018, Uranium isotope evidence for two episodes of deoxygenation during Oceanic Anoxic Event 2: Proceedings of the National Academy of Sciences, p. 201715278, doi: 10.1073/pnas.1715278115.

Curiale, J.A., 1994, Geochemical anomalies at the Cenomanian-Turonian boundary, northwest New Mexico: Organic Geochemistry, v. 22, p. 487–500, doi: 10.1016/0146-6380(94)90121-X.

De Boeck, H.J., Lemmens, C.M.H.M., Gielen, B., Bossuyt, H., Malchair, S., Carnol, M., Merckx, R., Ceulemans, R., and Nijs, I., 2007, Combined effects of climate warming and plant diversity loss on above- and below-ground grassland productivity: Environmental and Experimental Botany, v. 60, p. 95–104, doi: 10.1016/j.envexpbot.2006.07.001.

Döös, K., Nilsson, J., Nycander, J., Brodeau, L., and Ballarotta, M., 2012, The World Ocean Thermohaline Circulation: Journal of Physical Oceanography, v. 42, p. 1445–1460, doi: 10.1175/JPO-D-11-0163.1.

Dunk, R., Mills, R., and Jenkins, W., 2002, A reevaluation of the oceanic uranium budget for the Holocene: Chemical Geology, v. 190, p. 45–67.

Eicher, D.L., 1967, Depth of the Greenhorn Sea, *in* Paleoenvironments of the Cretaceous Seaway in the Western Interior—A symposium. Colorado School of Mines, Golden, p. 145–172.

Eicher, D.L., and Worstell, P., 1970, Cenomanian and Turonian Foraminifera from the Great Plains, United States: Micropaleontology, v. 16, p. 269–324, doi: 10.2307/1485079.

Elderbak, K., and Leckie, R.M., 2016, Paleocirculation and foraminiferal assemblages of the Cenomanian–Turonian Bridge Creek Limestone bedding couplets: productivity vs. dilution during OAE2: Cretaceous Research, v. 60, p. 52–77.

Föllmi, K.B., 2012, Early Cretaceous life, climate and anoxia: Cretaceous Research, v. 35, p. 230–257, doi: 10.1016/j.cretres.2011.12.005.

Forster, A., Schouten, S., Moriya, K., Wilson, P.A., and Sinninghe Damsté, J.S., 2007, Tropical warming and intermittent cooling during the Cenomanian/Turonian oceanic anoxic event 2: Sea surface temperature records from the equatorial Atlantic: Paleoceanography, v. 22.

Friedrich, O., Erbacher, J., and Mutterlose, J., 2006, Paleoenvironmental changes across the Cenomanian/Turonian boundary event (oceanic anoxic event 2) as indicated by benthic foraminifera from the Demerara Rise (ODP Leg 207): Revue de micropaléontologie, v. 49, p. 121–139.

Fujii, Y., Higuchi, N., Haruno, Y., Nomura, M., and Suzuki, T., 2006, Temperature dependence of isotope effects in uranium chemical exchange reactions: Journal of nuclear science and technology, v. 43, p. 400–406.

Gale, A.S., Christensen, W.K., Gale, A.S., and others, 1996, Occurrence of the belemnite Actinocamax plenus in the Cenomanian of SE France and its significance, *in* Bulletin of the Geological Society of Denmark, Citeseer, http://citeseerx.ist.psu.edu/viewdoc/summary?doi=10.1.1.574.3517 (accessed October 2017).

German, C.R., and von Damm, K.L., 2003, Hydrothermal Processes: Treatise on Geochemistry, v. 6, p. 625, doi: 10.1016/B0-08-043751-6/06109-0.

Glasspool, I.J., and Scott, A.C., 2010, Phanerozoic concentrations of atmospheric oxygen reconstructed from sedimentary charcoal: Nature Geoscience, v. 3, p. 627–630, doi: 10.1038/ngeo923.

Hay, W.W., and Floegel, S., 2012, New thoughts about the Cretaceous climate and oceans: Earth-Science Reviews, v. 115, p. 262–272, doi: 10.1016/j.earscirev.2012.09.008.

van Helmond, N.A.G.M., Ruvalcaba Baroni, I., Sluijs, A., Sinninghe Damsté, J.S., and Slomp, C.P., 2014, Spatial extent and degree of oxygen depletion in the deep proto-North Atlantic basin during Oceanic Anoxic Event 2: Geochemistry, Geophysics, Geosystems, v. 15, p. 4254–4266, doi: 10.1002/2014GC005528.

Henderson, G.M., and Anderson, R.F., 2003, The U-series toolbox for paleoceanography: Reviews in Mineralogy and Geochemistry, v. 52, p. 493–531.

Hetzel, A., Böttcher, M.E., Wortmann, U.G., and Brumsack, H.-J., 2009, Paleo-redox conditions during OAE 2 reflected in Demerara Rise sediment geochemistry (ODP Leg 207): Palaeogeography, Palaeoclimatology, Palaeoecology, v. 273, p. 302–328, doi: 10.1016/j.palaeo.2008.11.005.

Hetzel, A., Brumsack, H.-J., Schnetger, B., and Böttcher, M.E., 2006, Inorganic geochemical characterization of lithologic units recovered during ODP Leg 207 (Demerara Rise), *in* Proc. ODP Sci. Results, v. 207, p. 1–37.

Holmden, C., Amini, M., and Francois, R., 2015, Uranium isotope fractionation in Saanich Inlet: A modern analog study of a paleoredox tracer: Geochimica et Cosmochimica Acta, v. 153, p. 202–215, doi: 10.1016/j.gca.2014.11.012.

Holmden, C., Jacobson, A.D., Sageman, B.B., and Hurtgen, M.T., 2016, Response of the Cr isotope proxy to Cretaceous Ocean Anoxic Event 2 in a pelagic carbonate succession from the Western Interior Seaway: Geochimica et Cosmochimica Acta, v. 186, p. 277–295.

Hood, A. v S., Planavsky, N.J., Wallace, M.W., Wang, X., Bellefroid, E.J., Gueguen, B., and Cole, D.B., 2016, Integrated geochemical-petrographic insights from component-selective δ238U of Cryogenian marine carbonates: Geology, v. 44, p. 935–938, doi: 10.1130/G38533.1.

Huber, B.T., Norris, R.D., and MacLeod, K.G., 2002, Deep-sea paleotemperature record of extreme warmth during the Cretaceous: Geology, v. 30, p. 123–126, doi: 10.1130/0091-7613(2002)030<0123:DSPROE>2.0.CO;2.

Jefferies, R.P.S., 1961, The palaeoecology of the: Actinocamax plenus, p. 609–647.

Jefferies, R.P.S., 1963, The stratigraphy of the Actinocamax plenus subzone (Turonian) in the Anglo-Paris Basin: Proceedings of the Geologists' Association, v. 74, p. 1–IN4.

Jenkyns, H.C., 2010, Geochemistry of oceanic anoxic events: Geochemistry, Geophysics, Geosystems, v. 11, p. Q03004, doi: 10.1029/2009GC002788.

Jenkyns, H.C., Dickson, A.J., Ruhl, M., and van den Boorn, S.H.J.M., 2017, Basalt-seawater interaction, the Plenus Cold Event, enhanced weathering and geochemical change: deconstructing Oceanic Anoxic Event 2 (Cenomanian–Turonian, Late Cretaceous): Sedimentology, v. 64, p. 16–43, doi: 10.1111/sed.12305.

Kauffman, E.G., 1977, GEOLOGICAL AND BIOLOGICAL OVERVIEW: WESTERN INTERIOR CRETACEOUS BASIN: The Mountain Geologist, http://archives.datapages.com/data/rmag/mg/1977/kauffman.htm (accessed August 2016).

Keller, G., and Pardo, A., 2004, Age and paleoenvironment of the Cenomanian–Turonian global stratotype section and point at Pueblo, Colorado: Marine Micropaleontology, v. 51, p. 95–128.

Ku, T.-L., Knauss, K.G., and Mathieu, G.G., 1977, Uranium in open ocean: concentration and isotopic composition: Deep Sea Research, v. 24, p. 1005–1017.

Kuypers, M.M.M., Lourens, L.J., Rijpstra, W.I.C., Pancost, R.D., Nijenhuis, I.A., and Sinninghe Damsté, J.S., 2004, Orbital forcing of organic carbon burial in the proto-North Atlantic

during oceanic anoxic event 2: Earth and Planetary Science Letters, v. 228, p. 465–482, doi: 10.1016/j.epsl.2004.09.037.

Lau, K.V., Macdonald, F.A., Maher, K., and Payne, J.L., 2017, Uranium isotope evidence for temporary ocean oxygenation in the aftermath of the Sturtian Snowball Earth: Earth and Planetary Science Letters, v. 458, p. 282–292.

Leckie, R.M., Yuretich, R.F., West, O.L.O., Finkelstein, D., and Schmidt, M., 1998, Paleoceanography of the Southwestern Western Interior Sea During the Time of the Cenomanian-Turonian Boundary (Late Cretaceous):, http://archives.datapages.com/data/sepm_sp/csp6/Paleoceanography_of_the_Southwestern.htm (accessed February 2018).

Meisner, J.D., Goodier, J.L., Regier, H.A., Shuter, B.J., and Christie, W.J., 1987, An Assessment of the Effects of Climate Warming on Great Lakes Basin Fishes: Journal of Great Lakes Research, v. 13, p. 340–352, doi: 10.1016/S0380-1330(87)71656-6.

Miller, K.G., Kominz, M.A., Browning, J.V., Wright, J.D., Mountain, G.S., Katz, M.E., Sugarman, P.J., Cramer, B.S., Christie-Blick, N., and Pekar, S.F., 2005, The Phanerozoic Record of Global Sea-Level Change: Science, v. 310, p. 1293–1298, doi: 10.1126/science.1116412.

Monaco, S.L., López, L., Rojas, H., Garcia, D., Premovic, P., and Briceño, H., 2002, Distribution of major and trace elements in La Luna Formation, southwestern Venezuelan basin: Organic geochemistry, v. 33, p. 1593–1608.

Montoya-Pino, C., Weyer, S., Anbar, A.D., Pross, J., Oschmann, W., Schootbrugge, B. van de, and Arz, H.W., 2010, Global enhancement of ocean anoxia during Oceanic Anoxic Event 2: A quantitative approach using U isotopes: Geology, v. 38, p. 315–318, doi: 10.1130/G30652.1.

Morford, J.L., and Emerson, S., 1999, The geochemistry of redox sensitive trace metals in sediments: Geochimica et Cosmochimica Acta, v. 63, p. 1735–1750, doi: 10.1016/S0016-7037(99)00126-X.

Murdmaa, I.O., 1978, 18. INORGANIC GEOCHEMISTRY OF THE LEG 44 SEDIMENTS:

Orth, C.J., Attrep, M., Quintana, L.R., Elder, W.P., Kauffman, E.G., Diner, R., and Villamil, T., 1993, Elemental abundance anomalies in the late Cenomanian extinction interval: a search for the source(s): Earth and Planetary Science Letters, v. 117, p. 189–204, doi: 10.1016/0012-821X(93)90126-T.

Partin, C.A., Bekker, A., Planavsky, N.J., Scott, C.T., Gill, B.C., Li, C., Podkovyrov, V., Maslov, A., Konhauser, K.O., Lalonde, S.V., Love, G.D., Poulton, S.W., and Lyons, T.W., 2013, Large-scale fluctuations in Precambrian atmospheric and oceanic oxygen levels from the record of U in shales: Earth and Planetary Science Letters, v. 369–370, p. 284–293, doi: 10.1016/j.epsl.2013.03.031.

Reeder, R.J., Nugent, M., Lamble, G.M., Tait, C.D., and Morris, D.E., 2000, Uranyl Incorporation into Calcite and Aragonite: XAFS and Luminescence Studies: Environmental Science & Technology, v. 34, p. 638–644, doi: 10.1021/es990981j.

Romaniello, S.J., Herrmann, A.D., and Anbar, A.D., 2013, Uranium concentrations and 238 U/235 U isotope ratios in modern carbonates from the Bahamas: Assessing a novel paleoredox proxy: Chemical Geology, v. 362, p. 305–316.

Sageman, B.B., 1985, High-resolution stratigraphy and paleobiology of the Hartland Shale Member: analysis of an oxygen-deficient epicontinental sea:

Sageman, B.B., 1989, The benthic boundary biofacies model: Hartland Shale Member, Greenhorn Formation (Cenomanian), Western Interior, North America: Palaeogeography, Palaeoclimatology, Palaeoecology, v. 74, p. 87–110.

Sageman, B.B., Meyers, S.R., and Arthur, M.A., 2006, Orbital time scale and new C-isotope record for Cenomanian-Turonian boundary stratotype: Geology, v. 34, p. 125–128, doi: 10.1130/G22074.1.

Savrda, C.E., 1998, Ichnology of the Bridge Creek Limestone: Evidence for Temporal and Spatial Variations in Paleo-Oxygenation in the Western Interior Seaway:, http://archives.datapages.com/data/sepm_sp/csp6/Ichnology_of_the_Bridge.htm (accessed March 2018).

Schlanger, S.O., and Jenkyns, H.C., 1976, Cretaceous oceanic anoxic events: causes and consequences: Geologie en mijnbouw, v. 55, p. 179–184.

Sinninghe Damsté, J.S., van Bentum, E.C., Reichart, G.-J., Pross, J., and Schouten, S., 2010, A CO2 decrease-driven cooling and increased latitudinal temperature gradient during the mid-Cretaceous Oceanic Anoxic Event 2: Earth and Planetary Science Letters, v. 293, p. 97–103, doi: 10.1016/j.epsl.2010.02.027.

Sinton, C.W., and Duncan, R.A., 1997, Potential links between ocean plateau volcanism and global ocean anoxia at the Cenomanian-Turonian boundary: Economic Geology, v. 92, p. 836–842, doi: 10.2113/gsecongeo.92.7-8.836.

Snow, L.J., Duncan, R.A., and Bralower, T.J., 2005, Trace element abundances in the Rock Canyon Anticline, Pueblo, Colorado, marine sedimentary section and their relationship to Caribbean plateau construction and oxygen anoxic event 2: Paleoceanography, v. 20.

Stirling, C.H., Andersen, M.B., Potter, E.-K., and Halliday, A.N., 2007, Low-temperature isotopic fractionation of uranium: Earth and Planetary Science Letters, v. 264, p. 208–225, doi: 10.1016/j.epsl.2007.09.019.

Stirling, I., and Derocher, A.E., 2012, Effects of climate warming on polar bears: a review of the evidence: Global Change Biology, v. 18, p. 2694–2706, doi: 10.1111/j.1365-2486.2012.02753.x.

Taylor, S.R., and McLennan, S.M., 1995, The geochemical evolution of the continental crust: Reviews of Geophysics, v. 33, p. 241–265, doi: 10.1029/95RG00262.

Thurow, J., Moullade, M., Brumsack, H.J., Masure, E., Taugourdeau-Lantz, J., and Dunham, K., 1988, 35. The Cenomanian/Turonian boundary event (CTBE) at Hole 641A, ODP Leg 103 (compared with the CTBE interval at site 398): Boillot, G. et al., Ocean Drilling Program, Scientific Results, Proceedings, Leg, v. 103, p. 587–634.

Tissot, F.L., and Dauphas, N., 2015, Uranium isotopic compositions of the crust and ocean: Age corrections, U budget and global extent of modern anoxia: Geochimica et Cosmochimica Acta, v. 167, p. 113–143.

Topper, R.P.M., Trabucho Alexandre, J., Tuenter, E., and Meijer, P.T., 2011, A regional ocean circulation model for the mid-Cretaceous North Atlantic Basin: implications for black shale formation: Clim. Past, v. 7, p. 277–297, doi: 10.5194/cp-7-277-2011.

Trabucho Alexandre, J., Tuenter, E., Henstra, G.A., van der Zwan, K.J., van de Wal, R.S.W., Dijkstra, H.A., and de Boer, P.L., 2010, The mid-Cretaceous North Atlantic nutrient trap: Black shales and OAEs: Paleoceanography, v. 25, p. PA4201, doi: 10.1029/2010PA001925.

Tucholke, B.E., Sibuet, J.C., and Klaus, A., 2006, 10. Data Report: Multiproxy Geochemical Characterization of OAE-Related Black Shales at Site 1276, Newfoundland Basin:

Tucholke, B.E., and Vogt, P.R., 1979, Introduction and explanatory notes, leg 43 deep Sea Drilling Project: Initial Reports of the Deep Sea Drilling Project, v. 43, p. 5–27.

Turgeon, S., and Brumsack, H.-J., 2006, Anoxic vs dysoxic events reflected in sediment geochemistry during the Cenomanian–Turonian Boundary Event (Cretaceous) in the Umbria–Marche Basin of central Italy: Chemical Geology, v. 234, p. 321–339.

Turgeon, S.C., and Creaser, R.A., 2008, Cretaceous oceanic anoxic event 2 triggered by a massive magmatic episode: Nature, v. 454, p. 323–326.

Weyer, S., Anbar, A.D., Gerdes, A., Gordon, G.W., Algeo, T.J., and Boyle, E.A., 2008, Natural fractionation of 238U/235U: Geochimica et Cosmochimica Acta, v. 72, p. 345–359, doi: 10.1016/j.gca.2007.11.012.

Zhang, F., Algeo, T.J., Romaniello, S.J., Cui, Y., Zhao, L., Chen, Z.-Q., and Anbar, A.D., 2018, Congruent Permian-Triassic δ238U records at Panthalassic and Tethyan sites: Confirmation of global-oceanic anoxia and validation of the U-isotope paleoredox proxy: Geology, v. 46, p. 327–330.

APPENDIX Core photographs (Box 45 to 54) of the USGS PO #1 Core from the USGS Core Research Center online library. White stars denote sample locations within the core.

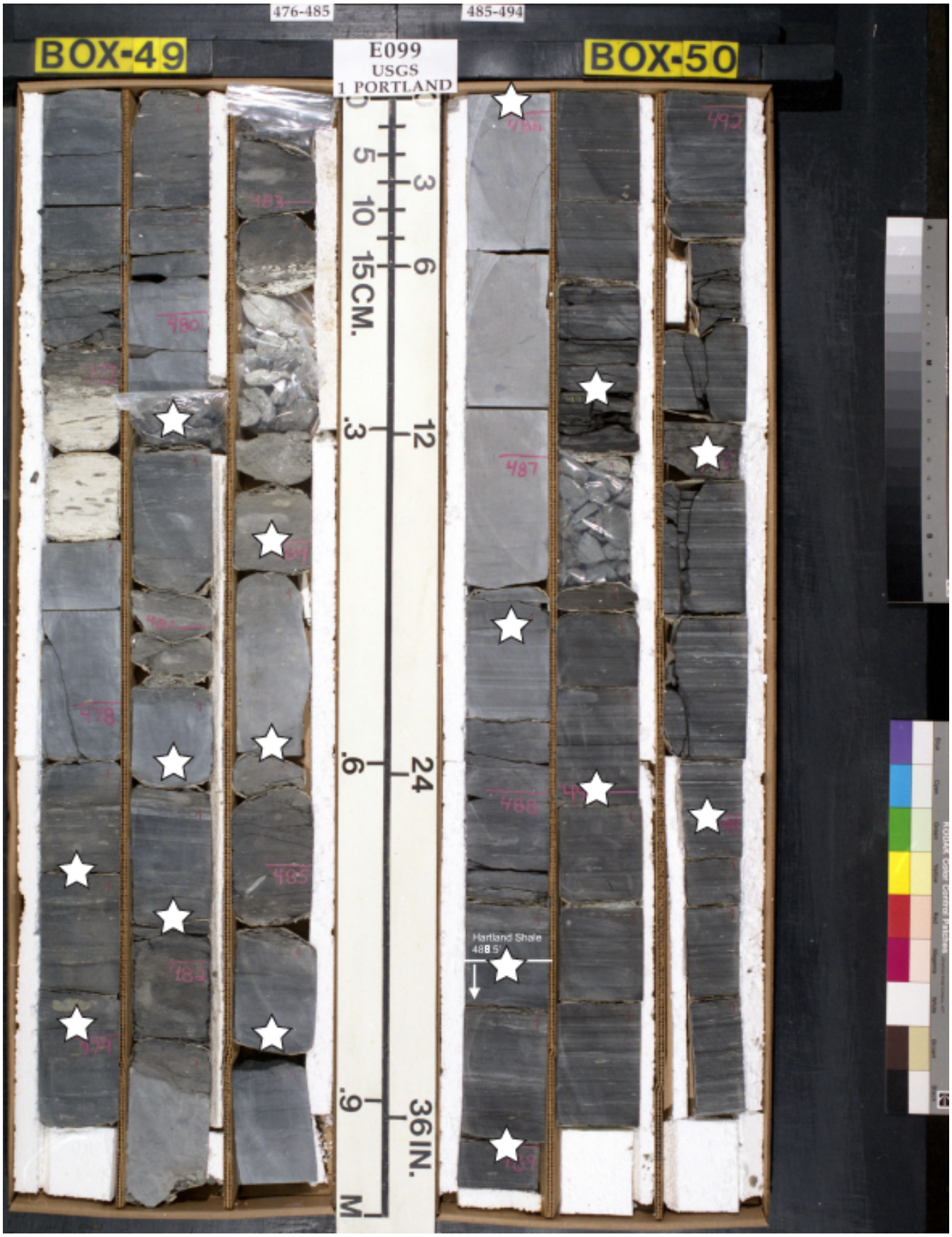
476-485
485-494
BOX-49
BOX-50
E099
USGS
1 PORTLAND
15CM.
36 IN.
Hartland Shale
488.5'

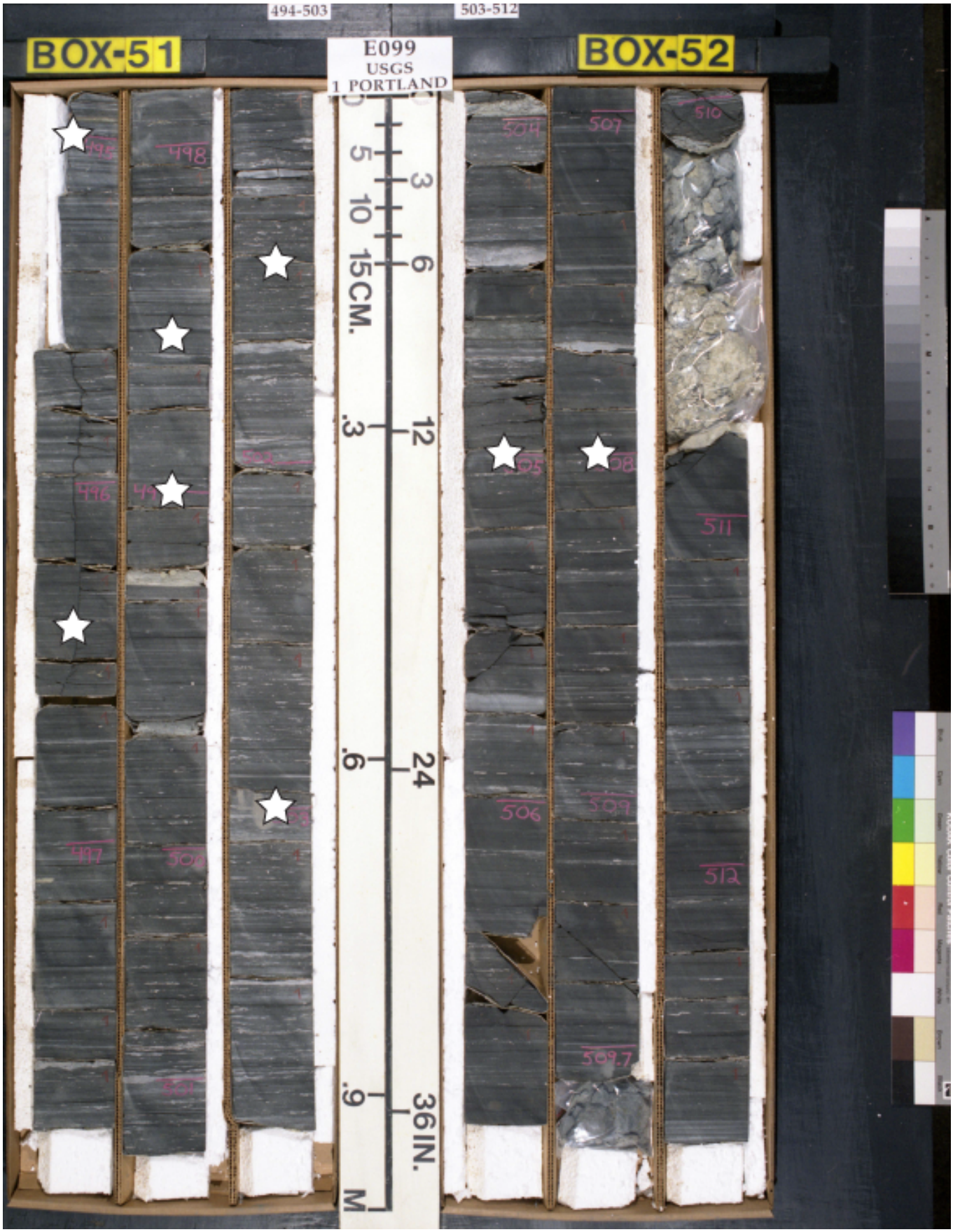
494-503
503-512
BOX-51
BOX-52
E099
USGS
1 PORTLAND
15CM.
36IN.